A Thesis for the Degree of Doctor of Philosophy in Pharmacology

Discovery of New Peptides Modulating Autophagy from Actinobacteria and Reinvestigation of the Structures of Tripartilactam and Lydiamycin A

방선균 유래 신규 자가포식 조절 펩타이드의 발견과 Tripartilactam 및 Lydiamycin A에 대한 구조적 재해석

January 2021

Sunghoon Hwang

Natural Products Science Major, College of Pharmacy
Doctoral Course in the Graduate School
Seoul National University

Discovery of New Peptides Modulating Autophagy from Actinobacteria and Reinvestigation of the Structures of Tripartilactam and Lydiamycin A

Under the Direction of Prof. Dong-Chan Oh
Submitted to the Faculty of the Graduate School
Seoul National University

By
Sunghoon Hwang
Pharmacy in Natural Products Science Major
Doctoral Course in the Graduate School
Seoul National University

Approved as a qualified thesis of Sunghoon Hwang
For the degree Doctor of Philosophy in Pharmacy
By the committee members
January 2021

CHAIRMAN	Jongheon Shin	(인)
VICE-CHAIRMAN	Yeo Joon Yoon	(인)
MEMBER	Minsoo Noh	(인)
MEMBER	Dong-Chan Oh	(인)
MEMBER	Hyukjae Choi	(인)

Abstract

Discovery of New Peptides Modulating Autophagy from Actinobacteria and Reinvestigation of the Structures of Tripartilactam and Lydiamycin A

Sunghoon Hwang
Natural Products Science Major
College of Pharmacy
Doctoral Course in the Graduate School
Seoul National University

During my doctoral course, my research works were concentrated to the structure determination of secondary metabolites derived from insect associated actinomycetes for drug discovery. Especially, my study was divided into discovery of new peptide type compounds from actinomycetes (Part A) and reinvestigation of inaccurate structures of already reported compounds (Part B).

Part A. New Peptides Modulating Autophagy from Actinomycetes

Five new tripeptides, acidiphilamides A-E (**1**-**5**), were discovered along with two previously reported compounds, L-isoleucinamide and L-valinamide, from *Streptacidiphilus rugosus* AM-16, an acidophilic actinobacterium isolated from acidic forest soil. The structures of **1**-**5** were

elucidated as modified tripeptides bearing phenylalaninol or methioninol fragments with C_3~C_5 acyl chains based mainly on NMR and mass spectroscopic data. The absolute configurations of the amino units were established by advanced Marfey's method and GITC (2,3,4,6-tetra-*O*-acetyl-β-d-glucopyranosyl isothiocyanate) derivatization followed by LC/MS analysis. Acidiphilamides A and B (**1**-**2**), the first secondary metabolites isolated from the rare actinobacterial genus *Streptacidiphilus*, significantly inhibited autophagic flux but not proteasome activity in HeLa cells. These compounds appeared to block mainly the autophagosome-lysosome fusion step in the late stage of cellular autophagy.

Pentaminomycins C–E (**6**–**8**) were isolated from the culture of the *Streptomyces* sp. GG23 strain from the guts of the mealworm beetle, *Tenebrio molitor*. The structures of the pentaminomycins were determined to be cyclic pentapeptides containing a modified amino acid, N^5-hydroxyarginine, based on 1D and 2D NMR and mass spectroscopic analyses. The absolute configurations of the amino acid residues were assigned using Marfey's method and bioinformatics analysis of their nonribosomal peptide biosynthetic gene cluster (BGC). Detailed analysis of the BGC enabled us to propose that the structural variations in **6**–**8** originate from the low specificity of the adenylation domain in the nonribosomal peptide synthetase (NRPS) module 1, and indicate that macrocyclization can be catalyzed noncanonically by penicillin binding protein type thioesterase (PBP-type TE). Furthermore, pentaminomycins C and D (**6** and **7**) showed significant autophagy-inducing activities and were cytoprotective against oxidative stress *in vitro*.

Part B. Reinvestigation of the Structures of Tripartilactam and Lydiamycin A

Tripartilactam (**9**) is a natural macrocyclic lactam originally reported to have a unique [18,8,4]-tricyclic framework. However, the validity of this structure has been contested since niizalactam C (**10**) bearing a [18,6,6]-tricyclic skeleton was proposed as an alternative structure in 2015. In this study, a comprehensive reinvestigation of NMR spectroscopic data and a ^{13}C-^{13}C COSY NMR experiment identified direct ^{13}C-^{13}C coupling, thus leading to the unequivocal revision of the structure of tripartilactam as niizalactam C (**10**). In addition, whole-genome sequencing analysis of the tripartilactam-producing bacterial strain and subsequent bioinformatics and mutagenesis analyses identified its biosynthetic pathway, which probably utilizes one of the type I polyketide synthase (PKS) modules iteratively during its biosynthesis and exhibits spontaneous [4+2] cycloaddition from the precursor compound, sceliphrolactam, in the post-PKS process.

Lydiamycin A (**11**) is a previously reported piperazic acid-bearing cyclic peptide from *Streptomyces*. The absolute configuration of lydiamycin A has not been fully determined despite multiple total syntheses being reported. The absolute configuration of **11** was reinvestigated by the advanced Marfey's method, chemical derivatization, and quantum mechanics-based computational analysis, eventually resulting in a structural revision and establishment of the complete configuration. Lydiamycin A (**11**) displayed weak antituberculosis activity *in vitro*.

Key words; actinomycetes, microbial secondary metabolites, biosynthetic pathway, structural revision

Student number: 2015-21908

List of Contents

Part A.

New Peptides Modulating Autophagy from Actinomycetes

I. Introduction

The long history of the discovery of microbial natural products demonstrates that actinobacteria are the most prolific bacterial group in producing bioactive secondary metabolites.[1] In the early years of this field (1940~1974), chemical studies of actinobacteria mainly focused on the genus *Streptomyces*, accounting for 85% of the total reported actinobacterial metabolites.[2] But as more microbial compounds have been reported, the discovery of structurally unique and biologically active compounds has become more difficult. Thus, the development and application of new approaches to microbial chemical reservoirs in exploring new or less-investigated metabolites is particularly important in the field of microbial natural product chemistry.

To solve this matter, natural product scientists often try to isolate rare strains that live in new environments, or to express silent genes of previously discovered strains. From this point of view, genetic based natural product science becomes one of the most important approaches of the field compared to the past. Therefore, it has also become very important to analyze genome of the strains and identify the biosynthetic pathway of the natural compounds. The most of microbial secondary metabolites were produced by two kinds of biosynthetic pathways which are polyketides synthases (PKSs) and non-ribosomal peptides synthetases (NRPSs). PKS pathway is the process of producing metabolites by assembling certain acetate building blocks. And NRPS pathway is the process of producing peptidic compounds based on amino acids building blocks. In this study, we focus on new autophagic active peptidic compounds which were produced by NRPS pathways.

Autophagy is an intracellular proteolytic process involving lysosomal

degradation of a variety of substrates that are either endogenous or exogenous. Autophagy occurs in all eukaryotes ranging from yeast to plants and mammals but does not occur in prokaryotes. The major function of autophagy is to maintain protein homeostasis during various cellular stresses, including nutrient deficiency and genomic instability. In addition, one type of selective autophagy degrades cytoplasmic bacteria (termed bacterial xenophagy).[3] Autophagy inhibitors have been reported to modulate cellular autophagic flux, promoting the death of tumor cells where autophagy is often upregulated.[4]

In this study, we highlight the structural determination of acidiphilamides A-E (**1**-**5**), which are the first secondary metabolites from *Streptacidiphilus* species, and disclose their novel mechanism of inhibiting autophagy at a relatively late stage. And also we report the structural elucidation and autophagic inducing activity of three new cyclic peptides from mealworm beetle associated bacterium: pentaminomycins C-E (**6**-**8**).

II. Acidiphilamides A-E, Modified Peptides as Autophagy Inhibitors from an Acidophilic Actinobacterium, *Streptacidiphilus rugosus*

II. 1. Results and discussions.

Acidiphilamide A (**1**) was isolated as a white powder. The molecular formula of **1** was assigned as $C_{28}H_{39}N_3O_4$ based on its HRFAB mass spectroscopic data. The molecular formula, which corresponds to 11 degrees of unsaturation, was also consistent with the ^{1}H and ^{13}C NMR data (Table 2). The ^{1}H and ^{13}C NMR data showed signals typical of amino acid-derived compounds with three amide proton signals (δ_H 8.07, 7.84, and 7.82) and α-amino proton signals (δ_H 4.54, 4.10, and 3.92). In addition to these ^{1}H resonances, ten aromatic protons (δ_H 7.24~7.14), 11 aliphatic methylene and methine protons (δ_H 3.32~1.37), three methyl groups (δ_H 0.78, 0.74, and 0.68), and one hydroxy proton (δ_H 4.79) were detected in the ^{1}H NMR spectrum. The ^{13}C NMR spectrum displayed three carbonyl carbon resonances (δ_C 172.0, 171.1, and 170.3) and three α-amino carbon signals (δ_C 57.0, 53.6, and 52.1) along with 12 aromatic carbons (δ_C 139.0~125.8), one oxygenated carbon (δ_C 62.4), and ten aliphatic carbon peaks (δ_C 37.2~11.0). Interpretation of the HSQC NMR spectrum allowed the assignment of all $^{1}J_{CH}$ correlations. Comprehensive analysis of the 1D (^{1}H and ^{13}C) and 2D (COSY, TOCSY, and HMBC) NMR spectroscopic data of **1** indicated the presence of two amino acid residues, phenylalanine and isoleucine, in acidiphilamide A (**1**) (Figure 1). In addition, an array of COSY and TOCSY correlations from 1-OH to H_2-3 and among the aromatic protons (H-5 to H-9) along with HMBC correlations from H-6/8 and H-3 to C-4 (δ_C 139.0) revealed the existence of phenylalaninol. Lastly, a short acyl chain, butanoic acid, was constructed based on H-26/H-27 and H-27/H-28 COSY and H-26/C-25 (δ_C 172.0) HMBC correlations. Once phenylalanine, isoleucine, phenylalaninol, and butanoic acid were identified, these partial structures were assembled by HMBC

correlations around amide carbonyl carbons. The 11 double bond equivalents were fully explained by two aromatic rings and three carbonyl functional groups, and acidiphilamide A (**1**) must be a combination of the four substructures in a linear molecule. The 2-NH (δ_H 7.84) signal of phenylalaninol correlated with the amide carbonyl carbon C-10 (δ_C 170.3), belonging to the isoleucine residue, which connected phenylalaninol to isoleucine. The HMBC correlation from 11-NH (δ_H 7.82) of isoleucine to the carbonyl carbon C-16 (δ_C 171.1) of phenylalanine established the sequence to isoleucine to phenylalanine. The amide proton of phenylalanine (17-NH; δ_H 8.07) displayed $^2J_{CH}$ coupling with the carbonyl carbon C-25 (δ_C 172.0) of butanoic acid, the terminal acyl chain, elucidating the planar structure of acidiphilamide A (**1**) (Figure 1).

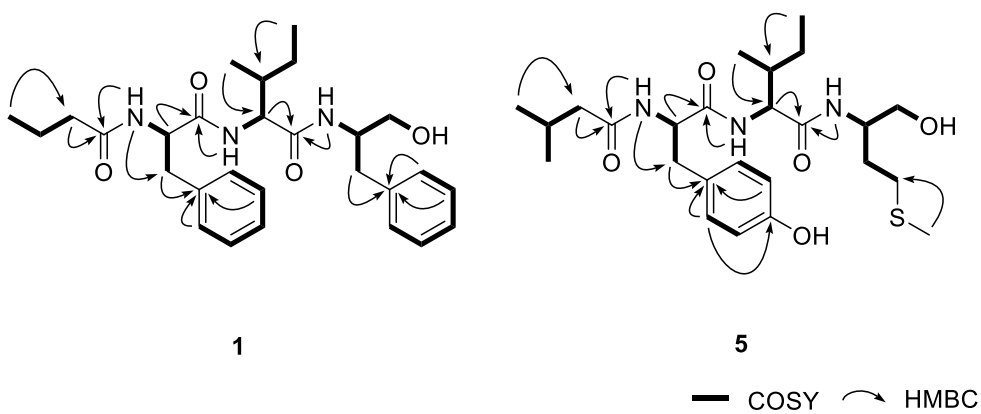

Figure 1. Key ^{1}H-^{1}H COSY and HMBC correlations of **1** and **5**.

Acidiphilamide B (**2**) was purified as a white powder, and its molecular formula was determined to be $C_{28}H_{39}N_3O_4$ based on the corresponding HRFAB mass spectroscopic data. This molecular formula is identical to that

of acidiphilamide A (**1**). The ^{1}H and ^{13}C NMR data of **2** in DMSO-d_6 were also highly similar to those of **1** (Table 2). However, detailed examination of the 1D and 2D NMR data of **2** revealed the structural difference between **1** and **2**. In particular, the ^{1}H and HSQC NMR spectra of acidiphilamide B (**2**) displayed four methyl doublets (δ_H 0.78, 0.78, 0.73, and 0.65), whereas acidiphilamide A (**1**) had two methyl triplets and one methyl doublet. Further analysis of the COSY and HMBC NMR spectra identified phenylalanine, valine, phenylalaninol, and 3-methylbutanoic acid moieties. The sequence of these partial structures was established to be phenylalaninol-valine-phenylalanine-3-methylbutanoic acid by analysis of the HMBC correlations. In brief, the isoleucine and butanoic acid units of **1** were replaced with valine and 3-methylbutanoic acid moieties in the structure of **2**.

Acidiphilamide C (**3**) was isolated as a white powder. Its HRFAB mass spectroscopic data indicated a molecular formula of $C_{29}H_{41}N_3O_4$, which has one CH_2 unit more than **1** and **2**. Although the NMR data of **3** displayed high similarity to those of **1** and **2**, unlike **1** and **2**, acidiphilamide C (**3**) showed one methyl triplet and three methyl doublets in its ^{1}H NMR data (Table 2), indicating variations in the methyl-bearing substructures such as the acyl chain and isoleucine/valine. Comprehensive analysis of its 1D and 2D NMR spectra identified phenylalanine, isoleucine, phenylalaninol, and 3-methylbutanoic acid moieties. The full structure (phenylanalinol-isoleucine-phenylalanine-3-methylbutanoic acid) of acidiphilamide C (**3**) was then constructed by analysis of the HMBC correlations in the same manner as discussed above.

Acidiphilamide D (**4**) was also purified as a white powder. The molecular formula of this compound was determined to be $C_{27}H_{37}N_3O_5$ based

on its HRFAB mass spectroscopic data. The molecular formula of **4** has one more oxygen and one less CH_2 compared to that of acidiphilamide A (**1**) (Table 2). The ^{1}H NMR spectra of **1** and **4** exhibited significant differences in their aromatic regions. Acidiphilamide D displayed ^{1}H resonance signals typical of a para-substituted aromatic ring at δ_H 7.01 (d, J = 8.0 Hz) and 6.62 (d, J = 8.0 Hz). Further analysis of its 1D and 2D NMR spectroscopic data indicated the presence of tyrosine instead of the phenylalanine, but the isoleucine, phenylalaninol, and propanoic acid moieties remained. These partial structures were in the sequence phenylalaninol-isoleucine-tyrosine-propanoic acid based on the HMBC correlations.

In addition to acidiphilamides A-D (**1**-**4**), acidiphilamide E (**5**) was discovered as a minor metabolite. Its molecular formula was determined to be $C_{25}H_{41}N_3O_5S$ by HRFAB MS analysis. The ^{1}H and ^{13}C NMR data of **5** showed resonance distinct from those of **1**-**4** (Table 2). Acidiphilamide E has only one aromatic ring containing four protons and six carbons, whereas the other congeners bear the two aromatic rings of phenylalanine/tyrosine and phenylalaninol. Moreover, acidiphilamide E displayed a methyl singlet (δ_C 14.7; δ_H 2.01). Interpretation of its ^{1}H, ^{13}C, COSY, HSQC and HMBC NMR spectra suggested that acidiphilamide E (**5**) possesses tyrosine, isoleucine, and 3-methylbutanoic acid moieties, which were also present in acidiphilamides A-D (**1**-**4**). These three partial structures accounted for $C_{20}H_{29}N_2O_4$, and the additional substructure must contain $C_5H_{12}NOS$. The triplet hydroxy proton (1-OH; δ_H 4.69) correlated with H_2-1 (δ_H 3.35 and 3.20). C-1 (δ_C 63.0) was connected to C-2 (δ_C 49.9) based on their H_2-1/H-2 COSY correlations. C-2 was identified as an α-amino carbon by the three bond ^{1}H-^{1}H coupling between H-2 (δ_H 3.79) and 2-NH (δ_H 7.70). The H-2/H_2-3 and H_2-3/H_2-4 COSY correlations extended the carbon chain to C-4 (δ_C

29.9). The chain was terminated by S-CH_3 based on the HMBC correlation from the singlet methyl group to C-4, constructing a methioninol moiety. The full planar structure of acidiphilamide E (**5**) was determined as methioninol-isoleucine-tyrosine-3-methylbutanoic acid (Figure 1). Notably, methioninol is incorporated into acidiphilamide E by replacing the phenylalaninol moiety present in the other compounds in this series. To the best of our knowledge, acidiphilamide E (**5**) is the first natural product bearing a methioninol fragment based on our comprehensive literature search.

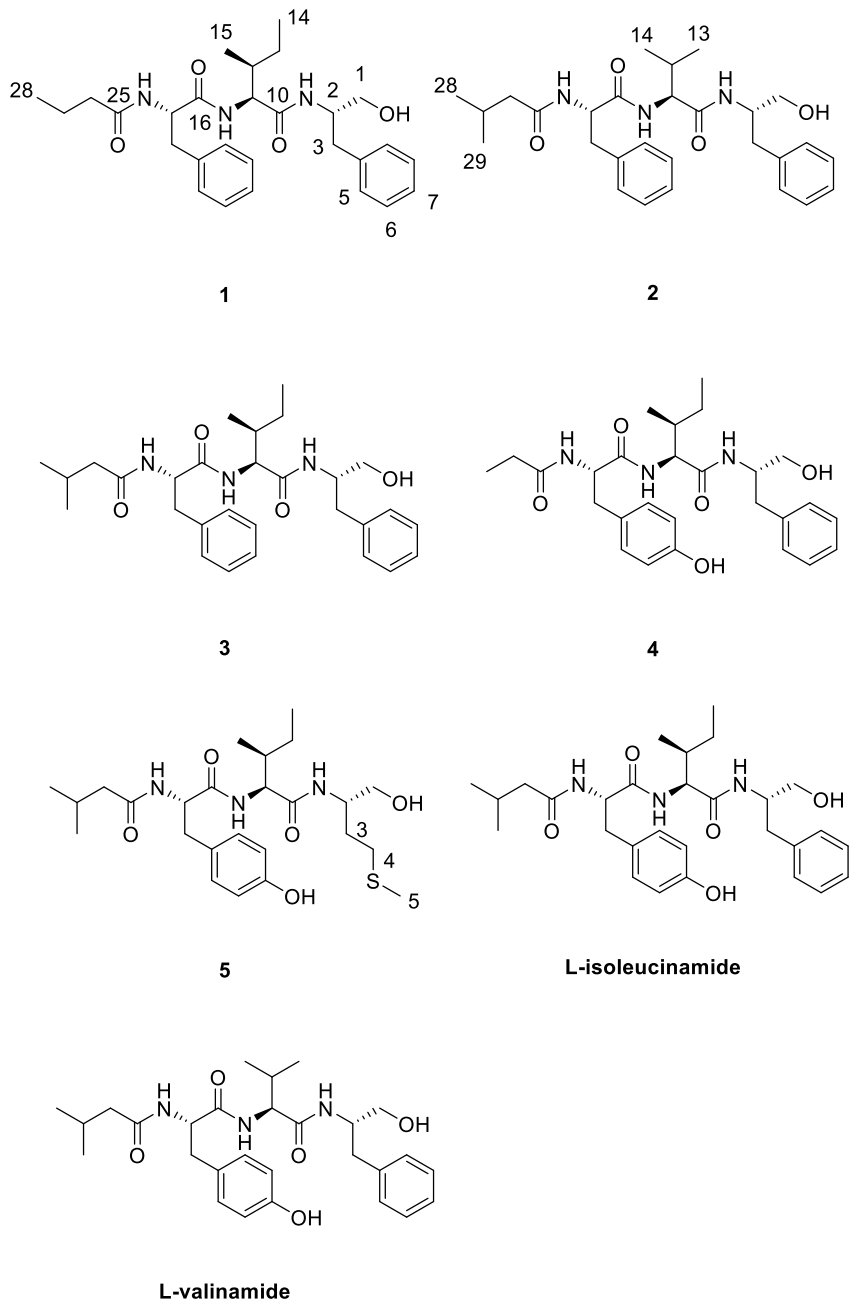

Figure 2. Chemical structures of acidiphilamides A-E (**1-5**), L-isoleucinamide and L-valinamide.

To determine the absolute configurations of acidiphilamides A-E (**1**-**5**), chemical derivatization of the hydrolysates of **1**-**5** using advanced Marfey's reagents[5] [*N*-(5-fluoro-2,4-dinitrophenyl)-L-alanine amide (L-FDAA) and D-FDAA] and GITC[6] (2,3,4,6-tetra-*O*-acetyl-*β*-D-glucopyranosyl isothiocyanate) was conducted. By LC/MS analysis of the FDAA derivatives, the *α*-carbons of the phenylalanine, isoleucine, valine, and tyrosine residues in acidiphilamides A-E (**1**-**5**) all possess L-configurations. The absolute configuration of the C-3 stereogenic center in the phenylalaninol fragments of **1**-**4** was assigned as being *S* by comparison with the L- and D-FDAA adducts of an authentic standard of *S*-phenylalaninol (Table 1). The configuration of the *β*-position in Ile was established by comparing the retention time of its GITC derivative with the retention times of the GITC derivatives of authentic L-Ile and L-allo-Ile. This analysis revealed that the isoleucine residues in **1** and **3**-**5** are L-Ile, not L-allo-Ile. The C-3 stereogenic center of methioninol in acidiphilamide E (**5**) was also demonstrated to be in the *S*-configuration based on a comparison of the retention times of its L- and D-FDAA derivatives with those of the derivatives of authentic *S*-methioninol.

During the purification of the acidiphilamides (**1**-**5**), previously reported metabolites L-isoleucinamide[7] and L-valinamide[8] were also obtained. Since these molecules were previously reported to inhibit the activity of a lysosomal endopeptidase enzyme, cathepsin L,[9] we examined whether these new metabolites affect cellular autophagic flux. When HeLa cells were treated with acidiphilamides A and B (**1**-**2**), the levels of key autophagic marker protein LC3-II were robustly elevated in a moderately dose-dependent manner, while the levels of autophagic receptor p62/SQSTM1 were

unchanged (Figure 3a). In contrast, L-isoleucinamide, L-valinamide, and acidiphilamides C, D, and E had virtually no effect on the levels of LC3-II (Figure 3a-3c). The time-course evaluation of LC3-II indicated that both acidiphilamides A and B perturb the cellular autophagy flux with acidiphilamide B having more potent and prolonged inhibitory effects than acidiphilamide A (Figure 3a-3c). The effects of the acidiphilamides on the proteasome were assessed using purified human 26S proteasomes, and it was found that the acidiphilamides did not affect proteasome activity as measured by fluorogenic reporter substrate suc-LLVY-AMC (Figure 3d). Consistently, after treatment with the acidiphilamides, the levels of total polyubiquitin conjugates and proteasome subunit α3 were also unchanged (Figure 3a). Together, these results indicated that treatment with acidiphilamides A and B (**1** and **2**) resulted in aberrant cellular autophagy without affecting the ubiquitin-proteasome system.

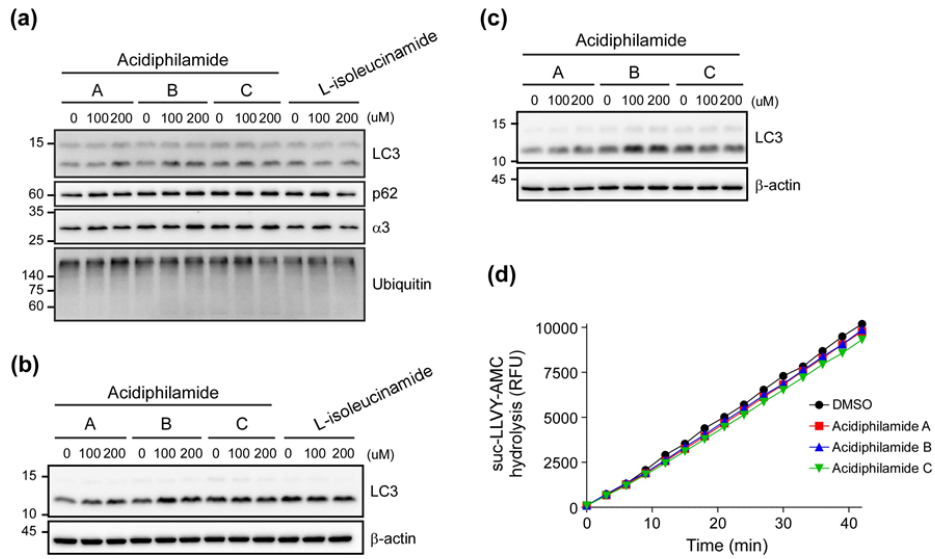

Figure 3. Acidiphilamides A and B (**1** and **2**) affect autophagic flux in mammalian cells. HeLa cells were treated with different acidiphilamides for various incubation times (4 h, 8 h, and 12 h for panels a, b, and c, respectively) at the indicated final concentrations. Whole cell lysates were collected and analyzed by SDS-PAGE and immunoblotting against the indicated antibodies. (d) The proteasome activity measured using purified proteasomes, acidiphilamides, and suc-LLVY-AMC. The hydrolysis of suc-LLVY-AMC was monitored for the indicated time periods. RFU, relative fluorescence unit.

Elevated levels of cellular LC3-II due to treatment with acidiphilamides may originate from either increased overall autophagic flux or inhibition of autolysosomal degradation of LC3-II.[10] To determine the molecular mechanism, the cells were treated with bafilomycin A1 (BafA1) prior to treatment with acidiphilamide A or B. BafA1 inhibits autophagy at a late stage by blocking the fusion between the autophagosome and lysosome.

We found little change in LC3-II upon exposure to acidiphilamides when the cells were cotreated with BafA1 (Figure 4), suggesting that the acidiphilamides may not directly induce the autophagy signal but most likely have an effect on the downstream of the autophagic flux. Consistent with this observation, when overall autophagy was induced through amino acid deprivation, treatment with acidiphilamides A and B (**1**-**2**) led to mild elevation of the LC3-II levels, indicating that the effects of acidiphilamides on autophagy are independent of the initial stages of autophagy.

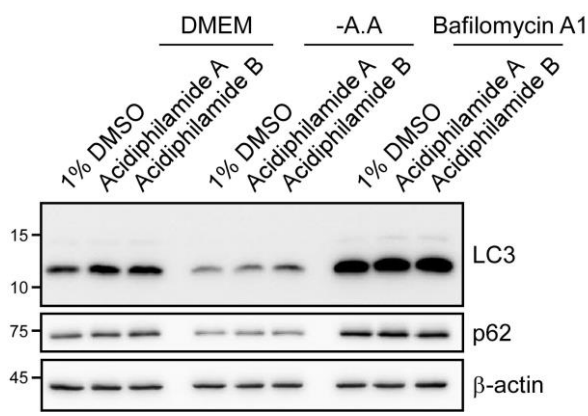

Figure 4. Acidiphilamides A and B (**1**-**2**) inhibit autolysosomal activity. HeLa cells were cotreated with **1** or **2** (200 μM) and bafilomycin A1 (100 nM) or under amino acid-depleted (-A.A, EBSS media) conditions for 8 h. *β*-Actin served as the loading control.

To further validate the mechanism of the activity of acidiphilamides A and B (**1**-**2**), HeLa cells were treated with BODIPY dye conjugated to a bovine serum albumin probe (DQ-BSA), and its fluorescence was monitored. In the assay, the fluorescence of DQ-BSA becomes dequenched when

endocytosed DQ-BSA is captured and degraded in the autolysosome.[11] Consistent with this, cells under starvation conditions in EBSS media showed elevated levels of fluorescent puncta representing autophagic lysosomes (Figure 5). Treatment with **1** or **2**, however, significantly reduced the intensity of the DQ-BSA signal compared to treatment with DMSO. These results demonstrated the inhibitory effect of acidiphilamides on lysosomes, further supporting the hypothesis that the ability of acidiphilamides to elevate LC3-II levels may reflect the inhibition of autophagy at the late stages instead of the upregulation of overall cellular autophagy.

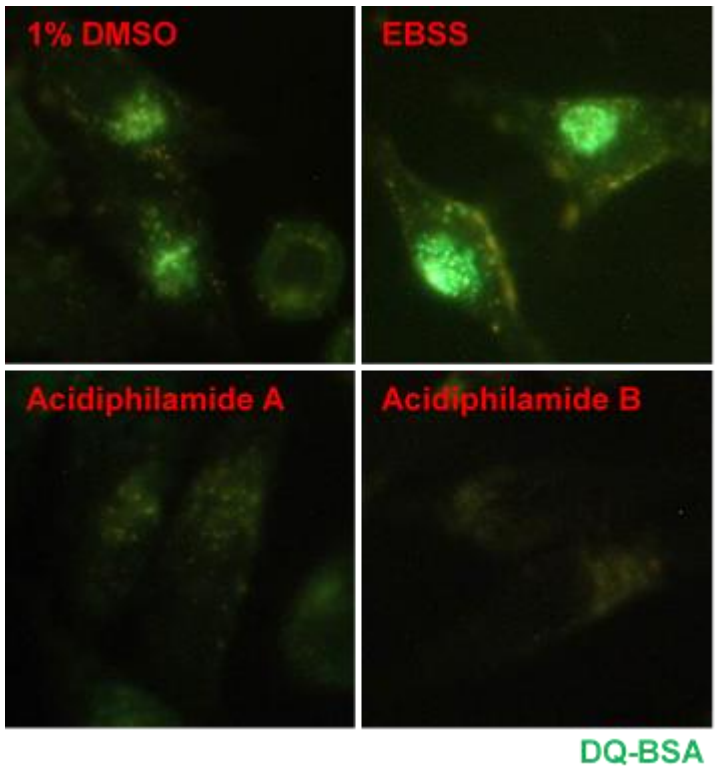

Figure 5. Lysosomal proteolytic activity is reduced by acidiphilamides A and B (**1**-**2**). HeLa cells were treated with self-quenching DQ-BSA green (10 μg/mL) for 1 h and then treated with DMSO, EBSS media, **1**, or **2** (200 μM) for 4 h.

The biosynthesis of acidiphilamides A-E (**1**-**5**), L-isoleucinamide, and L-valinamide from *Streptacidiphilus rugosus* AM-16 could be rationally proposed through a modular nonribosomal peptide synthetase (NRPS) pathway (Figure 6). The structural diversity of these peptides lies on the modification of the short C_3~C_5 acyl chains and the composition of the amino acid-derived units. Various short acyl chains could be introduced as starting units for a NRPS pathway because of the substrate promiscuity of fatty acyl

CoA ligase, which activates fatty acids for biosynthesis.[12] The composition of amino acid-derived units is determined by adenylation domains in the acidiphilamide NRPS biosynthetic module, which recognize and activate specific amino acids. The Ile/Val variation between acidiphilamides A and B could be easily explained based on the previously-reported high similarity of the specificity pockets of Ile and Val adenylation domains.[13] Another precedent biochemical study reported that the adenylation domain for L-Phe in tyrocidine A, a bacterial NRPS metabolite, can also activate both L-Tyr and L-Met even though the catalytic efficiencies for L-Tyr and L-Met are much lower than L-Phe,[14] possibly rationalizing the production of acidiphilamides D and E (**4**-**5**) bearing Tyr and/or Met-derived methioninol as minor metabolites. The terminal phenylalaninol and methioninol of **1**-**5** could be biosynthesized from Phe and Met through the reduction of their carboxylic acids to primary alcohols in the post modular biosynthesis (Figure 6).

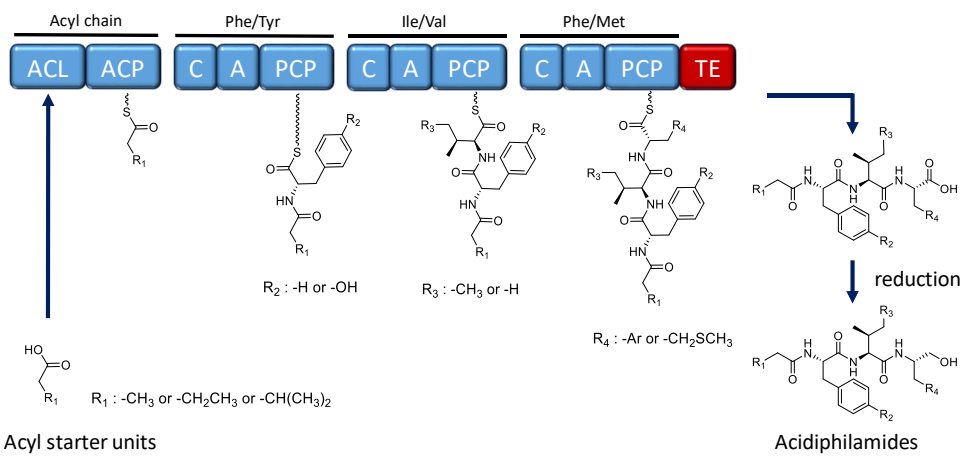

Figure 6. Proposed biosynthesis of the acidiphilamides through a putative NRPS pathway.

Table 1. LC/MS analysis of L- and D-FDAA derivatives of the amino acid-derived units in acidiphilamides (**1**-**5**). Retention times (min) are notified.

Acidiphilamide A (**1**)	Phenylalanine	Isoleucine	Phenylalaninol
+ L-FDAA	31.4	30.5	30.7
+ D-FDAA	34.2	34.4	33.7
Elution order	L→ D	L→ D	L→ D
Acidiphilamide B (**2**)	Phenylalanine	Valine	Phenylalaninol
+ L-FDAA	31.0	31.0	30.5
+ D-FDAA	34.1	34.1	33.9
Elution order	L→ D	L→ D	L→ D
Acidiphilamide C (**3**)	Phenylalanine	Isoleucine	Phenylalaninol
+ L-FDAA	31.2	30.4	30.5
+ D-FDAA	34.4	34.8	33.9
Elution order	L→ D	L→ D	L→ D
Acidiphilamide D (**4**)	Tyrosine	Isoleucine	Phenylalaninol
+ L-FDAA	30.8	39.5	39.8
+ D-FDAA	33.0	45.3	43.3
Elution order	L→ D	L→ D	L→ D
Acidiphilamide E (**5**)	Tyrosine	Isoleucine	Methioninol
+ L-FDAA	27.3	33.1	27.6
+ D-FDAA	27.6	36.4	30.5
Elution order	L→ D	L→ D	L→ D

Table 2. NMR data for acidiphilamides A-E (**1**-**5**) in DMSO-d_6

		Acidiphilamide A (**1**)		Acidiphilamide B (**2**)		Acidiphilamide C (**3**)		Acidiphilamide D (**4**)		Acidiphilamide E (**5**)	
	Position	δ_C, type	δ_H, mult (J in Hz)	δ_C, type	δ_H, mult (J in Hz)	δ_C, type	δ_H, mult (J in Hz)	δ_C, type	δ_H, mult (J in Hz)	δ_C, type	δ_H, mult (J in Hz)
Met/Phe-OH	1a	62.4, CH_2	3.32, m	62.4, CH_2	3.32, m	62.4, CH_2	3.32, m	62.4, CH_2	3.32, m	63.0, CH_2	3.35, m
	1b		3.24, m		3.24, m		3.24, m		3.25, m		3.20, m
	1-OH		4.79, br s		4.80, br s		4.77, t (5.0)		4.78, br s		4.69, t (4.5)
	2	52.1, CH	3.92, m	52.2, CH	3.92, m	52.2, CH	3.92, m	52.2, CH	3.92, m	49.9, CH	3.79, m
	2-NH		7.84, d (8.5)		7.83, d (8.5)		7.79, d (8.5)		7.78, d (8.5)		7.70, d (8.5)
	3a	36.3, CH_2	2.87, dd (14.0, 5.5)	36.4, CH_2	2.86, dd (14.0, 5.5)	36.3, CH_2	2.87, dd (14.0, 5.5)	36.3, CH_2	2.86, dd (14.5, 5.5)	30.6, CH_2	1.83, m
	3b		2.61, dd (14.0, 8.5)		2.61, dd (14.0, 8.5)		2.61, dd (14.0, 8.5)		2.62, m		1.53, m
	4a	139.0, C		139.1, C		139.1, C		139.1, C		29.9, CH_2	2.46, m
	4b										2.37, m
	5, 9	129.0, 2CH	7.20, d (7.0)	129.1, 2CH	7.20, d (7.0)	129.0, 2CH	7.20, d (7.0)	129.0, 2CH	7.20, d (7.0)	14.7, CH_3	2.01, s
	6, 8	128.1, 2CH	7.23, dd (7.0, 7.0)	128.1, 2CH	7.23, dd (7.0, 7.0)	128.1, 2CH	7.23, dd (7.0, 7.0)	128.1, 2CH	7.22, dd (7.0, 7.0)	-	
	7	125.8, CH	7.14, dd (7.0, 7.0)	125.9, CH	7.14, dd (7.0, 7.0)	125.8, CH	7.14, dd (7.0, 7.0)	125.9, CH	7.14, dd (7.0, 7.0)	-	
Ile/Val	10	170.3, C		170.3, C		170.4, C		170.4, C		170.6, C	
	11	57.0, CH	4.10, dd (9.0, 8.0)	57.8, CH	4.09, dd (9.0, 7.0)	57.0, CH	4.10, dd (8.5, 7.5)	57.0, CH	4.09, dd (8.5, 7.5)	57, CH	4.09, t (8.0)
	11-NH		7.82, d (9.0)		7.81, d (9.0)		7.80, d (8.5)		7.77, d (8.5)		7.82, d (8.5)
	12	36.9, CH	1.64, m	30.9, CH	1.89, m	36.9, CH	1.64, m	36.9, CH	1.63, m	36.6, CH	1.68, m

	13a	24.2, CH_2	1.37, m	19.1, CH_3	0.78, d (7.0)	24.2, CH_2	1.37, m	24.3, CH_2	1.36, m	24.4, CH_2	1.43, m
	13b		1.0, m				1.00, m		0.99, m		1.04, m
	14	11.0, CH_3	0.78, t (7.5)	18.1, CH_3	0.78, d (7.0)	11.0, CH_3	0.78, t (7.5)	11.0, CH_3	0.78, t (7.0)	11.0, CH_3	0.81, t (7.5)
	15	15.2, CH_3	0.74, d (7.0)	-		15.2, CH_3	0.75, d (7.0)	15.3, CH_3	0.74, d (7.0)	15.3, CH_3	0.80, d (6.5)
Tyr/Phe	16	171.1, C		171.3, C		171.2, C		171.2, C		171.4, C	
	17	53.6, CH	4.54, ddd (10.0, 8.5, 4.0)	53.7, CH	4.56, ddd (10.0, 8.5, 4.0)	53.7, CH	4.56, ddd (10.0, 8.5, 4.0)	54.0, CH	4.42, ddd (10.0, 8.5, 4.0)	54.0, CH	4.47, ddd (10.0, 8.5, 4.0)
	17-NH		8.07, d (8.5)		8.07, d (8.5)		8.04, d (8.5)		7.98, d (8.5)		7.94, d (9.0)
	18a	37.2, CH_2	2.93, dd (14.0, 4.0)	37.1, CH_2	2.94, dd (14.0, 4.0)	37.2, CH_2	2.92, dd (14.0, 4.0)	36.3, CH_2	2.82, dd (14.0, 4.0)	36.4, CH_2	2.84, dd (14.0, 4.0)
	18b		2.70, dd (14.0, 10.0)		2.71, dd (14.0, 10.0)		2.70, dd (14.0, 10.0)		2.60, dd (14.0, 10.0)		2.59, dd (14.0, 10.0)
	19	138.0, C		138.2, C		138.2, C		128.1, C		128.1, C	
	20, 24	129.1, 2CH	7.24, d (7.0)	129.1, 2CH	7.25, d (7.0)	129.1, 2CH	7.25, d (7.0)	130.0, 2CH	7.01, d (8.0)	130.0, 2CH	7.02, d (8.0)
	21, 23	127.9, 2CH	7.22, dd (7.0, 7.0)	127.9, 2CH	7.23, dd (7.0, 7.0)	127.9, 2CH	7.22, dd (7.0, 7.0)	114.8, 2CH	6.62, d (8.0)	114.7, 2CH	6.61, d (8.0)
	22	126.1, CH	7.16, dd (7.0, 7.0)	125.9, CH	7.15, dd (7.0, 7.0)	126.1, CH	7.16, dd (7.0, 7.0)	155.7, C		155.7, C	
Acyl	25	172.0, C	1.98, td (7.5, 2.0)	171.5, C	1.88, d (6.5)	171.4, C	1.87, d (6.5)	172.9, C		171.4, C	
	26	28.3, CH_2	1.37, m	44.5, CH_2	1.81, m	44.5, CH_2	1.82, m	28.3, CH_2	2.02, qd (7.5, 2.5)	44.5, CH_2	1.89, d (6.5)
				25.6, CH		25.5, CH			0.88, d (7.5)	25.5, CH	1.84, m
	27	18.6, CH_2	0.68, t (7.5)		0.73, d (7.0)		0.73, d (7.0)	9.9, CH_3			
	28	13.4, CH_3		22.2, CH_3		22.2, CH_3				22.2, CH_3	0.76, d (6.5)
	29			22.1, CH_3	0.65, d (7.0)	22.1, CH_3	0.66, d (7.0)			22.3, CH_3	0.70, d (6.5)

II. 2. Conclusion

In the present study, we discovered the first secondary metabolites, acidiphilamides A-E (**1**-**5**), from the rare actinobacterial genus *Streptacidiphilus* by chemical investigation of an *S. rugosus* strain isolated from acidic forest soil. Among these new natural products, the structure of acidiphilamide E (**5**) is the most unique as it bears a methioninol fragment instead of the phenylalaninol fragment present in the other compounds in this class. Methioninol is widely used as a component in synthetic compounds, including a synthetic analogue of encephalin,[15] the morphomimetic pentapeptides of the mammalian brain. However, to the best of our knowledge, acidiphilamide E (**5**) is the first natural product bearing a methioninol moiety.

II. 3. Experimental section

General experimental procedures. Optical rotations were measured using a JASCO P-1020 polarimeter. UV spectra were acquired on a Chirascan plus Applied Photophysics spectrophotometer. IR spectra were recorded using a Thermo NICOLET iS10 spectrometer. ^{1}H, ^{13}C, and 2D NMR spectra were obtained on a Bruker Avance 600 MHz spectrometer at the National Center for Inter-university Research Facilities (NCIRF) at Seoul National University. Low-resolution electrospray ionization mass spectra were acquired with an Agilent Technologies 6130 quadrupole mass spectrometer coupled to an Agilent Technologies 1200 series high-performance liquid chromatography (HPLC) instrument. High-resolution fast-atom bombardment (HRFAB) mass spectra were obtained using a JEOL JMS-600W high-resolution mass spectrometer at the NCIRF. Semipreparative HPLC separations were achieved with a Gilson 305 pump and a Gilson UV/VIS-155 detector.

Bacterial strain. *Streptacidiphilus rugosus* strain AM-16 was isolated from the soil of a pine forest (*Pinus thunbergii*) as described previously.[16] Later, the strain was designated as *Streptacidiphilus rugosus*, a species recently described by Cho *et al*.[17] The 16S rRNA gene sequence of the strain is available in the GenBank database under the accession number DQ904547.

Cultivation and extraction. The *Streptacidiphilus rugosus* strain was initially cultivated in 50 mL of modified Bennett's medium (1 g of yeast extract, 1 g of peptone, 2 g of beef extract, 10 g of glucose in 1 L of distilled water acidified with HCl to pH 4.5). After the strain was cultivated for 4 days

on a rotary shaker at 170 rpm and 30 ℃, 10 mL of the culture was transferred to 1 L of modified Bennett's medium in a 2.8-L Fernbach flask. The entire culture (72 L) was extracted twice with ethyl acetate (150 L). The EtOAc extract was concentrated in vacuo to yield 10 g of dry material.

Isolation of acidiphilamides. The dried extract was directly subjected to reversed-phase HPLC (YMC-Triart C_{18} 250 × 10 mm, flow rate 2 mL/min, UV 230 nm detection, 30%–60% aqueous CH_3CN-H_2O gradient with 0.1% formic acid over 40 min). Under these purification conditions, the fractions containing acidiphilamides A and B (**1**-**2**) (17 mg), pure acidiphilamide C (**3**) (10 mg), and acidiphilamides D and E (**4**-**5**) (19 mg) were collected at retention times of 38, 40, and 25 min, respectively. Subjecting the fraction containing acidiphilamides A and B (**1**-**2**) to reversed-phase HPLC (YMC-Triart C_{18} 250 × 10 mm, flow rate 2 mL/min, UV 230 nm detection, 70% aqueous MeOH isocratic conditions with 0.1% formic acid over 40 min) for a second time yielded pure acidiphilamide A (**1**) (8 mg) and acidiphilamide B (**2**) (9 mg) at retention times of 31 min and 34 min, respectively. To separate acidiphilamide D and E (**4**-**5**), revered-phase HPLC (YMC-Triart C_{18} 250 × 10 mm, flow rate 2 mL/min, UV 230 nm detection, 50% aqueous MeOH isocratic solvent conditions with 0.1% formic acid over 60 min) was performed. Under these purification conditions, acidiphilamide D (**4**) (9 mg) and acidiphilamide E (**5**) (10 mg) were obtained at retention times of 57 min and 60 min, respectively.

Acidiphilamide A (1): White powder; $[\alpha]_D^{25}$ -0.7 (*c* 0.2, MeOH); UV (MeOH) λ_{max} (log ε) 203 (2.77) nm; IR (neat) ν_{max} 3366, 2951, 2843, 1635, 1409, 1052, 1031 cm^{-1}; for ^{1}H and ^{13}C NMR data, Table 2; HRFABMS *m*/*z* 482.3019 $[M+H]^+$ (calcd for $C_{28}H_{40}N_3O_4$, 482.3019).

Acidiphilamide B (**2**): White powder; $[\alpha]_D^{25}$ -3.1 (*c* 0.6, MeOH); UV (MeOH) λ_{max} (log ε) 206 (2.35) nm; IR (neat) ν_{max} 3389, 2965, 2864, 1634, 1411, 1032 cm^{-1}; for ^{1}H and ^{13}C NMR data, Table 2; HRFABMS *m*/*z* 482.3018 $[M+H]^+$ (calcd for $C_{28}H_{40}N_3O_4$, 482.3019).

Acidiphilamide C (3): White powder; $[\alpha]_D^{25}$ -2.2 (*c* 0.5, MeOH); UV (MeOH) λ_{max} (log ε) 203 (2.30) nm; IR (neat) ν_{max} 3365, 2951, 2842, 1634, 1453, 1411, 1015 cm^{-1}; for ^{1}H and ^{13}C NMR data, Table 2; HRFABMS *m*/*z* 496.3173 $[M+H]^+$ (calcd for $C_{29}H_{42}N_3O_4$, 496.3175).

Acidiphilamide D (4): White powder; $[\alpha]_D^{25}$ -3.1 (*c* 0.6, MeOH); UV (MeOH) λ_{max} (log ε) 204 (2.32), 279 (1.27) nm; IR (neat) ν_{max} 3376, 2842, 1634, 1453, 1411, 1053 cm^{-1}; for ^{1}H and ^{13}C NMR data, Table 2; HRFABMS *m*/*z* 484.2814 $[M+H]^+$ (calcd for $C_{27}H_{38}N_3O_5$, 484.2811).

Acidiphilamide E (5): White powder; $[\alpha]_D^{25}$ -2.5 (*c* 0.5, MeOH); UV (MeOH) λ_{max} (log ε) 204 (2.32), 278 (1.31) nm; IR (neat) ν_{max} 3364, 3283, 2920, 2845, 1635, 1032 cm^{-1}; for ^{1}H and ^{13}C NMR data, Table 2; HRFABMS *m*/*z* 496.2848 $[M+H]^+$ (calcd for $C_{25}H_{42}N_3O_5S$, 496.2845).

Stereochemical analysis of the amino acid residues. Acidiphilamide A (2 mg) was hydrolyzed in 6 N HCl at 120 ℃ for 2 h. After removing the HCl *in vacuo*, 1 mg portions of the hydrolysate were transferred into two vials and

dissolved in 200 μL of 1 N $NaHCO_3$. L-FDAA (100 μL of 10 mg/mL in acetone) was added to one reaction vial, and D-FDAA was added to the other vial. The reactions were maintained at 80 ℃ for 3 min. Then, the reaction mixtures were neutralized by adding 100 μL of 2 N HCl and diluted with 300 μL of 50% aqueous CH_3CN-H_2O. Twenty microliters of each reaction mixture was analyzed by LC/MS using a Phenomenex C_{18}(2) column (Luna, 100 × 4.6 mm, 5 μm) with gradient solvent conditions (flow rate 0.7 mL/min; UV 340 nm detection; 10% to 60% CH_3CN-H_2O with 0.1% formic acid over 50 min). The L-FDAA derivatives of Phe, Ile, and phenylalaninol from acidiphilamide A eluted at 31.4, 30.5 and 30.7 min, respectively, whereas the D-FDAA derivatives of Phe, Ile, and phenylalaninol from the compound were detected at 34.2, 34.4, and 33.7 min, respectively. These experimentally acquired retention times were utilized to determine the absolute configurations of the α-amino carbons in these units. Because the L-FDAA derivatives eluted faster than the D-FDAA derivatives of Phe, Ile, the absolute configurations of the *α*-amino carbons of Phe and Ile were established as L. To confirm the absolute configuration of phenylalaninol, authentic L-phenylalaninol is derivatized in the same way. The result assigned absolute configuration of phenylalaninol as *S*.

To determine the absolute configuration of the *β*-position of the Ile unit of acidiphilamide A, the hydrolysate of the compound was derivatized with 100 μL of 1% GITC in acetone and 200 μL of 6% triethylamine at 25 °C. After 15 min of stirring, 100 μL of 5% acetic acid was added to quench the reaction. A 20-μL aliquot was injected into LC/MS for analysis under a reversed-phase gradient solvent system (column: Phenomenex C_{18} Gemini, 250 × 4.6 mm, 5 μm; flow rate 0.3 mL/min; UV 254 nm detection; 30% to

55% CH_3CN/H_2O with 0.1% formic acid for 80 min). The GITC adduct of the Ile fragment of acidiphilamide A eluted at 57.15 min. The GITC adducts of authentic standards of L-Ile and L-*allo*-Ile eluted at 57.2 min and 56.6 min, respectively, indicating that the Ile residue in **1** is L-Ile, not L-*allo*-Ile. The same procedure was used to establish the absolute configurations of acidiphilamides B-E (**2**-**5**) (Table 1).

Cell cultures. HeLa cells were cultured in Dulbecco's modified Eagle's medium (Welgene, LM001-05) supplemented with 10% fetal bovine serum (Tissue Culture Biologics, 101), 2 mM glutamine (Mediatech, 25-005-CI), and 100 unit/mL penicillin/streptomycin (Mediatech, 30-002-CI). After overnight preincubation, acidiphilamides A and B (**1**-**2**), L-isoleucinamide and L-valinamide were added to each well of a 24-well plate, and the cells were incubated for an additional 4-12 h. When we cultured cells under starvation conditions or autophagy inhibition conditions, the cells were initially grown in normal media, and when the cells reached >90% confluence, they were washed with PBS and then incubated with EBSS media or DMEM with 100 nM bafilomycin A1.

Immunoblotting. WCE from cells were prepared in RIPA buffer and used for IB. Proteins were separated by SDS-PAGE and transferred to a polyvinylidene difluoride (PVDF) membrane (Merck Millipore, Darmstadt, Germany). The membranes were blocked with 5% nonfat milk and probed with the following antibodies: anti-LC3 (L7543, Sigma-Aldrich), anti-SQSTM1 (sc-28359, Santa Cruz Biotechnology), anti-Ub (clone P4D1, Santa Cruz Biotechnology), anti-α3 (PW8115, Enzo), and anti-α-actin (A1978, Sigma). The membranes

were then incubated with a horseradish peroxidase-conjugated anti-mouse IgG antibody (81-6720, Invitrogen) or anti-rabbit IgG antibody (G21234, Invitrogen) and visualized using an ECL system (Thermo Fisher Scientific).

DQ-BSA assay. HeLa cells were seeded in 24-well plates with glass coverslips and treated with self-quenching, BODIPY dye conjugated with a bovine serum albumin probe (DQ-BSA, 10 μg/mL) for 1 h. The cells were then washed with PBS and incubated under different experimental conditions. After incubation for 4 h, they were fixed in 4% *para*-formaldehyde in PBS for 15 min. The slides were mounted with Fluoroshield mounting medium containing DAPI (Abcam, ab104139). The fluorescence was monitored and captured using an Olympus fluorescence microscope (IX71). All of the fluorescence micrographic images are representative of the total cell population.

Bioactivity experiments were performed by Prof. Min Jae Lee's laboratory from college of medicine in Seoul National University.

III. Pentaminomycins C–E: Cyclic pentapeptides as autophagy inducers from a mealworm beetle gut bacterium

III. 1. Results and discussions.

Pentaminomycin C (**6**) was purified as a white powder, and its molecular formula was established to be $C_{37}H_{51}N_9O_6$ based on HRFABMS data along with ^1H and ^{13}C NMR data (Table 4). Further analysis of the NMR spectra confirmed this compound as the previously reported cyclic peptide, pentaminomycin C[18], which consists of five amino acids: leucine, valine, tryptophan, N^5-hydroxyarginine, and phenylalanine. The sequence of the amino acids was confirmed as leucine-valine-tryptophan-N^5-hydroxyarginine-phenylalanine by HMBC correlations as reported in the literature[18].

Pentaminomycin D (**7**) was isolated as a white powder. Based on HRFABMS and NMR data, the molecular formula of **7** was determined to be $C_{36}H_{49}N_9O_6$ with 17 double bond equivalents. Based on this molecular formula, pentaminomycin D (**7**) possesses one less CH_2 group than **6**. The ^1H NMR spectrum of **7** showed the presence of five exchangeable amide NH groups (δ_H 8.85, 8.63, 8.45, 7.50, and 7.23) and five α-protons (δ_H 4.52, 4.28, 4.16, 4.12, and 3.70) in the amino acid residues, suggesting that **7** was also a pentapeptide-derived compound. The ^{13}C NMR spectrum also confirmed **7** to be a peptidic metabolite through its five carbonyl signals (δ_C 171.7, 171.4, 171.4, 170.7, and 170.4) and five α-carbon signals (δ_C 60.2, 57.5, 55.3, 53.5, and 52.9), which is consistent with the ^1H NMR spectrum. Further analysis of the ^{13}C NMR spectrum identified 15 sp^2 carbon atoms (δ_C 157.4–110.2) and 11 aliphatic carbon atoms (δ_C 50.5–18.3). The odd number of sp^2 carbon atoms indicated the existence of an imine-type functional group. Assuming that pentaminomycin D (**7**) possessed an imine group, eight double bonds and five carbonyl groups accounted for 13 double bond equivalents out of 17,

suggesting that this metabolite possessed four rings.

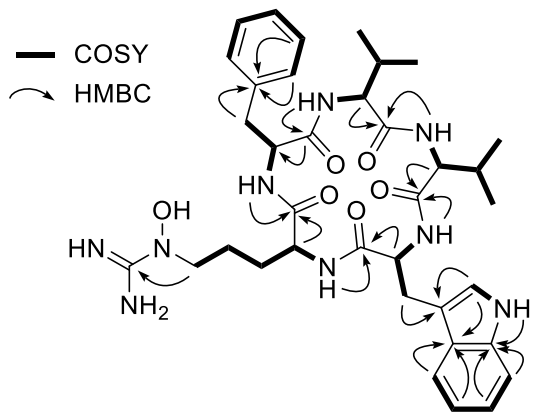

7

Figure 7. Key COSY and HMBC correlations of pentaminomycin D (**7**).

Analysis of the 1D (^{1}H and ^{13}C) and 2D (HSQC, COSY, and HMBC) NMR spectroscopic data of **7** identified the amino acid residues (Figure 7). More specifically, the conspicuous 1′-NH moiety (δ_H 10.78) was found to have a COSY correlation with H-2′ (δ_H 7.17), connecting C-1′ and C-2′. C-2′ was located adjacent to C-3′, as determined by the H-2′/C-3′ HMBC correlation. The $^{3}J_{HH}$ correlations of H-4′ (δ_H 7.51), H-5′ (δ_H 6.98), H-6′ (δ_H 7.04), and H-7′ (δ_H 7.30), and their ^{1}H-^{1}H coupling constants (J = 7.5 Hz), allowed the construction of an *ortho*-substituted 6-membered aromatic ring. HMBC signals from 1′-NH and H-7′ to C-7′a (δ_C 136.1) and from H-2′ and H-5′ to C-3′a (δ_C 126.8) secured the 1′-NH-C-7a' and C-3′-C-3′a connectivity and allowed the elucidation of the indole structure. H_2-3 (δ_H 3.19 and 2.91) displayed HMBC correlations with C-3′ (δ_C 110.2), indicating C-3 methylene substitution at C-3′. In addition, 2-NH (δ_H 8.63)/H-2 (δ_H 4.28) and H-2/H_2-3

COSY and H-2/C-1 HMBC correlations confirmed the presence of a tryptophan unit, while an array of COSY correlations starting from an NH group (δ_H 7.50) to H_3-4 and H_3-5 confirmed the existence of a valine residue. In a similar manner, COSY correlations from an amide NH moiety (δ_H 8.45) to a dimethyl group allowed the elucidation of an addition valine unit. Furthermore, correlation of the *α*-proton at δ_H 4.52 with an amide proton (δ_H 8.85) and *β*-protons (δ_H 2.98 and 2.79) was also observed, as were HMBC correlations between these *β*-protons with the quaternary C-1′ carbon atom of the aromatic ring (δ_C 138.0) and the C-2′ carbon atom (δ_C 129.0). Two overlapping methine carbon peaks (2 × CH) at δ_C 129.0 and 128.0, and the second-order signals observed for 5H indicated the presence of a phenylalanine residue. This unit was further assigned by HMBC correlations from H-2′ and H-5′ to C-6′ (δ_C 126.2) and from H-3′ and H-6′ to C-1′. The presence of the N^5-hydroxyarginine moiety was deciphered by consecutive COSY correlations from NH (δ_H 7.23) to H-5 (δ_H 3.42). The H_2-5 methylene protons showed COSY correlations only with H_2-4 (δ_H 1.33 and 1.15), placing the methylene unit at the terminus of this spin system. Moreover, the ^{13}C chemical shift of C-5 (δ_C 50.5) indicated that this carbon atom was bound to a nitrogen atom. This partial structure and the four elucidated amino acids (Trp, Phe, and two Val's) accounted for the $C_{35}H_{45}N_6O_5$ portion of the molecular formula $C_{36}H_{49}N_9O_6$, thereby leaving a CH_4N_3O unit for structural elucidation. Thus, this last carbon (δ_C 157.4), which was preliminarily diagnosed as an imine carbon, was correlated with H_2-5. Its chemical shift is typical for guanidine carbon, and the presence of three broad singlet protons at δ_H 7.50 confirmed the presence of a guanidine group containing the N^5-OH group (δ_H 10.55), thereby indicating that this last fragment is an N^5-hydroxyarginine residue.

The seven double bonds, one imine group, five carbonyl groups, and three ring structures of the Phe and Trp residues accounted for 16 double bond equivalents out of 17 for pentaminomycin D (**7**). An additional ring structure was therefore confirmed in the sequence analysis of the amino acids using the HMBC spectrum. More specifically, the HMBC correlations from the α-proton (δ_H 4.12) of Val-1 and the amide proton (δ_H 8.45) of Val-2 to the C-1 atom (δ_C 171.4) of Val-1 established the connectivity of Val-1 to Val-2. The connection of Val-2 to Trp was supported by the heteronuclear correlation from the NH moiety (δ_H 8.63) of Trp to the C-1 atom (δ_C 171.4) of Val-2 in the HMBC spectrum. An additional HMBC correlation from the amide NH group (δ_H 7.23) of N^5-OH-Arg to the amide carbonyl carbon atom (δ_C 171.7) of Trp secured the sequence of Trp to N^5-OH-Arg. Furthermore, the NH proton (δ_H 7.23) of N^5-OH-Arg correlated with the amide carbonyl carbon (δ_C 170.7) of Phe in the HMBC spectrum, which established the linkage of arginine to phenylalanine. Lastly, the cyclized structure was completed by the confirmation of an HMBC correlation from the NH unit (δ_H 8.85) of Phe to the carbonyl carbon atom (δ_C 171.4) of Val-1, finally establishing the planar structure of **7** as a new cyclic pentapeptide.

Pentaminomycin E (**8**) was also purified as a white powder. The molecular formula of this compound was determined to be $C_{40}H_{49}N_9O_6$ based on HRFABMS and NMR data (Table 4). Comparing the NMR spectra of **8** with those of **6** and **7**, additional aromatic protons and carbons were observed, indicating the presence of an additional aromatic group in **8**. Comprehensive analysis of the 1D and 2D NMR spectra confirmed the amino acid residues to be two phenylalanine residues, valine, tryptophan, and N^5-hydroxyarginine. The amino acid sequence of the structure was subsequently determined by analysis of the HMBC correlations, and was confirmed to be Phe-1-Val-Trp-

N^5-OH-Arg-Phe-2. The new metabolites, namely pentaminomycins D and E (**7** and **8**), share cyclic pentapeptide features with pentaminomycins A and B, including Trp and N^5-OH Arg[19]. However, pentaminomycins D and E incorporate Phe instead of Leu adjacent to N^5-OH-Arg, unlike in the cases of pentaminomycins A and B[19]. In addition, pentaminomycin E was identified as the first congener bearing two Phe units in the pentaminomycin series.

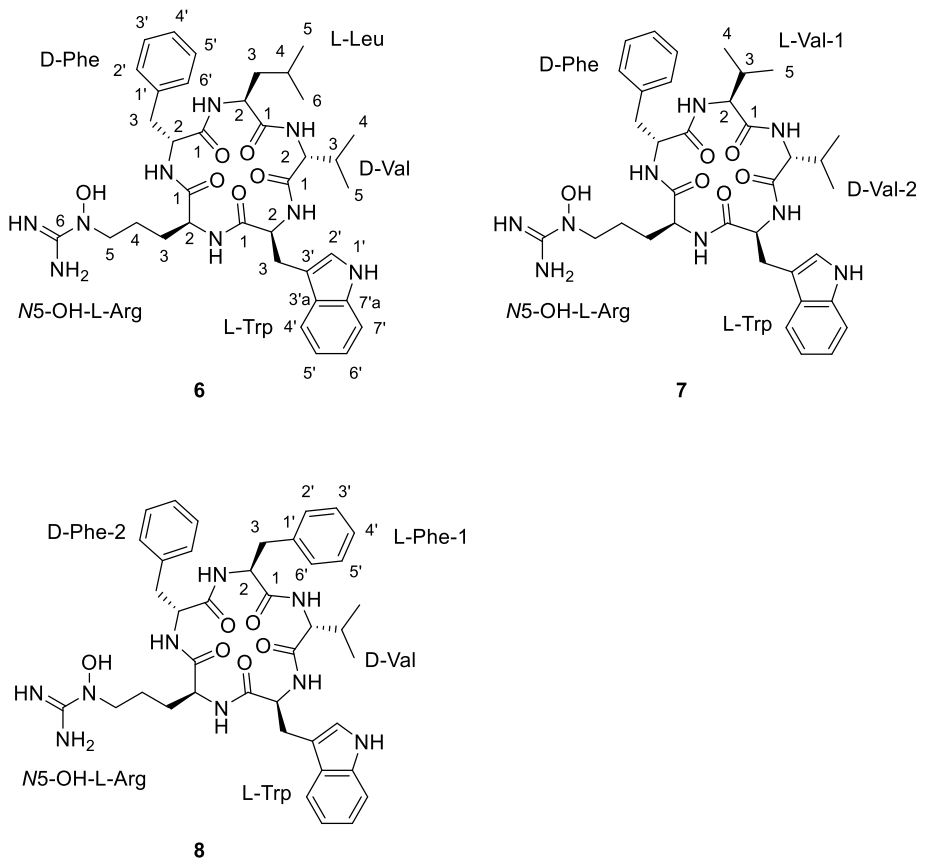

Figure 8. Structures of pentaminomycins C–E (**6**–**8**).

To determine the absolute configurations of pentaminomycins D and E (**7** and **8**), acid hydrolysis and derivatization of the hydrolysates with Marfey's reagents (*N*-(5-fluoro-2,4-dinitrophenyl)-L-leucine amide (L-FDLA)) were carried out[5]. By comparing the retention times from LC/MS analysis of the L-FDLA derivatives with the same reaction products of authentic L and D amino acids, the absolute configurations of the α-carbons were determined. The absolute configurations of the amino acids in pentaminomycin D (**7**) were established as L-valine, D-valine, L-tryptophan, N^5-hydroxy-L-arginine, and D-phenylalanine (Table 3). In a similar process, the absolute configurations of the amino acid residues present in pentaminomycin E (**8**) were determined to be D-valine, L-tryptophan, N^5-hydroxy-L-arginine, L-phenylalanine, and D-phenylalanine (Table 3). Since two valine residues of the opposite configuration exist in **7**, whereas **8** contains both L- and D-phenylalanine residues, the exact assignments of the configurations were subjected to genomic analysis of the biosynthetic gene cluster for the pentaminomycins because the L- and D-Val units in **7** and the L- and D-Phe residues in **8** are not distinguishable by NMR spectroscopic analysis.

Analysis of the whole genome sequence of the *Streptomyces* sp. GG23 strain identified the putative biosynthetic gene cluster responsible for the pentaminomycins. The 8.7 Mb draft genome consisting of three contigs was analyzed using antiSMASH 5.0[20]. In total, 31 gene clusters were involved in the biosynthesis of polyketides, nonribosomal peptides, and terpenes. The BGC of the pentaminomycins showed a high similarity to a previous report into pentaminomycin C[18]. The total length of the BGC is approximately 83.6 kb encompassing 53 open reading frames including two NRPS genes, three post-modification genes, seven transport and regulatory genes, and five

tryptophan biosynthesis genes (Figure 9A).

The NRPS (non-ribosomal peptide synthetase) gene for the pentaminomycins is *penN2*, which encodes five NRPS modules. Each module incorporates an amino acid to produce a pentapeptide chain. The first module without the epimerase domain flexibly recruits an amino acid of the group L-valine, L-leucine, and L-phenylalanine. The amino acid introduced by the second module is fixed as valine, whose absolute configuration is the d form because of the action of the epimerase domain in this module. This shows that the Val-2 residue introduced by module 2 has a d configuration and the other valine unit (Val-1) is in the L form in pentaminomycin D (**7**). Accordingly, L-Trp should be tethered after D-Val by module 3, and the arginine moiety is connected by module 4. The peptide chain is completed after the linkage of the last amino acid, D-Phe, by module 5 with the action of the epimerase domain. This also confirmed the absolute configuration of pentaminomycin E (**8**), in which Phe-2 is present in the d form, whereas Phe-1 possesses the L configuration. Post-modular modification by processes such as hydroxylation and cyclization finalized the biosynthesis of the pentaminomycins. *N*-hydroxylation on the arginine unit is possibly facilitated by the cytochrome P450 enzymes PenB and/or PenC. Cyclization of the pentapeptide chain was proposed to be catalyzed by serine hydrolase *penA* in a previously reported biosynthesis of pentaminomycin C[18]. However, our detailed analysis found that *penA* is the coding gene for penicillin binding protein (PBP)-type thioesterase (TE). PBP-type TE or the standalone cyclase is reported as a peptidyl cyclase included in the *β*-lactamase superfamily[21,22]. Cyclic peptides that use PBP-type TEs have been previously reported, including desotamide[23–25], surugamide[26], ulleungmycin[27], noursamycin[28], curacomycin[29], and mannopeptimycin[30]. These compounds share a

structurally common feature in that the initial NRPS module must introduce an L-amino acid, while the terminal module recruits a d-amino acid. This is due to the fact that the structure of PBP-type TE is analogous to the penicillin-binding protein[31]. The penicillin-binding protein detects the D-alanyl-D-alanine moiety in peptidoglycan precursors to contribute to transpepdidation for cell wall construction in bacteria[32]. Similarly, PBP-type TE also detects the D-amino acid at the C-terminus of the NRPS peptide chain and catalyzes peptidyl macrocyclization. Based on the NRPS modules, the biosynthesis of the pentaminomycins starts with an L-amino acid (L-Val, L-Leu, or L-Phe) and ends with D-Phe, facilitating the cyclization by PBP-type TE (PenA) (Figure 9B).

The BGC contains another NRPS gene, namely *penN1*, which is located close to the *penN2* gene (Figure 9B). Detailed analysis of the sequence revealed that *penN1* is also composed of five NRPS modules biosynthesizing another series of cyclic peptides, i.e., BE-18257A and B, which were reported to be endothelin-binding inhibitors[33]. In our chemical analysis of *Streptomyces* sp. GG23 based on LC/MS data, the production of these cyclic peptides was detected. The pentapeptide chains of BE-18257s are assumed to be cyclized by PenA because *penN1* does not possess canonical TE at the end of the NRPS module and no other PBP-type TE genes rather than *penA* were identified in the BGC. Furthermore, the NRPS gene of the BE-18267s initially introduces L-Leu and completes the biosynthesis of the pentapeptide chain with D-Val or D-Leu, which is suitable for the utilization of PBP-type TE. Additionally, tryptophan biosynthetic genes (i.e., *penD–H*) exist in the BGC[34]. The pentaminomycins and BE-18257s both contain tryptophan in their structures, and so it is hypothesized that the Trp units of these different cyclic peptides share the Trp biosynthetic gene. Even though sharing of the

PBP-type TE and Trp biosynthetic genes has to be proven by a follow-up study, if confirmed, the above example could be considered an unusual case in which independent NRPSs share core genes for their biosynthesis.

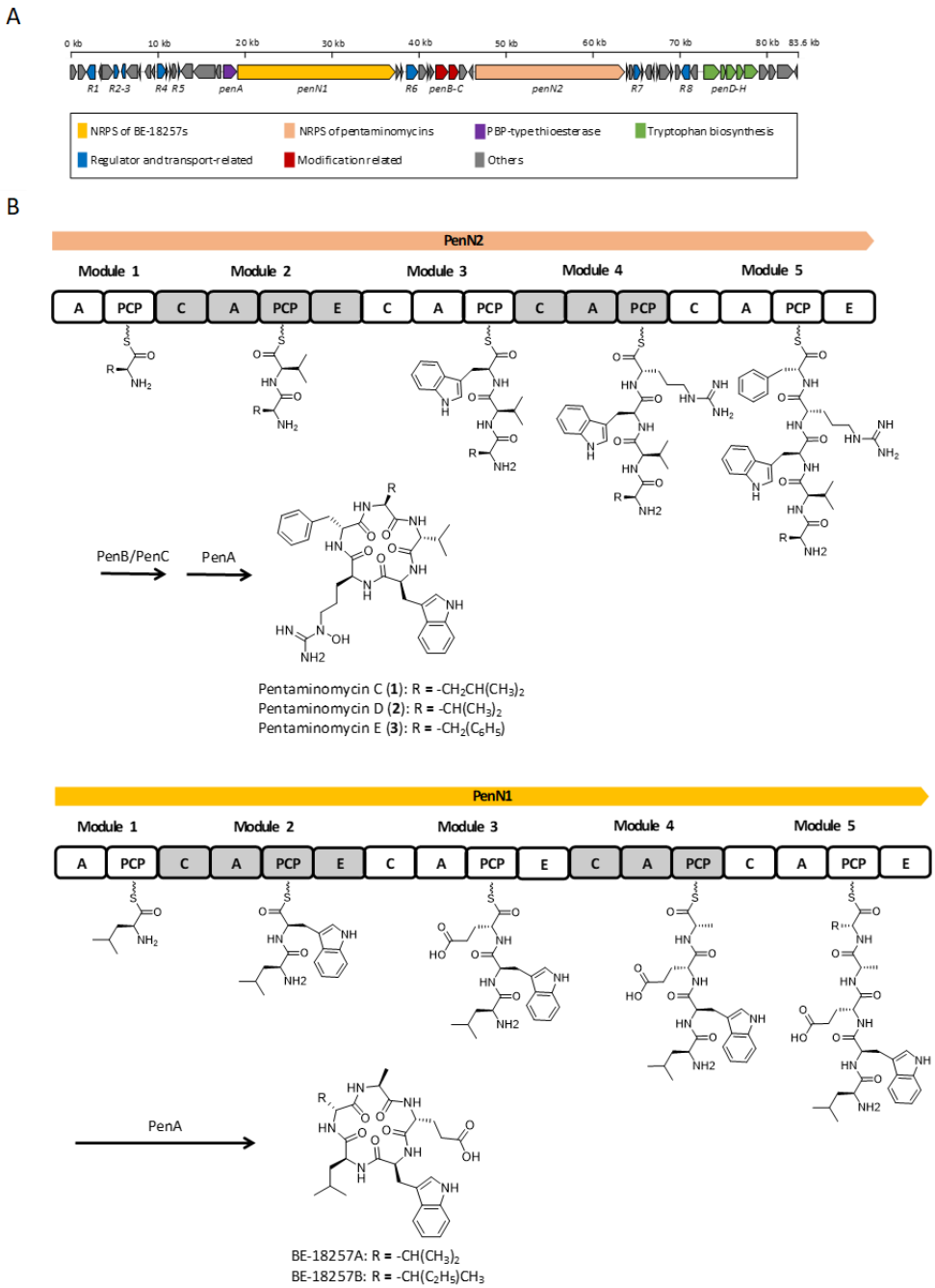

Figure 9. Proposed biosynthesis pathway for the BE-18257s and the pentaminomycins. (**A**) Genetic organization of putative biosynthetic gene

cluster of the pentaminomycins. (**B**) Putative biosynthetic pathway for the pentaminomycins and the BE-18257s with the nonribosomal peptide synthetase (NRPS) modular organization. C, condensation domain; A, adenylation domain; PCP, peptidyl carrier protein; E, epimerase domain.

The majority of amino acids constituting the pentaminomycins are non-polar residues that are expected to penetrate mammalian cells by simple diffusion and affect the membrane dynamics in the cell. In addition, similar cyclic peptides with lipophilic side chains often induce autophagy in cultured human cells[35,36]. We proceeded to examine whether pentaminomycins C–E affected the cellular autophagic flux by monitoring the conjugation of phosphatidylethanolamine (PE) to ATG8 proteins, such as microtubule-associated protein light chain 3 (LC3) and γ-aminobutyric acid receptor-associated protein (GABARAP), which is the hallmark of autophagy induction[37]. When HEK293T cells were treated with pentaminomycins C and D (**6** and **7**), the levels of lipidated forms of LC3 and GABARAPL1 (LC3-II and GABARAPL1-II, respectively) were significantly elevated in a moderate dose-dependent manner, while pentaminomycin E (**8**) did not exert a similar phenomenon (Figure 10A,B). The key autophagic receptor p62/SQSTSM1 remained virtually unchanged after compound treatment (Figure 10A).

Changes in the autophagic flux manifested as elevated levels of cellular LC3-II and GABARAPL1-II after treatment with pentaminomycins C and D may originate from either an increased overall cellular autophagy or the reduced autolysosomal degradation of LC3-II and GABARAPL1-II. To determine the molecular mechanism, the cells were treated with BafA1, which inhibits autophagy at a late stage by blocking the fusion between the

autophagosome and the lysosome, prior to treatment with the pentaminomycins. We observed a modest increase in GABARAPL1-II upon exposure to pentaminomycins C (**6**) and D (**7**), but not pentaminomycin E (**8**), when the cells were cotreated with BafA1 (Figure 10C,D). Taken together, our data largely point that pentaminomycins C and D induce global autophagy instead of inhibiting cellular autophagic flux, although the underlying molecular mechanism and direct target molecules of pentaminomycins should therefore be determined.

Due to the fact that autophagy contributes to the degradation of oxidized proteins[38], we examined the effect of pentaminomycins C and D (**6** and **7**) on the oxidative stress induced by menadione[39]. Measurement of the cell viability based on the intracellular ATP levels revealed that the autophagy inducers, pentaminomycins C and D, potently protected HEK293 cells against menadione-induced cytotoxicity (Figure 11). Pentaminomycins C and D showed significantly reduced cell death after 4 and 2 h cotreatment with menadione, respectively. These protective effects were more prominent with longer pentaminomycin incubation times (Figure 11), thereby suggesting that autophagy induction by the pentaminomycins may accelerate oxidized protein clearance in cells and be beneficial in terms of cell protection under oxidative stress. However, it has yet to be determined whether natural compounds originating from mealworm beetle-associated bacteria can delay the pathologic process involving oxidatively damaged proteins, such as neurodegeneration and aging. Our results may therefore offer a novel strategy to modulate cellular autophagy and oxidative stress responses in cells.

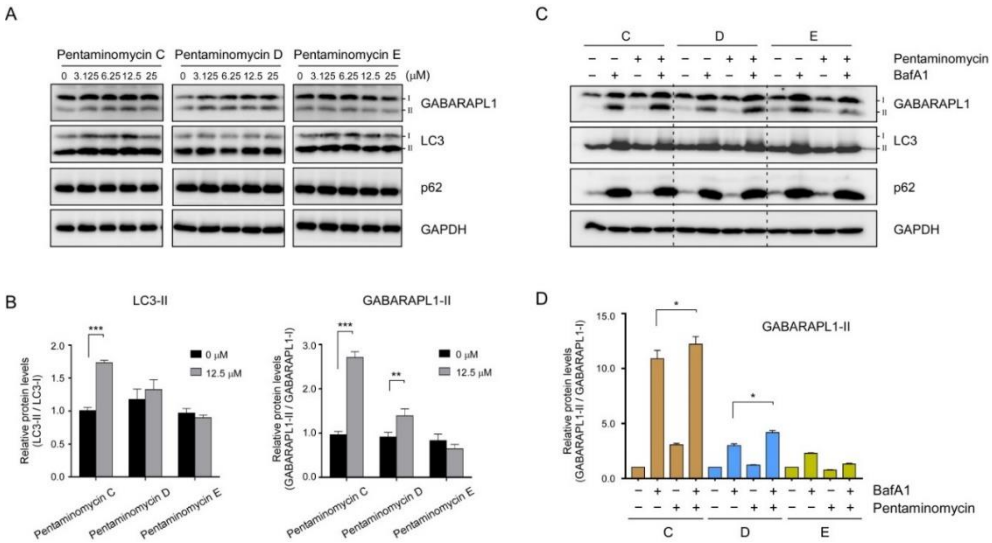

Figure 10. Effects of pentaminomycins C–E (**6**–**8**) on cellular autophagy in mammalian cells. HEK293T cells were treated with various concentrations of pentaminomycins for 8 h. (**A**) Whole cell lysates were harvested and subjected to SDS-PAGE followed by immunoblotting against the indicated antibodies. (**B**) Quantification of LC3-II and GABARAPL1-II in the presence of pentaminomycins (12.5 μM) using the multiple immunoblot images. Data were normalized to those of non-lipidated proteins. Data represent mean ± SD from three independent experiments. **, $p < 0.01$ and ***, $p < 0.001$ (one-way analysis of variance (ANOVA) with Bonferroni's multiple comparison test). (**C**) Pentaminomycins C and D, but not E, induce global cellular autophagy. HEK293T cells were cotreated with pentaminomycins C–E (20 μM) and a downstream autophagy inhibitor bafilomycin A1 (BafA1; 100 nM) for 12 h. (**D**) Quantification of GABARAPL1-II normalized to GABARAPL1-I in the presence or absence of pentaminomycins and BafA1. *, $p < 0.05$ (one-way ANOVA with Bonferroni's multiple comparison test).

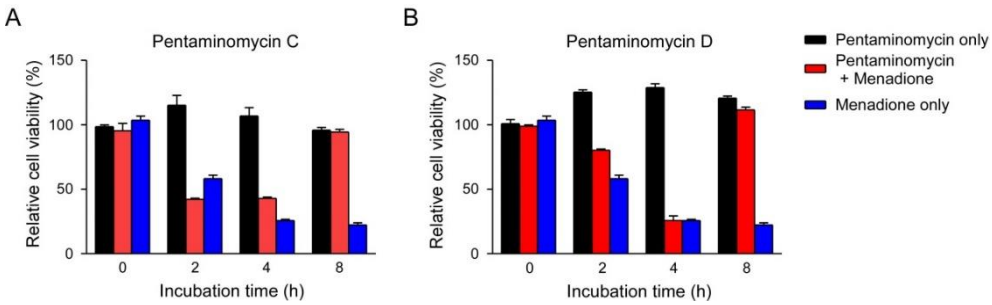

Figure 11. Alleviation of menadione-mediated cytotoxicity by (**A**) pentaminomycin C and (**B**) pentaminomycin D. Oxidative stress was induced by menadione (25 μM) for the indicated time periods in HEK293 cells, which were cotreated with either pentaminomycin C or D. The relative cell viability was assessed using the CellTiter-Glo assay and the values are represented as mean ± SD (n = 3).

Table 3. LC/MS analysis of L-FDLA derivatives of pentamnomycins D and E (**7**-**8**).

Pentaminomycin D				
Amino acids	Val	Arg	Trp	Phe
[M + H]⁺ (m/z)	412	469	499	460
Retention time (min)				
Reaction product	37.5/44.6	22.6	41.0	47.5
Authentic L with FDLA	37.3	22.1	40.2	41.2
Authentic D with FDLA	43.8	21.4	43.9	46.0
Supposed configuration	**L** and **D**	**L from co-injection**	**L**	**D**

Pentaminomycin E				
Amino acids	Val	Arg	Trp	Phe
[M + H]⁺ (m/z)	412	469	499	460
Retention time (min)				
Reaction product	37.5/44.6	22.6	41.0	47.5
Authentic L with FDLA	37.3	22.1	40.2	41.2
Authentic D with FDLA	43.8	21.4	43.9	46.0
Supposed configuration	**D**	**L from co-injection**	**L**	**L** and **D**

Table 4. NMR data for pentaminomycins C-E (**6-8**) in DMSO-d_6.

Pentaminomycin C (6)				**Pentaminomycin D (7)**				**Pentaminomycin E (8)**			
Position		δ_C, type	δ_H, mult (*J* in Hz)	Position		δ_C, type	δ_H, mult (*J* in Hz)	Position		δ_C, type	δ_H, mult (*J* in Hz)
L-Leu	1	172.2, C		L-Val	1	171.4, C		L-Phe	1	170.6, C	
	2	50.5, CH	4.40, ddd (15.0,9.0,7.0)		2	57.5, CH	4.12, dd (7.5,7.5)		2	52.8, CH	4.67, dt (9.0,7.5)
	3	41.1, CH_2	1.34, m		3	30.7, CH	1.77, m		3	38.1, CH_2	2.84, dd (13.5, 7.0) 2.78, dd (13.5,7.5)
	4	24.2, CH	1.43, m		4	19.0, CH_3	0.83, d (7.0)		1′	137.1, C	
	5	22.7, CH_3	0.85, d (6.5)		5	18.3, CH_3	0.76, d (7.0)		2′	129.1, CH	7.18, m
	6	22.0, CH_3	0.82, d (6.5)		NH		7.50, m		3′	128.0, CH	7.22, m
	NH		7.55, d (9.0)						4′	126.2, C	7.17, m
									NH		7.69, d (9.0)
D-Val	1	171.3, C		D-Val	1	171.4, C		D-Val	1	171.2, C	
	2	59.9, CH	3.70, dd (10.0,7.5)		2	60.2, CH	3.70, dd (10.0,7.5)		2	59.9, CH	3.70, dd (10.0,7.5)
	3	28.5, CH	1.65, m		3	28.1, CH	1.64, m		3	28.5, CH	1.65, m
	4	19.0, CH_3	0.75, d (6.5)		4	19.2, CH_3	0.77, d (7.0)		4	19.0, CH_3	0.75, d (6.5)
	5	18.5, CH_3	0.34, d (6.5)		5	18.5, CH_3	0.31, d (7.0)		5	18.5, CH_3	0.34, d (6.5)
	NH		8.41, d (7.5)		NH		8.45, d (7.5)		NH		8.41, d (7.5)
L-Trp	1	171.7, C		L-Trp	1	171.7, C		L-Trp	1	171.6, C	

	2	55.3, CH	4.29, ddd (11.0,8.0,3.5)		2	55.3, CH	4.28, ddd (11.5,8.0,3.0)		2	55.3, CH	4.27, ddd (11.5,8.0,3.5)
	3	26.9, CH_2	3.18, dd (14.5,3.0) 2.80, dd (14.5, 12.0)		3	26.9, CH_2	3.19, dd (14.5,3.0) 2.91, dd (14.5, 11.5)		3	26.9, CH_2	3.17, dd (14.5,3.0) 2.90, dd (14.5, 11.5)
	2-NH		8.59, d (8.0)		2-NH		8.63, d (8.0)		2-NH		8.58, d (8.0)
	1′(NH)		10.78, br s		1′(NH)		10.78, br s		1′(NH)		10.76, br s
	2′	123.9, CH	7.17, m		2′	123.9, CH	7.17, m		2′	123.8, CH	7.16, m
	3′	110.2, C			3′	110.2, C			3′	110.2, C	
	3′a	126.8, C			3′a	126.8, C			3′a	126.8, C	
	4′	117.9, CH	7.51, d (8.0)		4′	117.8, CH	7.51, m		4′	117.8, CH	7.50, d (8.0)
	5′	118.3, CH	6.98, t (7.5)		5′	118.2, CH	6.98, dd (7.5,7.5)		5′	118.2, CH	6.97, dd (7.5,7.5)
	6′	120.8, CH	7.05, t (7.5)		6′	120.8, CH	7.04, dd (7.5,7.5)		6′	120.8, CH	7.04, dd (7.5,7.5)
	7′	111.3, CH	7.31, d (8.0)		7′	111.3, CH	7.30, d (8.0)		7′	111.3, CH	7.30, d (8.0)
	7′a	136.1, C			7′a	136.1, C			7′a	136.1, C	
N^5-OH-L-Arg	1	170.4, C		N^5-OH-L-Arg	1	170.4, C		N^5-OH-L-Arg	1	170.4, C	
	2	52.8, CH	4.16, dt (7.0, 7.0)		2	52.9, CH	4.16, dt (8.0, 7.0)		2	53.0, CH	4.16, dt (7.0, 7.0)
	3	28.1, CH_2	1.53, m		3	28.2, CH_2	1.53, m		3	28.2, CH_2	1.52, m
	4	22.1, CH_2	1.33, m, 1.18, m		4	22.0, CH_2	1.33, m, 1.15, m		4	22.1, CH_2	1.34, m, 1.17, m

	5	50.4, CH_2	3.43, m		5	50.5, CH_2	3.42, m		5	50.5, CH_2	3.42, m
	N^5-OH		10.49, br s		N^5-OH		10.55, br s		N^5-OH		10.47, s
	6	157.3, C			6	157.4, C			6	157.3, C	
	6-NH(3H)		7.45, br s		6-NH(3H)		7.50, br s		6-NH(3H)		7.43, br s
	NH		7.29, d (7.5)		NH		7.23, m		NH		7.26, d (7.5)
D-Phe	1	170.6, C		D-Phe	1	170.7, C		D-Phe	1	170.6, C	
	2	53.7, CH	4.46, ddd (9.0,9.0,6.0)		2	53.5, CH	4.52, ddd (9.5,8.5,6.0)		2	53.5, CH	4.47, ddd (9.0,9.0,5.5)
	3	34.2, CH_2	2.96, dd (14.0, 5.5) 2.80, dd (14.0, 9.5)		3	33.9, CH_2	2.98, dd (14.0, 5.0) 2.79, dd (14.0, 10.0)		3	34.0, CH_2	2.93, dd (14.0, 5.5) 2.76, dd (14.0, 9.5)
	1′	137.9, C			1′	138.0, C			1′	137.9, C	
	2′, 6′	129.0, CH	7.24, m		2′, 6′	129.0, CH	7.24, m		2′, 6′	128.9, CH	7.20, m
	3′, 5′	128.0, CH	7.23, m		3′, 5′	128.0, CH	7.23, m		3′, 5′	128.0, CH	7.22, m
	4′	126.2, CH	7.17, m		4′	126.2, CH	7.17, m		4′	126.2, CH	7.17, m
	NH		8.85, d (8.0)		NH		8.85, d (8.0)		NH		8.89, d (8.5)

III. 2. Conclusion

Alteration of the culture conditions by changing the composition of culture medium, for a *Streptomyces* strain isolated from the gut of the mealworm beetle, *Tenebrio molitor*, enabled the production of cyclic pentapeptides, pentaminomycins C–E (**6**–**8**). The structures of **6**–**8** were assigned by combinational spectroscopic analysis. In addition, Marfey's analysis and bioinformatic investigations of the nonribosomal peptide synthetase (NRPS) biosynthetic gene cluster established the absolute configurations of the new metabolites, pentaminomycins D and E. Detailed sequence analysis of the adenylation domains in the NRPS modules revealed that the structural variations among **6**–**8** originate from the low specificity for hydrophobic amino acids in module 1. In addition, it was found that cyclization of the pentaminomycins can be catalyzed by a penicillin binding protein (PBP)-type thioesterase (TE), which is a noncanonical TE requiring l- and d-amino acids in the starting and terminal units, respectively. Pentaminomycins C and D (**6** and **7**), but not pentaminomycin E (**8**), exhibited significant autophagy-inducing activity based on LC3 and GABARAPL1 lipidation in both the presence and absence of BafA1. Importantly, cells treated with pentaminomycins C and D showed enhanced resistance to the oxidative stress induced by menadione, providing strong evidence that activation of cellular autophagic flux antagonizes the harmful effects of oxidized proteins. Although the underlying molecular mechanism requires further elucidation, our findings collectively suggest that some pentaminomycins may exhibit therapeutic potential against diseases associated with chronic oxidative stress and incompetent cellular responses. The discovery of pentaminomycins C–E therefore indicates that biotechnical

investigation into relatively unexploited insect-associated bacteria may be a promising strategy to explore microbial metabolites with unique biosynthetic pathways and interesting biological activities.

III. 3. Experimental section

General Experimental Procedures. Optical rotations were measured using a JASCO P-2000 polarimeter (JASCO, Easton, MD, USA). UV spectra were recorded using a Chirascan Plus Applied Photophysics Ltd. (Applied Photophysics, Leatherhead, Surrey, UK). Infrared (IR) spectra were obtained on a Thermo NICOLET iS10 spectrometer (Thermo Fisher Scientific, Waltham, MA, USA). ^{1}H, ^{13}C, and two dimensional nuclear magnetic resonance (NMR) spectra were acquired using a Bruker Avance 800 MHz spectrometer (Bruker, Billerica, MA, USA) with the NMR solvent of DMSO-d_6 (reference chemical shift: δ_C 39.5 ppm and δ_H 2.50 ppm) at the National Center for Inter-university Research Facilities (NCIRF) at Seoul National University. Electrospray ionization (ESI) low-resolution liquid chromatography-mass spectrometry (LC/MS) data were measured with an Agilent Technologies 6130 quadrupole mass spectrometer (Agilent, Santa Clara, CA, USA) coupled to an Agilent Technologies 1200 series high-performance liquid chromatography (HPLC) instrument using a reversed-phase C_{18}(2) column (Phenomenex Luna, 100 × 4.6 mm). High-resolution fast atom bombardment (HR-FAB) mass spectra were recorded using a Jeol JMS-600 W high-resolution mass spectrometer (JEOL, Akishima, Tokyo, Japan) at the NCIRF. Semi-preparative HPLC separations were achieved using a Gilson 305 pump and a Gilson UV/VIS-155 detector (Gilson, Middleton, WI, USA).

Bacterial Isolation and Identification. The mealworm beetle used in this study was randomly selected as the specimens of insects raised at the Seoul

Grand Park, Gwacheon-si, Gyeonggi Province, Republic of Korea. The selected specimen was identified as mealworm beetles, Tenebrio molitor Linnaues, based on external morphological characters. The mealworm beetle-associated actinomycete strain GG23 was isolated from the gut of adult mealworm beetles by using starch-casein agar (SCA), which contained 10 g of soluble starch, 0.3 g of casein, 2 g of KNO_3, 0.05 g of $MgSO_4 \cdot 7H_2O$, 2 g of K_2HPO_4, 2 g of NaCl, 0.02 g of $CaCO_3$, 0.01 g of $FeSO_4 \cdot 7H_2O$, and 18 g of agar in 1 L of distilled water. The strain was identified as Streptomyces sp. (GenBank accession number MT033037), which is closest to Streptomyces cacaoi (identity of 99.6%) (GenBank accession number NZ_MUBL 01000000) based on 16S rRNA gene sequence analysis.

Isolation of Pentaminomycin C-E. The dried extract was re-suspended with celite in MeOH followed by drying in vacuo. The celite-adsorbed extract was loaded onto 2 g of a pre-packed C_{18} Sepak resin. The extract was fractionated using five different compositions of aqueous MeOH (i.e., 20, 40, 60, 80, and 100 vol% MeOH). Pentaminomycins C–E (**6**–**8**) eluted in the 80 and 100 vol% MeOH fractions. The fractions were dried, redissolved in MeOH, and filtered to remove insoluble particles. Pentaminomycins C–E were further purified by preparative reversed-phase HPLC with a Phenomenex Luna 10 μm C_{18}(2) 250 × 21.20 mm column with a gradient system of 30–50 vol% aqueous MeCN over 30 min (flow rate: 10 mL/min, detection: UV 210 nm). Pentaminomycin D (**7**) eluted at 20 min under these HPLC conditions, whereas pentaminomycins C (**6**) and E (**8**) eluted together at 23 min. The eluates were subjected to semi-preparative reversed-phase HPLC using a YMC-Pack CN 250 × 10 mm, S-5 μm, 12 nm column with an isocratic system

of 35 vol% MeCN containing 0.05% trifluoroacetic acid (flow rate: 2 mL/min, detection: UV 210 nm). In the final purification, pentaminomycins C (**6**) (5 mg), D (**7**) (3 mg), and E (**8**) (4 mg) were collected at retention times of 20, 28, and 33 min, respectively.

Pentaminomycin C (6). White powder; $[\alpha]_D^{20}$ -50 (c 0.1, MeOH); UV (MeOH) λ_{max} (log ε) 218 (2.04), 281 (0.35) nm; IR (neat) ν_{max} 3302, 2965, 1673, 1537, 1444, 1199, 1140 cm^{-1}; ^1H and ^{13}C NMR data, see Table 4; HR-FAB-MS *m/z* 718.4041 $[M+H]^+$ (calcd. for $C_{37}H_{52}N_9O_6$ 718.4035).

Pentaminomycin D (7). White powder; $[\alpha]_D^{20}$ -8 (c 0.1, MeOH); UV (MeOH) λ_{max} (log ε) 218 (2.20), 281 (0.36) nm; IR (neat) ν_{max} 3296, 2964, 1672, 1536, 1444, 1199, 1140 cm^{-1}; ^1H and ^{13}C NMR data, see Table 4; HR-FAB-MS *m/z* 704.3876 $[M+H]^+$ (calcd. for $C_{36}H_{50}N_9O_6$ 704.3879).

Pentaminomycin E (8). White powder; $[\alpha]_D^{20}$ -31 (c 0.1, MeOH); UV (MeOH) λ_{max} (log ε) 216 (1.91), 282 (0.25) nm; IR (neat) ν_{max} 3300, 2964, 1672, 1536, 1445, 1199, 1140 cm^{-1}; ^1H and ^{13}C NMR data, see Table 4; HR-FAB-MS *m/z* 752.3879 $[M+H]^+$ (calcd. for $C_{40}H_{50}N_9O_6$ 752.3879).

Marfey's Analysis of Pentaminomycins D and E (7-8). A sample (1 mg) of pentaminomycin D (**7**) was hydrolyzed in 0.5 mL of 6 N HCl at 100 ℃ for 1 h. After hydrolysis, the reaction vial was cooled in an ice bucket for 3 min. After this time, the reaction solvent was evaporated in vacuo, and the

hydrolysate containing the free amino acids was dissolved in 100 µL of 1N $NaHCO_3$. Subsequently, 50 µL of a 10 mg/mL L-FDLA solution in acetone was added to the solution. The reaction mixture was stirred at 80 ℃ for 3 min, then 50 µL of 2 N HCl was used to neutralize the reaction mixture, which was subsequently diluted using 300 µL of a 50 vol% aqueous MeCN solution. An aliquot (20 µL) of the reaction mixture was analyzed by LC/MS using a Phenomenex C_{18}(2) column (Luna, 100 × 4.6 mm, 5 µm) under gradient solvent conditions (flow rate 0.7 mL/min; UV 340 nm detection; 10–60 vol% MeCN/H_2O containing 0.1% formic acid over 50 min). LC/MS analysis indicated that during acid hydrolysis, N^5-hydroxyarginine was converted to arginine. The L-FDLA derivatives of the two valine (37.5 and 44.6 min), tryptophan (41.0 min), arginine (22.6 min), and phenylalanine (47.5 min) residues of pentaminomycin D were detected by LC/MS analysis. The same procedure was performed for authentic L-and D-Val, Trp, Arg, and Phe to compare the retention times with those of the amino acids from **7** (Table 3). The absolute configurations of pentaminomycin E (**8**) were also established in the same manner.

Genome Analysis and the Biosynthetic Pathway. Whole genome sequencing of the GG23 strain was performed using PacBio RS II (Chunlab, Inc., Seocho-gu, Seoul, Republic of Korea). The sequencing data were assembled with PacBio SMRT Analysis v. 2.3.0, using a hierarchical genome assembly process (HGAP) protocol. Nucleotide sequences of the Streptomyces sp. GG23 genomes were generated in three contigs with a total of 8,666,993 base pairs. Gene prediction was performed using Prodigal v. 2.6.2, and sequences were annotated with EggNOG v. 4.5, Swissprot, KEGG,

and SEED (Chunlab, Inc., Seocho-gu, Seoul, Republic of Korea) The biosynthetic gene clusters (BGCs) were analyzed using antiSMASH v. 5.0[20].

Autophagic Flux Assay. To examine cellular autophagic flus after treatment of pentaminomycins, HEK293 cells (≈80% confluence) were treated with 0, 3.125, 6.25, 12.5, or 25 μM pentaminomycin C, D, or E for 8 h. Whole cell extracts were prepared using RIPA buffer (50 mM Tris-HCl (pH 8.0), 1% of NP-40, 0.5% of deoxycholate, 0.1% of sodium dodecyl sulfate (SDS), and 150 mM NaCl) supplemented with protease inhibitor cocktails. The lysates were then centrifuged at 16,000× g for 30 min at 4 ℃. The supernatants were separated by SDS-PAGE and transferred to a polyvinylidene difluoride (PVDF) membrane (Merck Millipore, Darmstadt, Germany). Subsequently, the membranes were blocked with 5% non-fat milk and probed with the following antibodies: anti-LC3 (L7543, MilliporeSigma, St. Louis, Missouri, USA), anti-SQSTM1 (sc-28359, Santa Cruz Biotechnology, Dallas, Texas, USA), anti-GABARAPL1 (D5R9Y, Cell Signaling Technology, Dallas, Texas, USA), and anti-GAPDH (A1978, MilliporeSigma). The membranes were then incubated with a horseradish peroxidase-conjugated anti-mouse IgG antibody (81-6720, Invitrogen, Carlsbad, California, USA) or an anti-rabbit IgG antibody (G21234, Invitrogen), and visualized using an ECL system (Thermo Fisher Scientific, Waltham, Massachusetts, USA).

Cytotoxicity Assay. The cell viability was assessed using the CellTiter-Glo Luminescent Cell Viability Assay (Promega) kit as previously described[40]. More specifically, the cells were grown in a black wall/clear-bottom 96-well

plate and treated with either pentaminomycins C–E (20 μM; **6**–**8**), menadione (25 μM), or combinations of pentaminomycins and menadione for 8 h at the indicated concentrations. After the addition of luminescence substrates in the same volume as the cell culture medium, the mixtures were incubated for 2 min at room temperature on a shaker, followed by 10 min incubation at room temperature to stabilize the luminescence signal prior to measurement.

Bioactivity experiments were performed by Prof. Min Jae Lee's laboratory from college of medicine in Seoul National University.

Part B.

Reinvestigation of the Structures of Tripartilactam and Lydiamycin A

I. Introduction

Structure elucidation of small molecules is a starting point for the development of new natural product derived medicines. Because the bioactivities are governed by the three-dimensional structures of the compounds.[41] For this reason, various methods have been devised to determine the structure of compounds during the history, among which NMR spectroscopy is now being used as the standard method to determine the planar structure of natural products. But basic 1D and 2D NMR experiments also have some limitations. Identifying novel and complex structure is still challenging because the data sometimes does not converge into a single strucuture, but there can be some possible structures. In this case, individual bias can affect the result, because all possible solutions discarded except the most logical one. Thus, there is a possibility that having errors in the reported compounds of unique and complex structures. In addition, absolute configuration determination was limited only in cases with typical structure features in the past. On the other hand, techniques for determination of absolute configuration has been developed through various approaches of chemistry, biology and computer science these days. Therefore, it is often easy to identify previously difficult structures with current methods which make possible to determine unknown structures or correct errors which were not in the past.

Tripartilactam (**9**) is a structurally unique natural macrocyclic lactam product originally identified in *Streptomyces* sp. SNA112 isolated from the brood ball of the dung beetle *Copris tripartitus* in 2012.[42] It was reported to have a tricyclic system consisting of cyclobutane, cyclooctene, and an 18-membered macrocyclic lactam. However, in 2015, the Abe research group

reported niizalactam C[43] from a combined culture of a *Streptomyces* strain and a mycolic acid-containing bacterium (*Tsukamurella pulmonis*) and proposed that the structure of niizalactam C (**10**), a [18,6,6]-tricyclic system is also the structure of tripartilactam. Even though the reported interpretation of 1D and 2D NMR data from niizalactam C in CD_3OD is reasonable, this claim should be reinvestigated because the structure of tripartilactam was originally proposed based on 2D NMR data acquired using DMSO-d_6.

The present study thus attempted to definitively determine the structure of tripartilactam by conducting a ^{13}C-^{13}C direct NMR coupling experiment, in which the SNA112 strain was cultivated in a medium containing universally-labeled ^{13}C-glucose to yield ^{13}C-enriched tripartilactam. Using this labeled tripartilactam, ^{13}C-^{13}C COSY NMR analysis allowed the structure of the carbon backbone to be unequivocally established. The biosynthetic pathway for tripartilactam was also elucidated using bioinformatics analysis of the entire SNA112 genome sequence, the mutagenesis of the identified biosynthetic gene cluster, and a cycloaddition experiment to prove the post-PKS non-enzymatic Diels-Alder reaction, producing tripartilactam from the precursor, sceliphrolactam. Here we report a definitive revision of the structure of tripartilactam and also describe its biosynthetic pathway.

Lydiamycins are piperazic acid-bearing cyclic depsipeptides originally reported from the soil-derived actinobacterium *Streptomyces lydicus* in 2006.[44] The compounds contain two piperazic acid-derived moieties, which are unusual amino units, and display antimycobacterial activity against *Mycobacterium* spp. Lydiamycin A (**11**) exhibited antituberculosis activity against *Mycobacterium tuberculosis* (TB) H37Rv

(MIC = 12.5 μg/mL) and a multidrug-resistant clinical TB strain (MIC = 25 μg/mL). The unique structural features of lydiamycin A, a rare 13-membered cyclodepsipeptide with piperazic acids, and its antituberculosis activity have attracted the attention of organic chemists who see it as an intriguing synthetic target. In particular, the original report of lydiamycins determined the absolute configurations of only four of the stereogenic centers, leaving two chiral centers, at the dehydropiperazic acid unit and the acyl chain, 2-pentyl-succinic acid, unassigned. Therefore, total syntheses were performed to establish the complete configuration of the lydiamycins, and four of the possible diastereomers were synthesized to established the undetermined stereogenic centers.[45,46] However, these synthetic efforts failed to assign the absolute configuration of the lydiamycins because the NMR spectra of the synthesized diastereomers of lydiamycin A and B's were noticeably different from those reported for natural lydiamycin A in the two independent synthetic reports in 2009[45] and 2010.[46] The discrepancy between the spectra of the natural and synthetic lydiamycins raised questions about the reported lydiamycins, but their exact structures remained unidentified.

In our chemical investigation of insect-associated bacteria, LC/MS analysis showed a peptide-derived metabolite was a major constituent of the extract of *Streptomyces* sp. GG23 strain from the gut of the mealworm beetle, *Tenebrio molitor*. Scale-up of the bacterial culture and subsequent purification of the metabolites allowed the identification of lydiamycin A based on spectroscopic analysis. As mentioned, because the accurate structures of lydiamycins are still in question, comprehensive re-examination of the stereochemistry by spectroscopic analysis, chemical derivatization, and quantum mechanics-based calculations was performed. Here, we report the structural revision of lydiamycin A as well as the re-evaluation of its

antituberculosis effects.

II. Structure Revision and the Biosynthetic Pathway of Tripartilactam

II. 1. Result and Discussion

Before conducting NMR experiments on tripartilactam (**9**), it was necessary to carefully analyze previously acquired 1D and 2D NMR spectra for the original report by our group (Table 5).[42] For consistency, the ^{1}H and ^{13}C numbering of the original structure of **9**[42] is used to discuss the structural analysis in this work. First, our previous report on tripartilactam (**9**) found no correlation between H-13 (δ_H 5.71) and H-14 (δ_H 4.52) in the COSY spectrum. Despite certain exceptions due to their dihedral angle, COSY correlations between two adjacent protons within three bonds are usually observed.[47] Actually, the H-13/H-14 COSY correlation should be observed if the structure of tripartilactam (**9**), possessing the C-13-C-14 connectivity, is correct, because the dihedral angle between H-13 and H-14 was estimated as 67.1° based on the energy-minimized structure of **9** by DFT calculation. Another problem arose in the interpretation of the COSY correlations of the overlapping signals of H-9 (δ_H 2.38) and H-17 (δ_H 2.43). Because of these overlapping protons, it was difficult to determine whether H-16 (δ_H 3.54) correlates with H-9 (δ_H 2.38), H-17 (δ_H 2.43), or both. H-16 was interpreted to correlate with both H-9 and H-17, which was crucial to the proposal of the cyclobutane structure in tripartilactam (**9**) (Figure 13).[42]

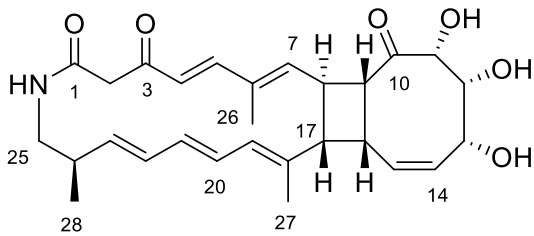

9

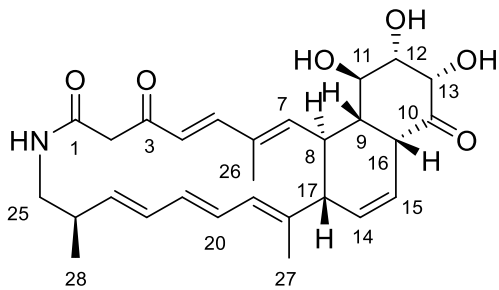

10

Figure 12. Structure of originally reported tripartilactam (**9**) and the revised structure (**10**).

When interpreting the HMBC data, no correlation was observed between H-14 (δ_H 5.71) to C-13 (δ_C 74.3) or H-13 (δ_H 4.52) to C-14 (δ_C 130.4) in the original report.[42] In addition, a four-bond HMBC correlation from H-17 (δ_H 2.43) to C-10 (δ_C 210.0) was previously reported. However, the overlap between H-17 (δ_H 2.43) and H-9 (δ_H 2.38) may have led to a misinterpretation (Figure 13).

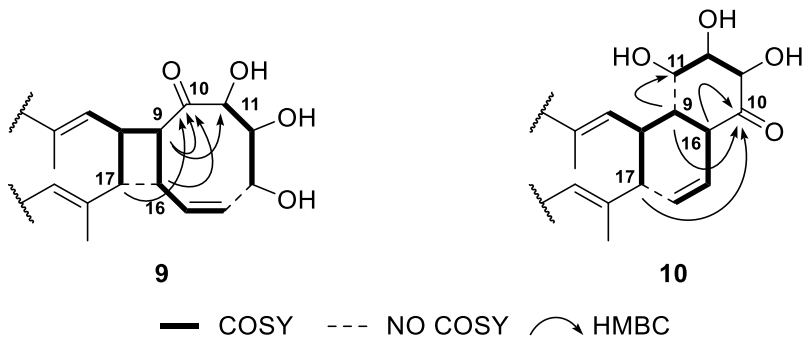

Figure 13. Previously reported key COSY and HMBC correlations for **9** and **10**.

To correctly determine the structure of tripartilactam (**9**), we conducted a ^{13}C-^{13}C COSY NMR experiment because this method can directly reveal the carbon backbone of a compound (Figure 13).[48] In particular, the chemical shifts of the carbons in the originally proposed cyclobutane and cyclooctene in **9** were well separated (Table 5), which is amenable for a ^{13}C-^{13}C direct coupling NMR experiment. However, ^{13}C-^{13}C COSY has an inherently low sensitivity due to the low abundance of the ^{13}C isotope in nature. Without ^{13}C labeling, a very large quantity of the compound is required to obtain the desired results. To avoid this, the ^{13}C-labeling experiment for tripartilactam (**9**) was performed by culturing the *Streptomyces* sp. SNA112 bacterial strain in a medium containing universally-labeled ^{13}C glucose. The production of ^{13}C-labeled tripartilactam was monitored using ESI-LC/MS. The mass spectrum for **9** clearly indicated that the compound had been enriched with ^{13}C. Even though not all of the ^{13}C-^{13}C connectivities were able to be observed, the analysis of the ^{13}C-^{13}C COSY NMR spectrum (Figure S9) enabled the crucial 1-bond ^{13}C-^{13}C correlations to be identified to a sufficient degree to allow the revision of the structure of tripartilactam (**9**) (Figure 15).

In the spectrum analysis, the C-9 methine (δ_C 48.6), which should be coupled with the C-10 ketone carbonyl carbon (δ_C 210.0) if the original structure is correct, instead demonstrated a 1-bond ^{13}C-^{13}C COSY correlation with C-11 (δ_C 70.3). The C-11 oxymethine carbon was directly connected to C-12 (δ_C 78.7) based on their ^{13}C-^{13}C correlation. Two hydroxylated carbons, C-12 (δ_C 78.7) and C-13 (δ_C 74.3), were then directly coupled to each other to confirm the C-12-C-13 connectivity. The two alkene carbons, C-14 (δ_C 130.4) and C-15 (δ_C 125.0), also had direct couplings, which agrees with both structures **9** and **10**.

In addition, the C-16 methine (δ_C 44.4), which should be coupled with C-15 or C-17 (δ_C 52.2) in the original structure, coupled with the C-10 ketone carbonyl carbon. In conjunction with the C-9-C-11 connectivity, this correlation proved crucial to the conclusion that the originally reported structure was erroneous. Further correlations in the ^{13}C-^{13}C COSY spectrum confirmed the previously identified carbon framework of the 18-membered ring. The carbonyl carbons C-1 (δ_C 164.4) and C-2 (δ_C 51.4) exhibited a direct coupling, and another carbonyl carbon C-3 (δ_C 191.3) also had a correlation with the olefinic carbon C-4 (δ_C 121.7). There was no coupling between C-5 and C-6, but C-7 (δ_C 145.6) correlated with C-8 (δ_C 38.0), confirming the C-7-C-8 connectivity. The assignment of C-19 (δ_C 130.0)-C-20 (δ_C 125.7) was confirmed based on the single-bond correlation between C-19 and C-20. Similarly, observations of C-21 (δ_C 132.5)/C-22 (δ_C 130.4) and C-23 (δ_C 137.9)/C-24 (δ_C 38.3) reconfirmed the presence of C-21-C-22 and C-23-C-24 bonds (Figure 14).

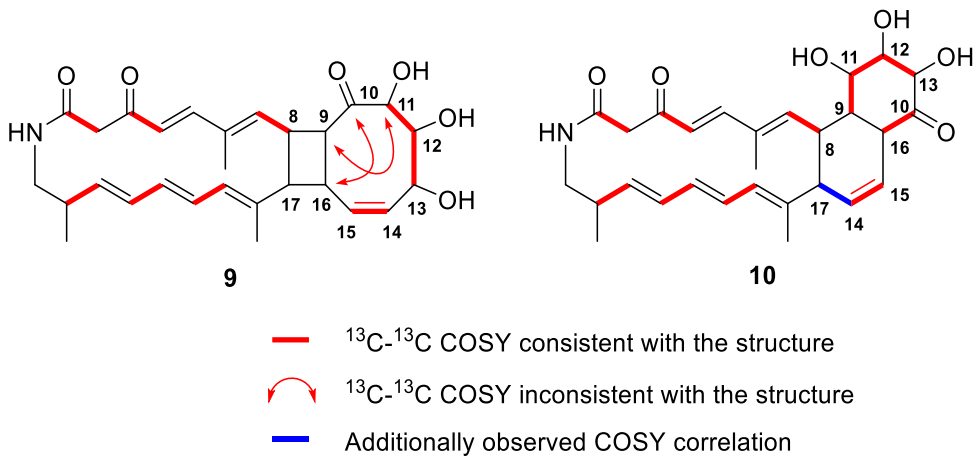

Figure 14. Assignment of 1-bond ^{13}C-^{13}C correlations observed in the ^{13}C-^{13}C COSY spectrum for structures **9** and **10** and an additionally observed COSY correlation supporting structure **10**.

Based on the overall single-bond ^{13}C-^{13}C COSY correlations, the structure of tripartilactam (**9**) was unequivocally determined to be identical to the structure of niizalactam C (**10**). This revised structure was further supported by the re-investigation of COSY correlations. Analysis of the weak peaks in the COSY spectrum in DMSO-d_6 identified a H-14/H-17 correlation (Figure 14), which was not observed in the DQF-COSY spectrum of niizalactam C in CD_3OD by Abe's research group.[43] Another overlooked correlation between H-9 and H-11 was also observed as a weak signal in the COSY spectrum in DMSO-d_6, confirming structure **10**.

To identify the biosynthetic gene cluster for tripartilactam, sequencing of *Streptomyces* sp. SNA112 DNA produced a draft genome. The draft genome obtained from 13 contigs was approximately 10.7 Mb, and genome analysis using antiSMASH 4.0[49] revealed the presence of 37 biosynthetic gene cluster regions putatively encoding polyketides, nonribosomal peptides,

ribosomally synthesized and post-translationally modified peptides, and others. Of these, we identified a continuous region containing type I polyketide synthases (PKSs), which was deemed a suitable candidate for the tripartilactam gene cluster (*tri* gene cluster). Within this gene cluster, the eight putative gene products involved in the biosynthesis of an amino acid starter unit exhibited 70% amino acid similarities to those found in the vicenistatin biosynthesis.[50] The *tri* cluster spanning at least 73.8 kb was found to contain 25 open reading frames, including six PKS genes, eight *β*-amino acid starter unit biosynthetic genes, two cytochrome P450 monooxygenase genes, five transport and regulatory genes, and several other genes (Figure 15a). This putative gene cluster was highly homologous to the recently reported sceliphrolactam gene cluster.[51] The proposed biosynthetic pathway for sceliphrolactam, which was first reported by Clardy's group and likely to be a precursor for tripartilactam, is almost identical to that of tripartilactam proposed in this report, except for the final cycloaddition step (Figure 15b).

The six PKS genes were divided into two regions, *triA1-A2* and *triA3-A6*, encoding a total of 11 modules, consisting of a loading module and 10 elongation modules. Sequence analysis of each domain revealed that the acyltransferase (AT) domains in modules 3 and 8 prefer methylmalonyl-CoA to malonyl-CoA, and other ATs are specific for malonyl-CoA. All of the ketoreductase (KR) domains are predicted to be type B1 KRs that contain the LDD motif. This sequence analysis is congruent with the structure of tripartilactam, which has two methyl groups at positions 26 and 27 and an *R*-configured hydroxylated carbon at position 12.

We propose that the biosynthesis of the macrolactam is initiated by incorporating a 3-aminoisobutyrate unit with amino protecting group as a starter unit, which is predicted to be biosynthesized by a set of genes encoding

the glutamate mutase subunits TriC and TriD (homologs of VinI and VinH in the vicenistatin gene cluster, respectively), decarboxylase TriE (a VinO homolog), two adenylation enzymes TriF and TriG (homologs of VinN and VinM), acyl carrier protein TriH (a homolog of VinL), and acyltransferase TriI (a homolog of VinK) in a manner similar to vicenistatin biosynthesis.[50] The polyketide chain is extended by 10 elongation modules, and then the terminal amino acyl group is removed by peptidase TriJ (a homolog of VinJ) prior to macrocyclization by the thioesterase domain of TriA6 (Figure 15b). Moreover, two cytochrome P450 monooxygenases encoded by *triK* and *triL* catalyze the formation of hydroxy groups at positions 11 and 13 to produce sceliphrolactam, which is also detected in the culture of the strain SNA112, followed by a [4+2] cycloaddition reaction to complete tripartilactam biosynthesis (Figure 15).

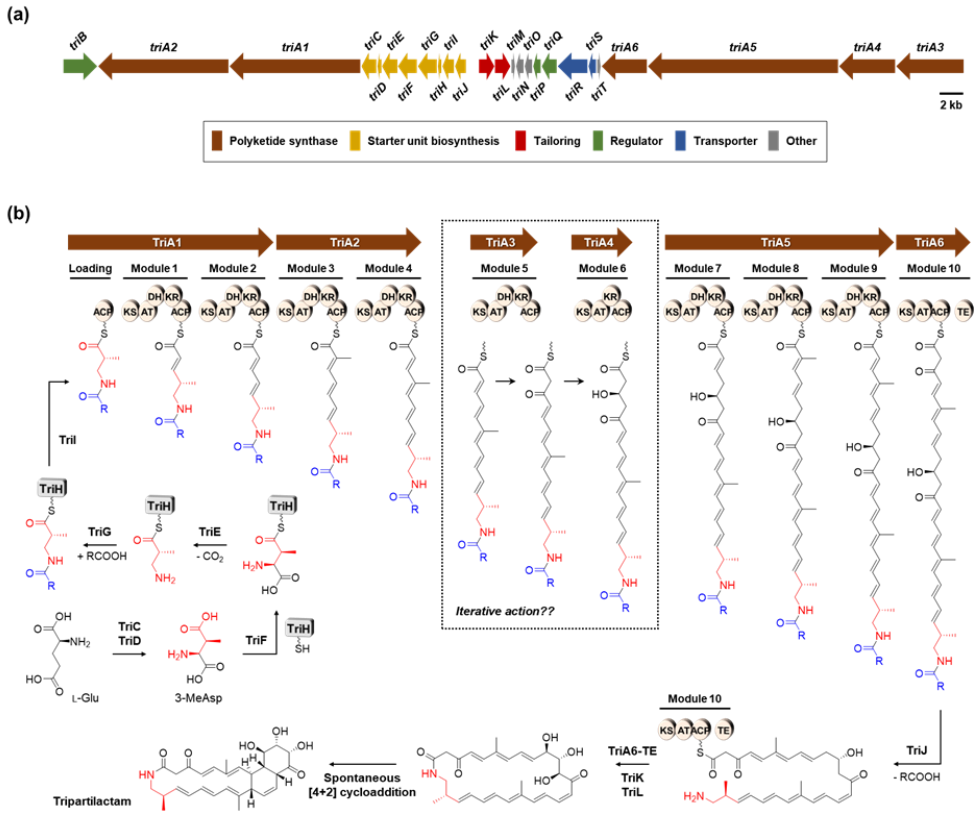

Figure 15. Proposed biosynthesis pathway for tripartilactam. (a) Organization of the *tri* biosynthetic gene cluster. (b) Putative biosynthetic pathway for tripartilactam and the modular organization of the tripartilactam PKSs. Predicted iterative module and its biosynthetic process is indicated by the box. Two P450s, TriK and TriL, would catalyze the hydroxylations on the macrolactam ring, or alternatively, are likely to act on the polyketide chain tethered to the PKS. ACP, acyl carrier protein; AT, acyltransferase; DH, dehydratase; KR, ketoreductase; KS, ketosynthase; TE, thioesterase.

Generally, [4+2] cycloaddition can be catalyzed biosynthetically using a Diels-Alderase.[52,53] However, there is no gene encoding for a Diels-

Alderase homologue in the genome of the SNA112 strain. Alternatively, the cycloaddition reaction can occur spontaneously without enzymes.[54,55] To prove this, the tripartilactam precursor sceliphrolactam was isolated and incubated in DMSO for five days at room temperature. LC/MS analysis revealed the formation of tripartilactam after three days, confirming the non-enzymatic production of tripartilactam from sceliphrolactam[56] (Figure 16), as observed in the biosynthesis of heronamides.[54] It has been reported that both heronamides D and E were non-enzymatically formed through spontaneous [4+6] and [6+6] cycloadditions of heronamide F, respectively, in DMSO solution.[54] In addition, natural products biosynthesized through non-enzymatic [4+2] cycloaddition reactions are not rare with the representative examples of anigorufone and galiellalactone.[55] Interestingly, the six *tri* PKSs have only 10 elongation modules, while 11 polyketide chain elongation cycles are required for the biosynthesis of tripartilactam based on its structure. One more module containing β-ketoacyl synthase (KS), AT, and acyl carrier protein (ACP) domains should be present between modules 5 and 6 based on the structure of tripartilactam. However, this module was not found near the *tri* biosynthetic gene cluster. Therefore, we can predict the repetitive catalysis of module 5 or module 6 without following the collinearity rule.[57] The iterative use of one or more modules has been found within modular PKSs such as borrelidin,[58] lankacidin,[59] aureothin,[60] and azalomycin F.[61] In the biosynthesis of azalomycin F, the first extension module, which contains the modification domains ketoreductase (KR), dehydratase (DH), and enoylreductase (ER) along with the minimal set of KS, AT, and ACP domains, acts twice for chain elongation. While the ER domain is skipped in the first cycle, the KR, DH, and ER domains are fully active in the second cycle.[61]

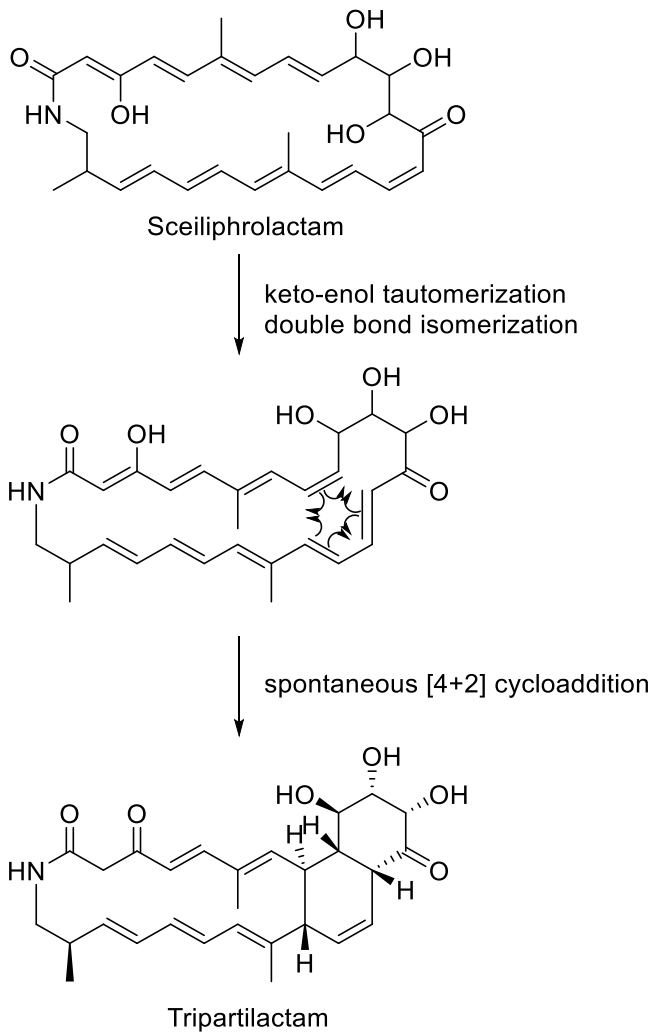

Figure 16. Proposed cycloaddition mechanism from sceliphrolactam to tripartilactam.

This form of switchable domain reaction with iterative modules can also be predicted for the growth of the tripartilactam chain, and we hypothesize that either module 5 or module 6 acts twice. If module 5, which is encoded by *triA3*, is used iteratively, it is proposed that the *β*-ketoacyl thioester intermediate is modified at the *β*-carbon by KR5 and DH5 in the first

cycle, but the reductive domains are not functional in the second cycle. If module 6, which is encoded by *triA4*, is used repeatedly, we can predict that the *β*-ketoacyl thioester intermediate is not modified in the first cycle, but the newly formed keto group is reduced by KR6 action in the second cycle. In a recent report on sceliphrolactam biosynthesis,[51] an equivalent biosynthetic mechanism involving the iterative use of PKS modules was proposed. In order to determine the identity of the iterative module for the tripartilactam PKS, inactivation mutagenesis of DH5, KR5, and KR6 was carried out. Site-specific mutations of His to Ala and Tyr to Phe were introduced to the active sites of DH and KR, respectively. With these mutations, we expected to produce unreduced derivatives bearing modifications associated with the iterative module. However, the production of tripartilactam was completely abolished and no related compounds were detected (Figure 17). In general, point mutations of the reductive domains for a PKS do not result in the complete loss of polyketide production, but such cases have been reported occasionally.[62] Although we could not confirm which module is employed iteratively, it was proven that these modules are functionally involved in tripartilactam biosynthesis.

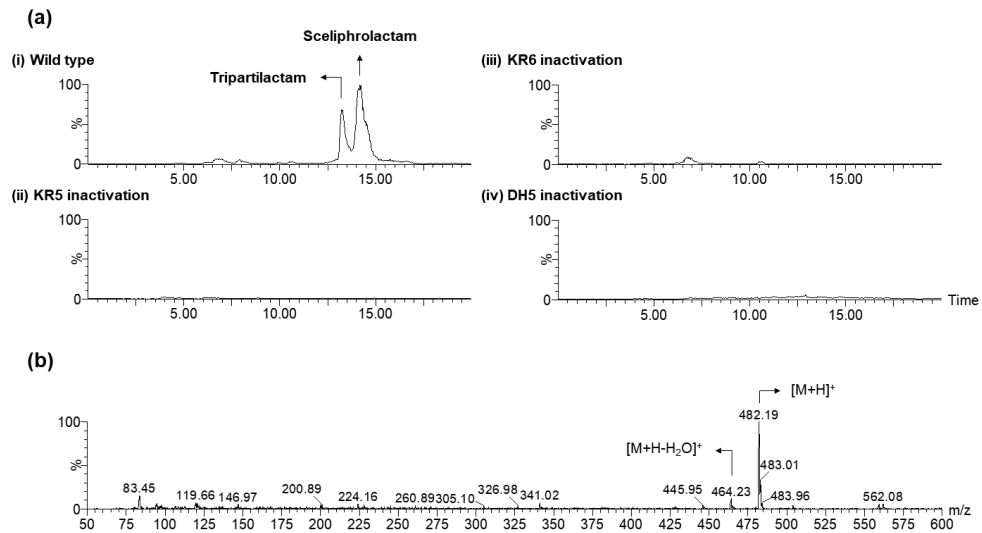

Figure 17. HPLC-ESI-MS analysis of SNA112 wild type and domain inactivation mutant strains. Chromatograms are shown for selected *m/z* values of naturally producing tripartilactam ($[M+H]^+$=482.25) and the expected derivatives of each mutant strain. (a) Chromatograms of wild type extract showing tripartilactam production (selected for *m/z*=482.25) (i), KR5 inactivation mutant strain extract (selected for *m/z*=482.25) (ii), KR6 inactivation mutant strain extract (selected for *m/z*=482.25) (iii), and DH5 inactivation mutant strain extract (selected for *m/z*=482.25) (iv). (b) MS/MS spectra of tripartilactam produced from wild type strain.

Table 5. NMR Data for Tripartilactam (**9**) in DMSO-d_6

Tripartilactam (**9**)			
Position	δ_C, type	δ_H, mult (*J* in Hz)	^{13}C–^{13}C
1	164.4, C		2
2a	51.4, CH_2	3.47, d (11.5)	1
2b		2.95, d (11.5)	
3	191.3, C		4
4	121.7, CH	6.03, d (15.5)	3
5	147.1, CH	7.10, d (15.5)	
6	135.4, C		
7	145.6, CH	5.70, m	8
8	38.0, CH	2.57, ddd (12.0, 10.0,	7
9	48.6, CH	10.0)	11
10	210.0, C	2.38, m	16
11	70.3, C		9
		3.82, br s	
11-OH		5.31, br d (2.5)	
12	78.7, CH	4.02, m	13
12-OH		4.96, br d (4.0)	
13	74.3, CH	4.52, dd (7.5, 3.5)	12
13-OH		4.67, br d (7.5)	
14	130.4, CH	5.71, m	15
15	125.0, CH	5.76, ddd (10.0, 5.0, 2.5)	14
16	44.4, CH	3.54, m	10
17	52.2, CH	2.43, ddd (10.0, 4.0, 2.5)	
18	134.3, C		
19	130.0, C	5.38, d (11.0)	20
20	125.7, CH	6.11, dd (14.5, 11.0)	19
21	132.5, CH	5.68, dd (14.5, 10.0)	22
22	130.1, CH	6.02, dd (14.5, 11.0)	21
23	137.9, CH	5.24, dd (15.0, 9.0)	24
24	38.3, CH	2.32, m	23
25a	44.1, CH_2	3.25, m	
25b		2.89, ddd (13.0, 4.0, 4.0)	
25-NH		8.01, dd (8.0, 4.0)	
26	13.1, CH_3	1.26, s	
27	12.9, CH_3	1.49, s	
28	19.0, CH_3	0.93, d (6.5)	

^1H and ^{13}C NMR data were recorded at 800 and 200 MHz, respectively.

II. 2. Conclusion

Comprehensive spectroscopic analysis of the ^{13}C-^{13}C COSY NMR spectrum led to the unequivocal revision of the contested structure of tripartilactam (**9**) as niizalactam C (**10**) by directly confirming its carbon framework. Bioinformatics analysis and mutagenesis experiments revealed the biosynthetic gene cluster of **9**, which possibly utilizes one of the PKS modules iteratively and undergoes spontaneous cycloaddition to form the [18,6,6]-tricyclic structure after modular biosynthesis.

II. 3. Experimental section

General Experimental Procedures. ^{1}H, ^{13}C, and 2D NMR spectra were obtained on Bruker 800 and 850-MHz spectrometers. Low-resolution electrospray ionization mass spectra were acquired using an Agilent Technologies 6130 quadrupole mass spectrometer coupled with an Agilent Technologies 1200 series high-performance liquid chromatography (HPLC) instrument. Preparative HPLC separation was achieved using a Dynamax Rainin 100 SC pump and a Gilson UV/VIS-155 detector.

Cultivation and Extraction. The *Streptomyces* sp. SNA112 strain isolated from the brood ball of the dung beetle *Corpris tripartitus*[42] was initially cultivated in 50 mL of YEME medium (4 g of yeast extract, 10 g of malt extract, and 4 g of glucose in 1 L of distilled H_2O) for three days on a rotary shaker at 200 rpm and 30 ℃. The spores in the medium were then transferred to 200 mL of YEME medium and cultivated for three days under identical conditions. After cultivation, the spores were transferred into 1 L of YEME medium which contained universally-labeled ^{13}C d-glucose instead of unlabeled d-glucose in a 2.8-L Fernbach flask. The entire culture (6 L) was extracted twice using EtOAc (12 L), with the extract shielded from light exposure. The EtOAc extract was concentrated *in vacuo* to yield 1 g of dry material.

Isolation of Tripartilactam. The dry material was resuspended in MeOH and dried again with celite. The celite-adsorbed material was loaded onto a 2-g Sep-Pak silica cartridge and fractionated with 30 mL each of 1:1

hexane/EtOAc, 100% EtOAc, 9:1, 5:1, 2:1 EtOAc–MeOH, and finally 100% MeOH to divide it into six fractions. Each fraction was analyzed with LC/MS, and tripartilactam was found in the 9:1 EtOAc–MeOH fraction. This fraction was injected into a reversed-phase preparative HPLC instrument (C_{18}(2) Luna 10 μm, 250 × 21.10 mm, flow rate 10 mL/min, UV 280 nm detection, 30–70% CH_3CN–H_2O gradient over 40 min). Under these purification conditions, pure tripartilactam was isolated with a retention time of 24 min.

Whole-Genome Sequencing Analysis. Genome sequencing of *Streptomyces* sp. SNA112 was performed by ChunLab Inc. using the PacBio RS II system. Genome assembly was conducted using PacBio SMRT Analysis 2.3.0 with the HGAP protocol (Pacific Biosciences). Functional annotations of the genome were carried out with EggNOG 4.5, Swissprot, KEGG, and SEED as references based on ChunLab's in-house pipeline. Secondary metabolite biosynthetic gene clusters were identified and analyzed using antiSMASH4.0.[49] The *tri* cluster was deposited in GenBank under the accession number MN305323.

Domain Inactivation by Site-Directed Mutagenesis. To inactivate the KR5 domain via the replacement of the amino acid at the active site of the KR5 domain, the following procedures were carried out. Two DNA fragments containing the mutations Y1548F and N1547S were amplified with two PCR primer pairs dKR5_LF/dKR5_LR and dKR5_RF/dKR5_RR (Table S3) from the genomic DNA of wild-type SNA112. A 1407-bp *Eco*RI-*Hind*III fragment harboring the upstream region of mutated KR5 and a 1348-bp *Hind*III-*Xba*I fragment containing the downstream region of mutated KR5 were ligated

together into the temperature-sensitive *E. coli-Streptomyces* shuttle vector pKC1139[63] through *Eco*RI-*Xba*I sites, generating pdKR5. To inactivate the KR6 domain, the same strategy was employed to create plasmid pdKR6 carrying the mutations Y1297F and N1296S generated by the primer pairs dKR6_LF/dKR6_LR and dKR6_RF/dKR6_RR.

To generate mutants with an inactivated DH5 domain, a plasmid carrying H956A and A957S mutations was constructed using PCR amplification with the PCR primer pairs dDH5_LF/dDH5_LR and dDH5_RF/dDH5_RR. A 640-bp *Eco*RI-*Bmt*I fragment and another 720-bp *Bmt*I-*Hind*III fragment were cloned into *Eco*RI-*Hind*III-digested pKC1139 to create pdDH5.

The mutated plasmids were introduced into wild-type SNA112 via conjugation using the non-methylating *E. coli* donor strain ET12567/pUZ8002.[64] The successful creation of the desired inactivated mutants via double-crossover homologous recombination was confirmed using PCR amplification, enzyme digestion, and the sequencing of the PCR products.

Spontaneous Cycloaddition. The cycloaddition mechanism for tripartilactam was assumed to be a spontaneous Diels-Alder reaction. Sceliphrolactam was isolated using normal-phase flash chromatography as previously reported[56] from an EtOAc extract from SNA112. Isolated sceliphrolactam was dissolved in DMSO at a concentration of 0.5 mM and stirred for five days at room temperature. The compound was analyzed every two days using LC/MS with an aqueous CH_3CN gradient solvent condition (10–100% CH_3CN/H_2O over 20 min, 0.1% formic acid, flow rate: 0.7

mL/min).

Genome analysis and mutagenesis experiments were performed by Prof. Yeo Joon Yoon's laboratory from college of pharmacy in Seoul National University.

III. Structural Revision of Lydiamycin A by Reinvestigation of the Stereochemistry

III. 1. Results and Discussion.

Lydiamycin A (**11**) was isolated as a white powder. The molecular formula was deduced as $C_{31}H_{49}N_7O_9$ based on HR-FAB mass spectrometry ($[M+H]^+$ *m*/*z* at 664.3666, calculated 664.3670). The ^1H NMR spectrum of **11** in DMSO-d_6 showed five exchangeable protons (δ_H 12.0, 8.27, 8.19, 7.93, and 4.52) and five α-amino proton signals (δ_H 5.04, 4.96, 4.41, 4.37, and 4.29). The ^{13}C NMR data also revealed six amide or ester carbonyl groups (175.2, 173.4, 172.0, 170.3, 169.6, and 169.4) and seven α-carbonyl or oxygenated carbons (62.9, 52.7, 51.6, 51.3, 50.8, 50.6, and 46.3), which were consistent with the structural features of peptide-derived compounds.

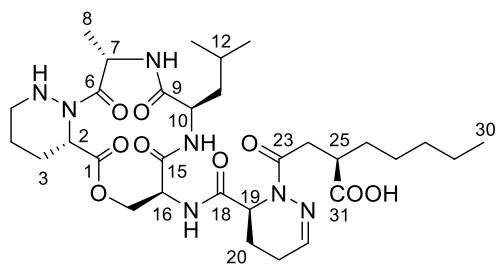

11

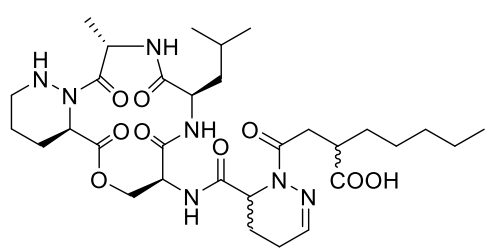

originally reported lydiamycin A

Figure 18. Structure of revised lydiamycin A (**11**) and originally reported structure.

Comprehensive analysis of the 2D NMR data of **11**, including its COSY, HSQC, HMBC, and ROESY spectra, indicated that an alanine, a leucine, a serine, a piperazic acid, and a dehydropiperazic acid residue along with 2-pentyl-succinic acid were present. The sequence of the amino units was confirmed by the HMBC correlations from the NH groups to the adjacent carbonyl carbons (Table 6). The cyclization between serine and piperazic acid via an ester bond was confirmed by the HMBC cross-peak from H-17 to C-1, completing the planar structure of **11**, which is identical to that of previously reported for lydiamycin A. The ^{1}H and ^{13}C NMR spectra of **11** acquired in $CDCl_3$ exactly matched those reported for lydiamycin A. The optical rotation of **11** ($[\alpha]_D^{20}$ = -21) was also consistent with the value ($[\alpha]_D^{20}$ = -20) reported for lydiamycin A.[44] However, detailed analysis of the 1D and 2D NMR spectra of **11** in $CDCl_3$ acquired in a high-field NMR spectrometer (800 MHz) indicated that the C-1, C-9, and C-15 amide carbons were incorrectly assigned in the previous report (Table 6).

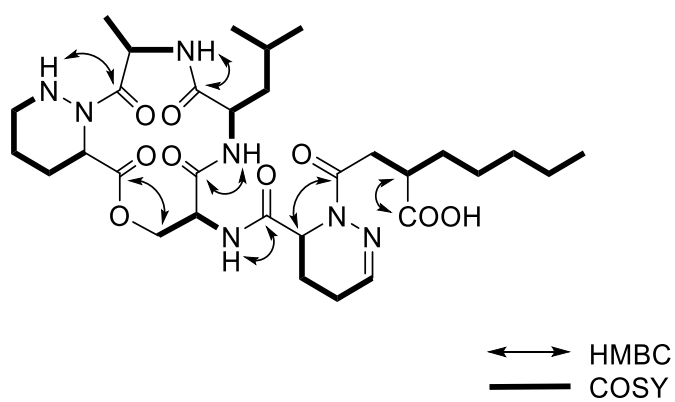

Figure 19. COSY and key HMBC correlations of lydiamycin A (**11**).

Because the absolute configuration of lydiamycin A has not been fully assigned, the stereochemistry of **11** was comprehensively reinvestigated. First, the absolute configurations of the α-positions of the Ala, Leu, and Ser residues of **11** were determined in a straightforward manner using advanced Marfey's method with L- and D-FDAA (1-fluoro-2,4-dinitrophenyl-5-alanine amide).[5] The result indicated that lydiamycin A possesses L-Ala, D-Leu, and L-Ser units, consistent with the reported structure.

For the piperazic acid moiety, the D-FDAA adduct of piperazic acid eluted faster than the L-FDAA derivative in the LC/MS analysis. The elution order of the Marfey's products of piperazic acid was empirically reported in a structural study of the piperazic acid-bearing cyclic peptide, dentigerumycin,[65] with authentic L- and D-piperazic acids; the L-Marfey's product of *R*-piperazic acid elutes faster than the D-Marfey's product, whereas the D-Marfey's product of *S*-piperazic acid elutes before the L-Marfey's product by reversed-phase HPLC. Since this first report of Marfey's analysis of piperazic acids, this elution order has been widely used for the configurational determination of piperazic acid moieties in natural products.[66-69]

Despite increasing use, the cause of the elution order and the exact structures of the Marfey's products of piperazic acid remain to be clarified. Because piperazic acid possesses two amine groups that could react with Marfey's reagent, the exact structures of the L- and D-FDAA adducts of piperazic acid were rigorously investigated. *S*-Piperazic acid was derivatized with L- and D-FDAA, and the products were purified. Analysis of the 1D and 2D NMR spectra allowed the assignment of the structures of the Marfey's products. The elution order of the L- and D-FDAA products of piperazic acid

was established. In particular, the COSY correlation between the α-proton of the piperazic acid moiety and the NH of the α-amine group established the presence of the α-amine NH, indicating that this amine did not participate in the Marfey's derivatization. The methyl group of the alanine residue of Marfey's reagent showed a ROESY correlation with δ-protons (CH_2) supported the structure shown in Figure 20a. Therefore, the δ-amine group of piperazic acid, not α-amine, reacts with Marfey's reagent to form the obtained adducts.

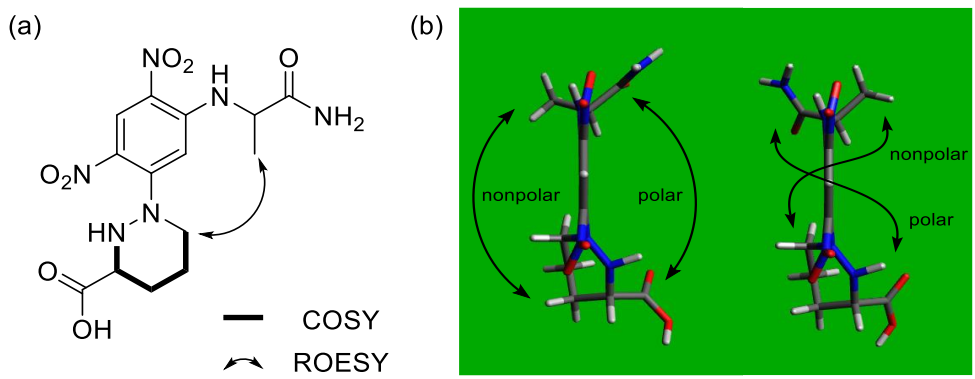

Figure 20. (a) The planar structure of the FDAA adduct of piperazic acid. (b) Energy-minimized structures of the reaction products of *S*-piperazic acid with L-FDAA (left) and D-FDAA (right).

Once the exact structures of the L- and D-FDAA adducts of piperazic acid were determined, their 3-dimensional conformations were examined by molecular modeling, which may elucidate the cause of the elution order in reversed-phased HPLC. After computational 3D modeling with energy minimization, the nonpolar methylene hydrocarbon region of *S*-piperazic acid

was pointed in the same direction as the alanyl methyl group of alaninamide of the L-FDAA product (Figure 20b). On the other hand, the nonpolar hydrocarbons of piperazic acid were in the opposite direction of the alanyl methyl of the D-FDAA product (Figure 20b). Therefore, the cause of the elution order was rationalized as follows: The L-FDAA adduct of *S*-piperazic acid possesses a stronger affinity for the reversed-phase HPLC stationary phase, thus eluting later than the D-FDAA product of *S*-piperazic acid because of their conformations.[5,65] Based on the empirical D→L elution order of the FDAA adducts and the established rationale, the absolute configuration of the piperazic acid unit in lydiamycin A (**11**) was determined to be *S*. This assignment is different from the originally proposed *R* configuration.

Although D-FDAA-dehydropiperazic acid was detected slightly earlier than the L-FDAA adduct of the amino acid in the LC/MS analysis of the analogous compound *S*-piperazic acid, this was not sufficient evidence to assign the absolute configuration of the dehydropiperazic acid moiety in lydiamycin A by advanced Marfey's method because there was no reference for the elution order for the FDAA products of dehydropiperazic acid. To circumvent this problem, the imine in the dehydropiperazic acid residue was reduced to the piperazic acid with sodium cyanoborohydride ($NaBH_3CN$) as a hydride source (Figure 21).[70] After confirmation of reduced product using LC/MS analysis, the residue was subjected to acid hydrolysis and FDAA derivatization for advanced Marfey's analysis. As a result, the L- and D-FDAA products of dehydropiperazic acid moiety, which was observed in the analysis of **11**, disappeared. Only one piperazic acid-derived FDAA product remained in each batch of FDAA derivatization. This result suggests dehydropiperazic acid has the same absolute configuration as the piperazic

acid unit in **11**, thus the configuration of C-19 was assigned to *S* same as C-2.

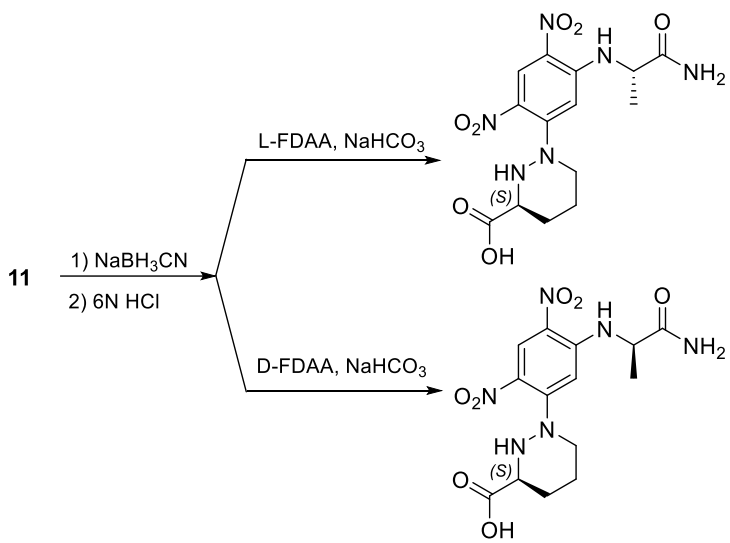

Figure 21. Application of Marfey's method after reduction for the identification of the absolute configuration at C-19 of **11**.

The last undetermined stereogenic center, C-25 in the 2-pentyl-succinic acid moiety, was successfully assigned by *S*- and *R*-phenylglycine methyl ester (PGME) derivatizations of the carboxylic acid group of **11**.[71] Comparing the ^{1}H NMR chemical shifts of the *S*- and *R*-PGME amides (**11a** and **11b**) of **11** based on the $\Delta\delta_{S-R}$ values calculated from the ^{1}H and COSY NMR data of the *S*- and *R*- PGME amides allowed us to determine the absolute configuration of C-25 as *R* (Figure 22).

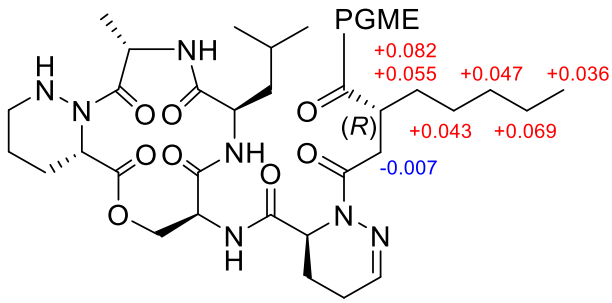

Figure 22. $\Delta\delta_{S\text{-}R}$ values of the *S*- and *R*-PGME products (**11a** and **11b**) of **11**.

The 19*S* configuration in the dehydropiperazic acid unit was also supported by quantum mechanics-based chemical shift calculations and subsequent statistical analysis by the DP4 method.[72] Two possible diastereomers (19*R* and 19*S*) were proposed with the determined configurations for the other stereogenic centers. For the diastereomers, the ^{1}H and ^{13}C chemical shifts of their 104 conformers were calculated and averaged based on their Boltzmann populations. Comparing the experimental ^{1}H and ^{13}C chemical shifts with Boltzmann averaged calculated chemical shifts, the DP4 calculation suggested that the 19*S* configuration shows the best fit with the experimental data (100% probability). This supported the results of advanced Marfey's analysis of the reduction product of **11**.

Overall, the absolute configuration of lydiamycin A (**11**) was finally determined as 2*S*, 7*S*, 10*R*, 16*S*, 19*S*, and 25*R*. In particular, the 2*S* configuration is opposite the originally proposed configuration. Therefore, the configuration of C-2 in lydiamycin A must be revised from *R* to *S*. It is now clear that the incorrect configuration of C-2 in the original report caused the discrepancy in the spectroscopic data of the natural and synthetic lydiamycins.[45,46]

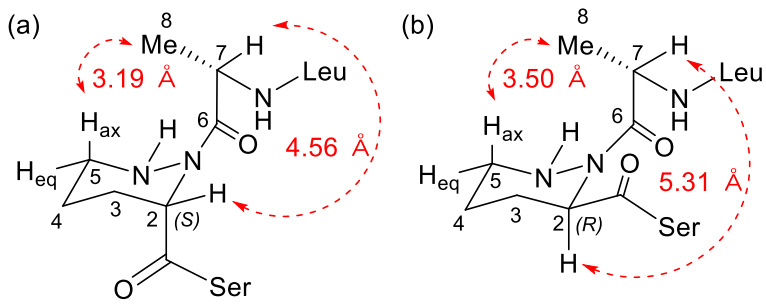

Figure 23. The piperazic acid and alanine fragments of **11** from the energy minimized computational (a) 2*S* model and (b) 2*R* model.

Then, we examined the reason that the original report arrived at this erroneous configuration. The Marfey's method-based determination of the absolute configuration of piperazic acid was established in 2009[5] and thus was not available at the time of the original report of the lydiamycins (in 2006).[44] Hence, the configurations of the piperazic acids in the lydiamycins were previously proposed based on computational modeling along with NOE correlations. In the original report, the absolute configuration of C-2 was proposed based on the distance between H_{ax}-5 and alanyl methyl proton H_3-8 in the original report. The distance between H_{ax}-5 and H_3-8 was calculated as 4.1 Å based on the ROESY peak areas, which was close to the H_{ax}-5/H_3-8 distance (4.06 Å) calculated from the molecular model of the 2*R*-configuration by conformational analysis and computation with the MM+ force field. The H_{ax}-5/H_3-8 distance in the molecular model of the 2*S*-configuration was calculated as 2.65 Å in that report. However, this calculation might be unreliable because the H_{ax}-5/H_3-8 distance was calculated only from fragmented models. The undetermined configurations and the acyl chain could affect the molecular conformation. The reliability

might be also lower because the calculations were with the MM+ force field rather than density functional theory (DFT), which is required to reproduce the actual dynamics.[73]

To improve the rigor of the molecular modeling, the energy-minimized structures of the 2*S* and 2*R* models of the entire structures of lydiamycin A (**11**) were constructed based on DFT calculations and validated by ROESY correlations. The H_{ax}-5/H_3-8 distances in our models were measured, and the distances in the 2*S* and 2*R* models were not dramatically different in this configurational analysis. Considering the entire structure, the distances were 3.19 Å in the 2*S* model and 3.50 Å in the 2*R* model (Figure 23). This result indicates that the absolute configuration of C-2 proposed based on fragmented models in the original report was not reliable and led to the erroneous configuration.

In addition to H_{ax}-5 and H_3-8, we focused on the distance and ROESY correlation between H-2 and H-7. The measured distance was 4.56 Å in the 2*S* model, whereas these protons were 5.31 Å apart in the 2*R* model. Even though the signal intensity was relatively weak, ROESY correlations are generally observed between protons within 5 Å of each other. Therefore, the 2*S* model is more consistent with the observed ROESY data, which again supports our 2*S* configuration.

Lydiamycins were originally reported as antimycobacterial natural products (MIC against *M. tuberculosis* was 12.5 μg/mL). Thus, the antimycobacterial activity of lydiamycin A (**11**) was first evaluated. MIC_{50} and MIC_{90} values were defined as the drug concentration at which 50% and 90% of the *M. tuberculosis* tested showed no visible growth, respectively. However, our MICs of lydiamycin A (**11**) against *M. tuberculosis* mc^2 6230

by a resazurin-based microtiter plate assay (REMA) indicated weaker activity than the original report.[74] As shown in Figure 24, lydiamycin A (**11**) showed very high MIC_{50} and MIC_{90} values (31.0 μg/ml; 46.8 μM and 285.6 μg/ml; 430.6 μM, respectively) and failed to kill *M. tuberculosis* even at high concentrations (MBC >200 μM). In conclusion, lydiamycin A (**11**) had no significant bactericidal effect against *M. tuberculosis*, although it showed weak antimycobacterial activity *in vitro*.

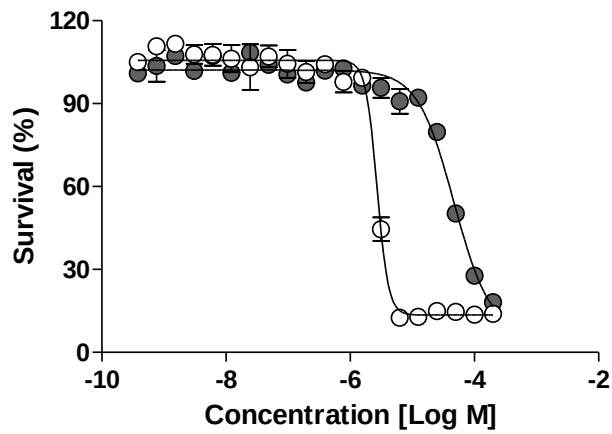

Figure 24. *In vitro* antituberculosis activity of **11** by REMA. The activity of **11** (closed circles) against *M. tuberculosis* mc^2 6230 was compared with ethambutol (open circle).

Lydiamycin A (**11**) was subjected to additional cytotoxicity and antimicrobial activity evaluations. However, no cytotoxic activity was observed against the tested cancer cell lines (SNU638: gastric cancer, SK-Hep-1: liver cancer, A549: lung cancer, HCT116: colon cancer, and MDA-MB-231: breast cancer). In the antimicrobial assay against pathogenic bacteria (*S. aureus*, *E. faecalis*, *E. faecium*, *K. pneumonia*, *S. enterica*, and *E.*

coli) and fungi (*C. albicans*, *A. fumigatus*, *T. rubrum*, and *T. mentagrophytes*), lydiamycin A (**11**) did not display any significant effects.

Table 6. NMR spectral data for lydiamycin A (**11**)[a]

No.	**11** (DMSO-d_6)		**11** ($CDCl_3$)		**11** (originally reported)[c] ($CDCl_3$)	
	δ_C, mult.[b]	δ_H (*J* in Hz)	δ_C, mult.[b]	δ_H (*J* in Hz)	δ_C, mult.[b]	δ_H (*J* in Hz)
1	169.4, qC		169.8, qC		169.1, qC	
2	50.6, CH	5.04, m	52.7, CH	5.30, m	52.7, CH	5.28, m
3	24.0, CH_2	2.10, 1.68, m	24.4, CH_2	2.38, 1.77, m	24.4, CH_2	2.35, 1.77, m
4	21.1, CH_2	1.51, 1.43, m	21.4, CH_2	1.63, 1.59, m	21.4, CH_2	1.60, m
5	46.3, CH_2	3.02, 2.62, m	47.1, CH_2	3.14, m, 2.77, qd (12.0, 3.0)	47.1, CH_2	3.12, br d (13.5), 2.75, br dq (13.5, 3.8)
5-NH		4.52, d (12.0)		4.32, d (12.0)		4.31, br d
6	172.0, qC		174.3, qC		174.3, qC	
7	51.6, CH	4.37, qd (9.0, 7.0)	50.5, CH	4.85, qd (10.5, 7.0)	50.5, CH	4.83, qd (10.5, 7.25)
7-NH		7.93, d (9.0)		7.30, d (10.5)		7.27, d (10.5)
8	16.1, CH_3	1.37, d (7.5)	18.3	1.44, d (7.0)	18.2	1.43, d (7.25)
9	170.0, qC		169.0, qC		169.3, qC	
10	50.8, CH	4.29, m	51.4, CH	4.35, td (8.5, 8.5)	51.4, CH	4.33, m
10-NH		8.19, m		7.46, d (8.5)		7.43, d (7.8)
11	37.6, CH_2	1.55, 1.44, m	36.4, CH_2	1.78, m	36.6, CH_2	1.77, m
12	24.2, CH	1.45, m	24.6, CH	1.65, m	24.6, CH	1.63, m
13	22.7, CH_3	0.89, d (6.0)	22.8, CH_3	0.93, d (6.5)	22.7, CH_3	0.93, d (6.5)
14	21.9, CH_3	0.82, d (6.0)	22.3, CH_3	0.88, d (6.5)	22.2, CH_3	0.87, d (7.8)
15	170.3, qC		169.3, qC		169.7, qC	
16	52.7, CH	4.42, td (9.0,7.0)	50.6, CH	5.31, m	50.7, CH	5.28, m
16-NH		8.27, m		8.30, d (10.0)		8.25, d (9.85)
17	62.9, CH_2	4.61, 3.81, dd (10.0,7.0)	68.3, CH_2	4.77, dd (11.5, 4.5), 4.04, d (11.5)	68.2, CH_2	4.75, dd (11.4, 4.4), 4.03, br d (11.4)
18	169.6, qC		171.0, qC		170.9, qC	
19	51.3, CH	4.95, m	55.6, CH	4.67, t (5.0)	55.6, CH	4.65, br t (5.7)
20	18.8, CH_2	2.24, 1.77, m	19.4, CH_2	2.35, 1.92, m	19.3, CH_2	2.35, 1.93, m
21	19.5, CH_2	2.15, 1.84, m	20.6, CH_2	2.17, 1.95, m	20.6, CH_2	2.15, 1.92, m
22	141.8, CH	6.91, d (4.0)	142.7, CH	6.92, m	142.7, CH	6.90, br s
23	173.3, qC		175.9, qC		175.9, qC	
24	35.4, CH_2	2.53, 2.28, m	36.6, CH_2	3.32, dd (17.0, 12.0), 2.62, dd (17.0, 5.5)	36.5, CH_2	3.30, dd (16.8, 12.2), 2.60, dd (16.8, 5.3)
25	36.4, CH	3.67, m	46.0, CH	3.04, m	46.0, CH	3.02, m

26	31.0, CH_2	1.54, 1.30, m	31.6, CH_2	1.72, 1.53, m	31.6, CH_2	1.71, 1.52, m
27	31.2, CH_2	1.19, m	26.9, CH_2	1.35, 1.25, m	26.8, CH_2	1.35, 1.24, m
28	25.6, CH_2	1.22, m	31.5, CH_2	1.29, 1.25, m	31.5, CH_2	1.27-1.26, m
29	21.8, CH_2	1.23, m	22.4, CH_2	1.27, m	22.4, CH_2	1.27-1.26, m
30	13.8, CH_3	0.83, t (7.0)	14.0, CH_3	0.86, t (7.0)	13.9, CH_3	0.85, t (6.5)
31	175.2, qC		177.3, qC		177.3, qC	
31-OH		12.01, br s		11.37, br s		-

[a] 800 MHz for ^{1}H NMR and 200 MHz for ^{13}C NMR.

[b] Numbers of attached protons were determined by analysis of 2D spectra.

[c] 500 MHz for ^{1}H NMR and 75.5 MHz for ^{13}C NMR.

III. 2. Conclusion

Our rigorous stereochemical reinvestigation allowed us to completely determine the absolute configuration of lydiamycin A (**11**) and ultimately revise its structure. In particular, the previously undetermined chiral center of the dehydropiperazic acid was successfully established by C=N bond reduction followed by Marfey's analysis. The stereogenic center in the carboxylic acid-bearing acyl side chain (2-pentyl-succinic acid) was determined by PGME derivatization for ^{1}H chemical shift analysis. The absolute configuration of C-2 in the piperazic acid moiety, which was unequivocally determined by advanced Marfey's analysis and supported by molecular modeling, was revised from *R* to *S*, explaining why the two syntheses[45,46] that sought to determine the absolute configurations of the lydiamycins failed.

III. 3. Experimental section

General Experimental Procedures. Optical rotations were measured by a JASCO P-200 polarimeter (sodium light source, JASCO, Easton, PA, USA) with a 1-cm cell. UV spectra were acquired on a Chirascan plus Applied Photophysics spectrophotometer. IR spectra were obtained using a Thermo NICOLET iS10 spectrometer (Thermo, Madison, CT, USA). ^{1}H, ^{13}C, and 2D nuclear magnetic resonance (NMR) spectra were recorded on a Bruker Avance 800 MHz spectrometer (Bruker, Billerica, MA, USA) at the Research Institute of Pharmaceutical Sciences at Seoul National University. Electrospray ionization (ESI) low-resolution LC/MS data were recorded using an Agilent Technologies 6130 quadrupole mass spectrometer (Agilent Technologies, Santa Clara, CA, USA) coupled with an Agilent Technologies 1200 series high-performance liquid chromatography (HPLC) instrument using a reversed-phase C_{18} column (Phenomenex Luna, 100 × 4.6 mm). High-resolution fast atom bombardment (HR–FAB) mass spectra were recorded using a Jeol JMS–600 W high-resolution mass spectrometer (Jeol, München, Germany) at the National Center for Inter-university Research Facilities at Seoul National University.

Collection and phylogenetic analysis. The mealworm beetle-associated actinomycete strain GG23 was isolated from the gut of a *Tenebrio molitor* specimen bred and collected from Seoul Grand Park. It was identified as a *Streptomyces* sp. that is phylogenetically closest to *Streptomyces cacaoi* (GenBank accession number NZ_MUBL01000000) based on 16S rRNA gene sequence analysis (GenBank accession number MT033037).

Cultivation and Extraction. The GG23 strain was cultured in 50 mL of modified K medium (4 g of yeast extract, 5 g of malt extract, 5 g of soytone, 5 g of soluble starch, 5 g of mannitol, 2 g of glucose, and 6 g of glycerol in 1 L of distilled water) in a 125-mL Erlenmeyer flask. After cultivation for 3 days on a rotary shaker at 200 rpm at 30 ℃, 5 mL of the culture medium was inoculated in 200 mL of modified K medium in a 500-mL Erlenmeyer flask. After cultivation for 3 days under the same conditions, 10 mL of the culture medium was inoculated in 1 L of modified K medium in 2.8-L Fernbach flasks (60 ea × 1 L, total volume 60 L) for 4 days at 170 rpm at 30 ℃. Sixty liters of GG23 culture medium was extracted with 120 L of ethyl acetate. The ethyl acetate and water fractions were separated, and the remaining water in the ethyl acetate was removed with anhydrous sodium sulfate. The ethyl acetate was removed by a rotary evaporator, and the extract was dried in vacuo to yield 25 g of organic material.

Isolation of Lydiamycin A. The crude extract was injected directly onto a preparative reversed-phase HPLC column (C_{18} Luna 10 μm C_{18}(2) 250 × 21.2 mm, 10 mL/min, detection: UV at 210 nm) and separated using a gradient solvent system from 30% to 70% CH_3CN/water over 40 min. Lydiamycin A (**11**) was isolated at a retention time of 31 min (10 mg). Compound **11** was further purified on a CN HPLC column (YMC CN, 250 × 10 mm, S-5 μm, 12 nm) using a gradient (30% CH_3CN/water to 70% CH_3CN/water over 40 min, UV detection at 210 nm, flow rate: 2 mL/min) to yield **11** (t_R 25 min, 7.7 mg).

Lydiamycin A (**11**): white amorphous solid; $[\alpha]_D^{20}$ – 21 (*c* 0.1, $CHCl_3$); UV (MeOH) λ_{max} (log ε) 200 (3.31) nm; IR (neat) ν_{max} 3310, 2941, 2829, 1407, 1022, 632 cm^{-1}; ^1H, ^{13}C and 2D-NMR (800 MHz, DMSO-d_6 and $CDCl_3$), see Table 6; HRMS (FAB) *m*/*z*: $[M+H]^+$ Calcd for $C_{31}H_{50}N_7O_9$, 664.3670; Found 664.3666.

Determination of the absolute configurations of the amino acid units. Lydiamycin A (**11**) (1.5 mg) was hydrolyzed in 6 N HCl at 115 ℃ for 2 h. After removing the HCl in vacuo, the hydrolysate was divided into two vials. The hydrolysate was dissolved in 200 μL of 1 N $NaHCO_3$, and L- and D-FDAA (100 μL of 10 mg/mL in acetone) were each added to one of the reaction vials. The reactions were maintained at 80 ℃ for 3 min. The reaction mixtures were then neutralized with 100 μL of 2 N HCl and dried in vacuo. The reaction products were dissolved in 300 μL of MeOH, and 20 μL of each reaction mixture was analyzed by LC/MS using a Phenomenex C_{18}(2) column (Luna, 100 × 4.6 mm, 5 μm) under gradient solvent conditions (flow rate 0.7 mL/min; UV 340 nm detection; 10% to 60% CH_3CN/H_2O with 0.1% formic acid over 50 min).

Table 7. LC/MS analysis of L- and D-FDAA derivatives of lydiamycin A (**1**)

Lydiamycin A (**1**)					
	Ala	Ser	Leu	Pip	ΔPip
$[M + H]^+$ (*m*/*z*)	342	358	384	383	381
Retention time (min)					
L-FDAA	23.4	18.3	38.2	24.3	23.3
D-FDAA	26.1	18.5	33.9	21.5	23.0
Elution order	L→D	L→D	D→L	D→L	D→L
Supposed configuration	L	L	D	S	?

Table 8. LC/MS analysis of L- and D-FDAA derivatives of the reduction product of **11**

Lydiamycin A (**1**)					
	Ala	Ser	Leu	Pip	ΔPip
$[M + H]^+$ (*m*/*z*)	342	358	384	383	381
Retention time (min)					
L-FDAA	23.4	18.3	38.2	24.3	not detected
D-FDAA	26.0	18.5	33.9	21.5	not detected
Elution order	L→D	L→D	D→L	D→L	
Supposed configuration	L	L	D	S	

Analysis of the structure of the FDAA adducts of piperazic acid. Depsidomycin B (10 mg), a previously reported S-piperazic acid-bearing depsipeptide,[1] was hydrolyzed in 6 N HCl at 115 ℃ for 2 h. After removing the HCl in vacuo, the hydrolysate was divided into two vials. The hydrolysate in the reaction vials was dissolved in 200 μL of 1 N $NaHCO_3$, and l- and d-FDAA (100 μL of 10 mg/mL in acetone) were each added to one reaction vial. The reaction was maintained at 80 ℃ for 3 min. The reaction mixtures were neutralized with 100 μL of 2 N HCl and dried in vacuo. The reaction products were dissolved in 500 μL of MeOH. l-FDAA-S-piperazic acid and d-FDAA-S-piperazic acid were purified by HPLC on a YMC-Triart C_{18} column (250 × 10 mm) with gradient solvent conditions (flow rate 2 mL/min; UV 360 nm detection; 30% to 50% CH_3CN/H_2O with 0.1% formic acid over 40 min). Both l-FDAA-S-piperazic acid (1.0 mg, 20% yield) and d-FDAA-S-piperazic acid (1.0 mg, 20% yield) eluted at 24 min under the purification conditions as yellowish amorphous solid.

Reduction of lydiamycin A and analysis of the FDAA adducts of piperazic acid. Lydiamycin A (**11**) (1 mg) was dried in a 40-mL vial under high vacuum. The dried compound was dissolved in 1 mL of a 2:1 mixture of acetic acid and MeOH. $NaBH_3CN$ (2 mg) was added to the solution, and the reaction mixture was stirred at room temperature under argon for 1 h. The reaction was quenched by adding 200 μL of 10% aqueous HCl solution. The reaction product was confirmed by the expected molecular ion by LC/MS analysis (ESI-LRMS m/z: $[M+H]^+$ Calcd for $C_{31}H_{52}N_7O_9$, 666; Found 666). The fraction of residue was subjected to the advanced Marfey's analysis following the same procedure mentioned above.

Conformational search and DP4 analysis of lydiamycin A (11). A conformational search of lydiamycin A (**1**) was performed using MacroModel with the Merck molecular force field (gas phase), a 10 kJ/mol upper energy limit, and a 0.001 kJ (mol Å)$^{-1}$ convergence threshold on the rms gradient to minimize computational complexity and expense. Twenty-three conformers were obtained for the 19S diastereomer, and 81 conformers were obtained for the 19R model under the 10 kJ/mol limit. The Boltzmann population of each conformer was calculated. Ground state geometry optimization of each conformer was carried out by density functional theory (DFT) modeling and TurbomoleX 4.3.2. The basis set for the calculation was def-SV(P) for all atoms, and the level of theory was B3-LYP at the functional level in the gas phase. The calculated ^{1}H and ^{13}C chemical shift values were averaged by the Boltzmann populations. By comparing these Boltzmann averaged chemical shifts and the experimental chemical shifts, the DP4 analyses indicated the 14S configuration of **1** with 100.0% probability.

Figure 25. Result of DP4 calculation from the simulated models of two possible diastereomers (19*S*, 19*R*).

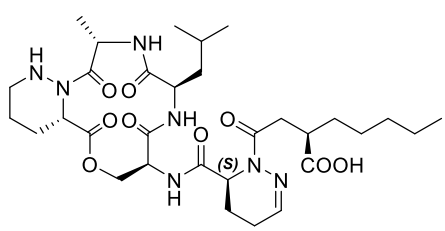

Diastereomer 1 (19*S*)

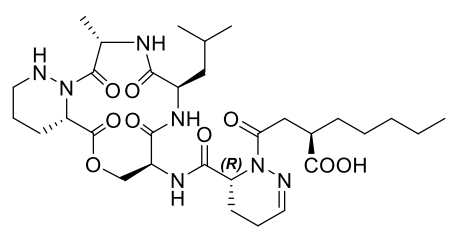

Diastereomer 2 (19*R*)

DP4 Calculation result

Both carbon and proton data:
Diastereomer 1 (19*S*) – 100.0%
Diastereomer 2 (19*R*) – 0.0%

Carbon data only:
Diastereomer 1 (19*S*) – 100.0%
Diastereomer 2 (19*R*) – 0.0%

Proton data only:
Diastereomer 1 (19*S*) – 100.0%
Diastereomer 2 (19R) – 0.0%

PGME derivatization of lydiamycin A (11). Lydiamycin A (**11**) (2 mg) was dissolved in 1 mL of dimethylformamide (DMF) and equal portions were transferred into two vials. The vials were treated with 5 mg of benzotriazol-1-yl-oxytripyrrolidinophosphonium hexafluorophosphate (PyBOP), 2 mg of hydroxybenzotriazole (HOBt) and 100 μL of 4-methylmorpholine. *S*-PGME reagent (5 mg) was added to one vial, and *R*-PGME (5 mg) was added to the other. The reaction mixtures were stirred at rt for 1 h, and the reactions were quenched with 5% HCl. After the reaction mixtures were dried *in vacuo*, the mixtures were purified on a reversed-phase HPLC column (C_{18} Luna 10 μm C_{18}(2) 250 × 21.2 mm, 10 mL/min, detection: UV at 210 nm) with a gradient solvent system from 40% to 70% CH_3CN/H_2O over 40 min. The *S*- and *R*-PGME products (**11a** and **11b**) of **1** eluted at 46 min as white amorphous solid. The weights of reaction products were 0.7 mg (**11a**, 57% yield) and 0.8 mg (**11b**, 66% yield), respectively. The molecular formular of **11a** and **11b** were determined as $C_{40}H_{58}N_8O_{10}$ by LRMS (ESI) (*m/z*: $[M+H]^+$ 811 Calcd for $C_{40}H_{59}N_8O_{10}$; Found 811 / $[M+Na]^+$ 833 Calcd for $C_{40}H_{58}N_8O_{10}Na$; Found 833). The $\Delta\delta_{S-R}$ values of the products were calculated based on their ^1H and

COSY NMR spectra data.

S-PGME product (**11a**) (0.7 mg): ^{1}H NMR (DMSO-d_6, 800 MHz) δ_H 8.67 (1H, d, *J* = 7.2 Hz), 8.49 (1H, br s), 8.23 (1H, d, *J* = 7.0 Hz), 8.18 (1H, d, *J* = 8.8 Hz), 7.93 (1H, d, *J* = 9.0 Hz), 7.39-7.33 (5H, m), 6.89 (1H, d, *J* = 4.2 Hz), 5.35 (1H, d, *J* = 7.0 Hz), 5.04 (1H, d, *J* = 5.5 Hz), 4.93 (1H, m), 4.60 (1H, dd, *J* = 10.5, 6.9 Hz), 4.52 (1H, d, *J* = 12.5 Hz), 4.41 (1H, dt, *J* = 9.3, 7.2 Hz), 4.37 (1H, dt, *J* = 8.5, 7.5 Hz), 4.29 (1H, m), 3.80 (1H, t, *J* = 10.0 Hz), 3.75 (1H, m), 3.60 (3H, s), 3.02 (1H, d, *J* = 12.5 Hz), 2.62 (1H, m), 2.34 (1H, dd, *J* = 15.3, 6.2 Hz), 2.21 (1H, m), 2.15-2.09 (2H, m), 1.84 (1H, m), 1.74 (1H, m), 1.69 (1H, m), 1.56-1.50 (2H, m), 1.47-1.41 (2H, m), 1.37 (3H, d, *J* = 7.4 Hz), 1.34 (1H, m), 1.27-1.17 (10H, m), 0.88 (3H, d, *J* = 6.1 Hz), 0.85 (3H, t, *J* = 7.0 Hz), 0.81 (3H, d, *J* = 6.0 Hz)

R-PGME product (**11b**) (0.6 mg): ^{1}H NMR (DMSO-d_6, 800 MHz) δ_H 8.69 (1H, d, *J* = 7.6 Hz), 8.50 (2H, br s), 8.30 (1H, d, *J* = 7.0 Hz), 8.22 (1H, d, *J* = 8.7 Hz), 7.93 (1H, d, *J* = 8.9 Hz), 7.38-7.32 (5H, m), 6.86 (1H, d, *J* = 4.1 Hz), 5.40 (1H, d, *J* = 7.6 Hz), 5.04 (1H, d, *J* = 6.0 Hz), 4.96 (1H, m), 4.61 (1H, dd, *J* = 10.6, 6.8 Hz), 4.52 (1H, d, *J* = 12.6 Hz), 4.42 (1H, dt, *J* = 9.5, 7.0 Hz), 4.37 (1H, dt, *J* = 8.5, 7.5 Hz), 4.30 (1H, m), 3.82 (1H, t, *J* = 10.0 Hz), 3.75 (1H, m), 3.60 (3H, s), 3.02 (1H, d, *J* = 12.5 Hz), 2.62 (1H, m), 2.34 (1H, dd, *J* = 15.1, 6.5 Hz), 2.23 (1H, m), 2.16-2.09 (2H, m), 1.84 (1H, m), 1.77 (1H, m), 1.69 (1H, m), 1.56-1.51 (2H, m), 1.49-1.41 (4H, m), 1.37 (3H, d, *J* = 7.3 Hz), 1.31-1.12 (12H, m), 0.89 (3H, d, *J* = 6.2 Hz), 0.82 (3H, d, *J* = 6.5 Hz), 0.81 (3H, t, *J* = 7.3 Hz)

Determination of MIC value of lydiamycin A (11) for *Mycobacterium tuberculosis* by resazurin microtitre assay (REMA). The MIC values of lydiamycin A (**11**) were determined as described previously. Briefly, the *M.*

tuberculosis mc^2 6230 strain was grown at 37 ℃ in Middlebrook 7H9 broth containing 0.2% casamino acids and 0.24 µg/mL pantothenate. A 100-µL aliquot of media was added to each well of a 96-well microtiter plate, and two-fold serial dilutions of lydiamycin A (**11**) were carried out directly in each well. Log-phase *M. tuberculosis* cultures were added to each well to a final OD600 of 0.05, and the plates were incubated at 37 ℃ for 5 days. Resazurin (0.025% [wt/vol]) was added to each well, and the fluorescence was measured (ex/em 560/590 nm) using a SpectraMax® M3 Multi-Mode Microplate Reader (Molecular Devices, CA, USA). The MIC values were calculated using Prism 6 (GraphPad Software, Inc., La Jolla, CA).

Summary

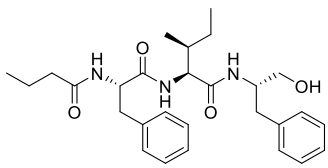

1

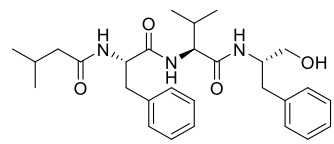

2

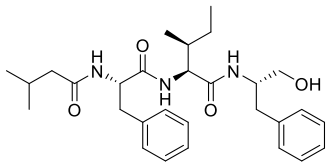

3

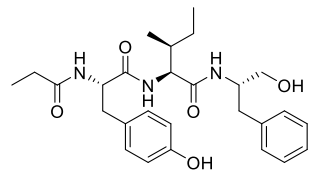

4

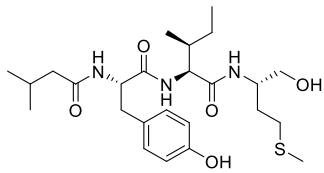

5

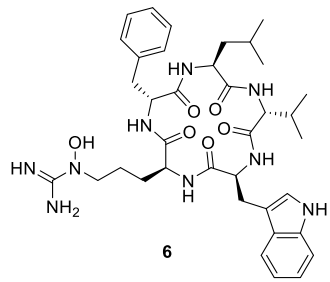

6

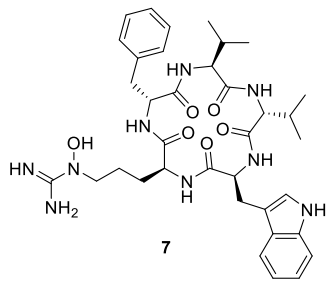

7

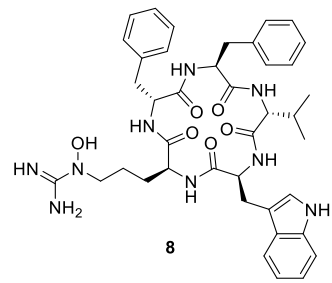

8

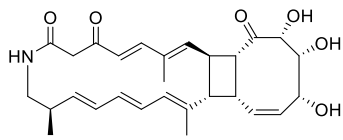

9

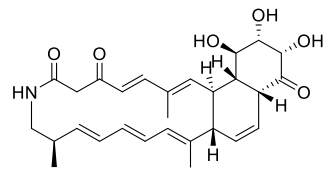

10

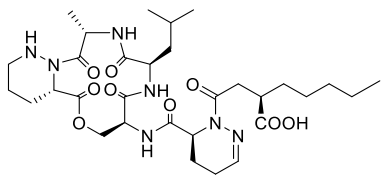

11

In this thesis for degree of doctor of philosophy, I focused on discovery of new peptides from actinomycetes (Part A, **1**-**8**) and structural revision of known compounds (Part B, **9**-**11**).

In part A, five new peptides, acidiphilamides A-E (**1**-**5**) were discovered by acidophilic actinomycetes, *Streptacidiphilus rugosus* AM-16. The strain was isolated from acidic soil of pine tree forest, so the strain need to be cultured using acidic media acidized by HCl. The structures of these compounds were identified by 1D and 2D spectra and the absolute configurations were confirmed by advanced Marfey's method and GITC derivatization followed by LC/MS analysis. Acidiphilamide A and B have moderate autophagy inhibition activities *in vitro*.

Pentaminomycins C-E (**6**-**8**) were isolated by the strain of *Streptomyces* sp. GG23 which was derived from the gut of mealworm beetles. These cyclic peptides were the derivatives of the known compounds, pentaminomycin A and B. The structures were similar with the reported structures except the composition of amino acid units. The biosynthetic pathway of the compounds could be proposed by whole genome sequence analysis. The pentapeptide chain was assembled by 5 NRPS modules and the cyclization was performed by penicillin binding protein type thioesterase (PBP-type TE). Hydroxylation of arginine moiety was catalyzed by cytochrome P450. Pentaminomycin C and D (**7** and **8**) have autophagic inducing activities *in vitro*.

In part B, structural uncertainty of a unique tricyclic lactam compound, tripartilactam (**9**) had been raised. To figure out the exact structure of tripartilactam, ^{13}C-^{13}C COSY NMR experiment was performed. ^{13}C labeled tripartilactam was produced using the culture media composed of ^{13}C isotope universally labeled glucose. It was determined that the originally reported

structure of tripartilactam (**9**) was wrong and the revised structure (**10**) was right. The biosynthetic pathway was proposed by whole genome sequence analysis with mutagenesis experiments.

Lydiamycin A (**11**) was discovered from the strain, GG23 which producing pentaminomycins using different culture media. Lydiamycin A is cyclic depsipeptide containing two piperazic acid moieties. In spite of a couple of total synthetic trials, the absolute configuration of lydiamycin A was not determined completely. The planar structure of lydiamycin A was determined by NMR spectroscopic data which was identical with the reported structure. The absolute configuration of α position of the amino acids were determined by advanced Marfey's method. The absolute configuration of piperazic acid in the macro ring was determined as *S* which was opposite with the originally reported. The stereochemistry of dehydropiperazic acid was identified by CN double bond reduction followed by additional Marfey's method. Only *S* piperazic acid product was detected by LC/MS analysis which means the absolute configuration of dehydropiperazic acid is *S*. The last chiral center of 2-pentyl succinic acid moiety was determined by PGME derivatization. The absolute configuration of dehydropiperazic acid was reconfirmed by DP4 calculation.

Reference

1. Baltz, R. H. Renaissance in antibacterial discovery from actinomycetes *Curr. Opin. Pharmacol.* **2008**, *8*, 557–563.

2. Bérdy, J. Thoughts and facts about antibiotics: where we are now and where we are heading *J. Antibiot.* **2012**, *65*, 385–395.

3. Galluzzi, L.; Baehrecke, E. H.; Ballabio, A.; Boya, P.; Bravo-San Pedro, J. M.; Cecconi, F.; Choi, A. M.; Chu, C. T.; Codogno, P.; Colombo, M. I.; Cuervo, A. M.; Debnath, J.; Deretic, V.; Dikic, I.; Eskelinen, E. L.; Fimia, G. M.; Fulda, S.; Gewirtz, D. A.; Green, D. R.; Hansen, M.; Harper, J. W.; Jaattela, M.; Johansen, T.; Juhasz, G.; Kimmelman, A. C.; Kraft, C.; Ktistakis, N. T.; Kumar, S.; Levine, B.; Lopez-Otin, C.; Madeo, F.; Martens, S.; Martinez, J.; Melendez, A.; Mizushima, N.; Munz, C.; Murphy, L. O.; Penninger, J. M.; Piacentini, M.; Reggiori, F.; Rubinsztein, D. C.; Ryan, K. M.; Santambrogio, L.; Scorrano, L.; Simon, A. K.; Simon, H. U.; Simonsen, A.; Tavernarakis, N.; Tooze, S. A.; Yoshimori, T.; Yuan, J.; Yue, Z.; Zhong, Q.; Kroemer, G. Molecular definitions of autophagy and related processes *EMBO J.* **2017**, *36*, 1811–1836.

4. Cheng, Y.; Ren, X.; Hait, W. N.; Yang, J.-M. Therapeutic targeting of autophagy in disease: biology and pharmacology *Pharmacol. Rev.* **2013**, *65*, 1162–1197.

5. Fujii, K.; Ikai, Y.; Oka, H.; Suzuki, M.; Harada, K. A Nonempirical Method Using LC/MS for Determination of the Absolute Configuration of Constituent Amino Acids in a Peptide:

Combination of Marfey's Method with Mass Spectrometry and Its Practical Application *Anal. Chem.* **1997**, *69*, 5146–5151.

6. Hess, S.; Gustafson, K. R.; Milanowski, D. J.; Alvira, E.; Lipton, M. A.; Pannell, L. K. Chirality determination of unusual amino acids using precolumn derivatization and liquid chromatography–electrospray ionization mass spectrometry *J. Chromatogr. A* **2004**, *1035*, 211–219.
7. Kokai Tokkyo Koho Jpn. Patent No. JP 07179412, 1995
8. Hirao, T.; Tsuge, N.; Imai, S.; Shin-Ya, K.; Seto, H. Nerfilin I, a novel microbial metabolite inducing neurite outgrowth of PC12 cells *J. Antibiot.* **1995**, *48*, 1494–1496.
9. Teramura, K.; Orita, M.; Matsumoto, H.; Yasumuro, K.; Abe, K. Effects of Ym-51084 and Ym-51085, new inhibitors produced by *Streptomyces* sp. Q21705, on Cathepsin L *J. Enzyme Inhib.* **1996**, *11*, 115–121.
10. Kim, E.; Park, S.; Lee, J. H.; Mun, J. Y.; Choi, W. H.; Yun, Y.; Lee, J.; Kim, J. H.; Kang, M. J.; Lee, M. J. Dual function of USP14 deubiquitinase in cellular proteasomal activity and autophagic flux *Cell Rep.* **2018**, *24*, 732–743.
11. Jiang, Y.; Lee, J.; Lee, J. H.; Lee, J. W.; Kim, J. H.; Choi, W. H.; Yoo, Y. D.; Cha-Molstad, H.; Kim, B. Y.; Kwon, Y. T.; Noh, S. A.; Kim, K. P.; Lee, M. J. The arginylation branch of the N-end rule pathway positively regulates cellular autophagic flux and clearance of proteotoxic proteins *Autophagy* **2016**, *12*, 2197–2212.

12. Arora, P.; Vats, A.; Saxena, P.; Mohanty, D.; Gokhale, R. Promiscuous fatty acyl CoA ligases produce acyl-CoA and acyl-SNAC precursors for polyketide biosynthesis *J. Am. Chem. Soc.* **2005**, *127*, 9388–9389.

13. Challis, G. L.; Ravel, J.; Townsend, C. A. Predictive, structure-based model of amino acid recognition by nonribosomal peptide synthetase adenylation domains *Chem. Biol.* **2000**, *7*, 211–224.

14. Schaffer, M. L.; Otten, L. G. Substrate flexibility of the adenylation reaction in the Tyrocidine non-ribosomal peptide synthetase *J. Mol. Catal. B-Enzym.* **2009**, *59*, 140–144.

15. Roemer, D.; Buescher, H. H.; Hill, R. C.; Pless, J.; Bauer, W.; Cardinaux, F.; Closse, A.; Hauser, D.; Huguenin, R. A synthetic enkephalin analogue with prolonged parenteral and oral analgesic activity *Nature* **1977**, *268*, 547–549.

16. Cho, S.-H.; Han, J.-H.; Seong, C. N.; Kim, S. B. Phylogenetic diversity of acidophilic sporoactinobacteria isolated from various soils *J. Microbiol*. **2006**, *44*, 600–606.

17. Cho, S.-H.; Han, J.-H.; Ko, H.-Y.; Kim, S. B. *Streptacidiphilus anmyonensis* sp. nov., *Streptacidiphilus rugosus* sp. nov. and *Streptacidiphilus melanogenes* sp. nov., acidophilic actinobacteria isolated from Pinus soils *Int. J. Syst. Evol. Microbiol*. **2008**, *58*, 1566–1570.

18. Kaweewan, I.; Hemmi, H.; Komaki, H.; Kodani, S. Isolation and structure determination of a new antibacterial peptide pentaminomycin C from *Streptomyces cacaoi* subsp. *cacaoi J. Antibiot.* **2020**, *73*, 224–229.

19. Jang, J.-P.; Hwang, G. J.; Kwon, M. C.; Ryoo, I.-J.; Jang, M.; Takahashi, S.; Ko, S.-K.; Osada, H.; Jang, J.-H.; Ahn, J. S. Pentaminomycins A and B, Hydroxyarginine-Containing Cyclic Pentapeptides from *Streptomyces* sp. RK88-1441 *J. Nat. Prod.* **2018**, *81*, 806–810.
20. Blin, K.; Shaw, S.; Steinke, K.; Villebro, R.; Ziemert, N.; Lee, S. Y.; Medema, M. H.; Weber, T. antiSMASH 5.0: updates to the secondary metabolite genome mining pipeline *Nucleic Acids Res.* **2019**, *47*, W81–W87.
21. Kuranaga, T.; Matsuda, K.; Sano, A.; Kobayashi, M.; Ninomiya, A.; Takata, K.; Matsunaga, S.; Wakimoto, T. Total synthesis of the nonribosomal peptide surugamide B and identification of a new offloading cyclase family *Angew. Chem. Int. Ed.* **2018**, *57*, 9447–9451.
22. Matsuda, K.; Kobayashi, M.; Kuranaga, T.; Takada, K.; Ikeda, H.; Matsunaga, S.; Wakimoto, T. SurE is a trans-acting thioesterase cyclizing two distinct non-ribosomal peptides *Org. Biomol. Chem.* **2019**, *17*, 1058–1061.
23. Miao, S.; Anstee, M. R.; LaMarco, K.; Matthew, J.; Huang, L. H. T.; Brasseur, M. M. Inhibition of Bacterial RNA Polymerases. Peptide Metabolites from the Cultures of *Streptomyces* sp. *J. Nat. Prod.* **1997**, *60*, 858–861.
24. Song, Y.; Li, Q.; Liu, X.; Chen, Y.; Zhang, Y.; Sun, A.; Zhang, W.; Zhang, J.; Ju, J. Cyclic Hexapeptides from the Deep South China Sea-Derived *Streptomyces scopuliridis* SCSIO ZJ46 Active Against

Pathogenic Gram-Positive Bacteria *J. Nat. Prod.* **2014**, *77*, 1937–1941.

25. Fazal, A.; Webb, M. E.; Seipke, R. F. The desotamide family of antibiotics *Antibiotics* **2020**, *9*, 452.

26. Takada, K.; Ninomiya, A.; Naruse, M.; Sun, Y.; Miyazaki, M.; Nogi, Y.; Okada, S.; Matsunaga, S. Surugamides A–E, Cyclic Octapeptides with Four d-Amino Acid Residues, from a Marine *Streptomyces* sp.: LC–MS-Aided Inspection of Partial Hydrolysates for the Distinction of d- and l-Amino Acid Residues in the Sequence *J. Org. Chem.* **2013**, *78*, 6746–6750.

27. Son, S.; Hong, Y.-S.; Jang, M.; Heo, K.T.; Lee, B.; Jang, J.-P.; Kim, J.-W.; Ryoo, I.-J.; Kim, W.-G.; Ko, S.-K.; Kim, B. Y. ; Jang, J.-H.; Ahn, J. S. Genomics-Driven Discovery of Chlorinated Cyclic Hexapeptides Ulleungmycins A and B from a *Streptomyces* Species *J. Nat. Prod.* **2017**, *80*, 3025–3031.

28. Mudalungu, C. M.; von Törne, W. J.; Voigt, K.; Rückert, C.; Schmitz, S.; Sekurova, O. N.; Zotchev, S. B.; Süssmuth, R. D. Noursamycins, Chlorinated Cyclohexapeptides Identified from Molecular Networking of Streptomyces noursei NTR-SR4 *J. Nat. Prod.* **2019**, *82*, 1478–1486.

29. Kaweewan, I.; Komaki, H.; Hemmi, H.; Kodani, S. Combining Mass Spectrometric Metabolic Profiling with Genomic Analysis: A Powerful Approach for Discovering Natural Products from Cyanobacteria *J. Org. Chem.* **2017**, *6*, 1838–1844.

30. Magarvey, N. A.; Haltli, B.; He, M.; Greenstein, M.; Hucul, J. A.

Biosynthetic pathway for mannopeptimycins, lipoglycopeptide antibiotics active against drug-resistant gram-positive pathogens *Antimicrob. Agents Chemother.* **2006**, *50*, 2167–2177.

31. Matsuda, K.; Zhai, R.; Mori, T.; Kobayashi, M.; Sano, A.; Abe, I.; Wakimoto, T. Heterochiral coupling in non-ribosomal peptide macrolactamization *Nat. Catal.* **2020**, *3*, 507–515.

32. Goffin, C.; Ghuysen, J. M. *Microbiol. Mol. Biol. Rev.* **2002** *66*, 702–738.

33. Kojiri, K.; Ihara, M.; Nakajima, S.; Kawamura, K.; Funaishi, K.; Yano, M.; Suda, H. Biochemistry and Comparative Genomics of SxxK Superfamily Acyltransferases Offer a Clue to the Mycobacterial Paradox: Presence of Penicillin-Susceptible Target Proteins versus Lack of Efficiency of Penicillin as Therapeutic Agent *J. Antibiot.* **1991**, *44*, 1342–1347.

34. Radwanski, E. R.; Last, R. L. Tryptophan biosynthesis and metabolism: biochemical and molecular genetics *Plant. Cell* **1995**, *7*, 921–934.

35. Peraro, L.; Zou, Z.; Makwana, K. M.; Cummings, A. E.; Ball, H. L.; Yu, H.; Lin, Y.-S.; Levine, B.; Kritzer, J. A. Diversity-oriented stapling yields intrinsically cell-penetrant inducers of autophagy *J. Am. Chem. Soc.* **2017**, *139*, 7792–7802.

36. Wang, L.; Li, M.-D.; Cao, P.-P.; Zhang, C.-F.; Huang, F.; Xu, X.-H.; Liu, B.-L.; Zhang, M. Astin B, a cyclic pentapeptide from Aster tataricus, induces apoptosis and autophagy in human hepatic L-02 cells *Chem. Biol. Interact.* **2014**, *223*, 1–9.

37. Kim, E.; Park, S.; Lee, J. H.; Mun, J. Y.; Choi, W. H.; Yun, Y.; Lee, J.; Kim, J. H.; Kang, M.-J.; Lee, M. J. *Cell Rep.* **2018**, *24*, 732–743.

38. Filomeni, G.; De Zio, D.; Cecconi, F. Dual function of USP14 deubiquitinase in cellular proteasomal activity and autophagic flux *Cell Death Differ.* **2015**, *22*, 377–388.

39. Choi, W. H.; De Poot, S. A.; Lee, J. H.; Kim, J. H.; Han, D. H.; Kim, Y. K.; Finley, D.; Lee, M. J. Open-gate mutants of the mammalian proteasome show enhanced ubiquitin-conjugate degradation *Nat. Commun.* **2016**, *7*, 1–12.

40. Choi, W. H.; Yun, Y.; Park, S.; Jeon, J. H.; Lee, J.; Lee, J. H.; Yang, S.-A.; Kim, N.-K.; Jung, C. H.; Kwon, Y. T.; Han, D.; Lim, S. M.; Lee, M. J. Aggresomal sequestration and STUB1-mediated ubiquitylation during mammalian proteaphagy of inhibited proteasomes *Proc. Natl. Acad. Sci. USA* **2020**, *117*, 19190–19200.

41. Chhetri, B. K.; Lavoie, S.; Sweeney-Jones, A. M.; Kubanek, J. Recent trends in the structural revision of natural products *Nat. Prod. Rep.* **2018**, *35(6)*, 514-531.

42. Park, S.-H.; Moon, K.; Bang, H.-S.; Kim, S.-H.; Kim, D.-G.; Oh, K.-B.; Shin, J.; Oh, D.-C. Tripartilactam, a Cyclobutane-Bearing Tricyclic Lactam from a *Streptomyces* sp. in a Dung Beetle's Brood Ball *Org. Lett.* **2012**, *14*, 1258–1261.

43. Hoshino, S.; Okada, M.; Wakimoto, T.; Zhang, H.; Hayashi, F.; Onaka, H.; Abe, I. Niizalactams A–C, Multicyclic Macrolactams Isolated from Combined Culture of *Streptomyces* with Mycolic Acid-Containing Bacterium *J. Nat. Prod.* **2015**, *78*, 3011–3017.

44. Huang, X.; Roemer, E.; Sattler, I.; Moellmann, U.; Christner, A.; Grabley, S. Lydiamycins A–D: cyclodepsipetides with antimycobacterial properties *Angew. Chem. Int. Ed.* **2006**, *45*, 3067−3072.

45. Li, W.; Gan, J.; Ma, D. A concise route to the proposed structure of lydiamycin B, an antimycobacterial depsipeptide *Org. Lett.* **2009**, *11*, 5694−5697.

46. Chen, B.; Dai, L.; Zhang, H.; Tan, W.; Xu, Z.; Ye, T. A concise route to the proposed structure of lydiamycin B, an antimycobacterial depsipeptide *Chem. Commun.* **2010**, *46*, 574−576.

47. Minch, M. Orientational dependence of vicinal proton-proton NMR coupling constants: The Karplus relationship *Concept. Magnetic Res.* **1994**, *6*, 41–56.

48. Kwon, Y.; Park, S.; Shin, J.; Oh, D.-C. Application of 13C-labeling and 13C–13C COSY NMR experiments in the structure determination of a microbial natural product *Arch. Pharm. Res.* **2014**, *37*, 967–971.

49. Blin, K.; Wolf, T.; Chevrette, M. G.; Lu, X.; Schwalen, C. J.; Kautsar, S. A.; Suarez Duran, H. G.; de Los Santos, E. L. C.; Kim, H. U.; Nave, M.; Dickschat, J. S.; Mitchell, D. A.; Shelest, E.; Breitling, R.; Takano, E.; Lee, S. Y.; Weber, T.; Medema, M. H. antiSMASH 4.0-improvements in chemistry prediction and gene cluster boundary identification *Nucleic Acids Res.* **2017**, *45*, W36–W41.

50. Miyanaga, A.; Kudo, F.; Eguchi, T. Mechanisms of β-amino acid incorporation in polyketide macrolactam biosynthesis *Curr. Opin. Chem. Biol.* **2016**, *35*, 58–64.

51. Low, Z. J.; Pang, L. M.; Ding, Y.; Cheang, Q. W.; Hoang, K. L. M.; Tran, H. T.; Li, J.; Liu X.-W.; Kanagasundaram, Y.; Yang, L.; Liang Z.-X. Identification of a biosynthetic gene cluster for the polyene macrolactam sceliphrolactam in a *Streptomyces* strain isolated from mangrove sediment *Sci. Rep.* **2018**, *8*, 1594.

52. Kim, H. J.; Ruszczycky, M. W.; Choi, S.-H.; Liu, Y.-N.; Liu, H.-W. Enzyme-catalysed [4+ 2] cycloaddition is a key step in the biosynthesis of spinosyn A *Nature* **2011**, *473*, 109–112.

53. Byrne, M. J.; Lees, N. R.; Han, L.-C.; van der Kamp, M. W.; Mulholland, A. J.; Stach, J. E. M.; Willis, C. L.; Race, P. R. The catalytic mechanism of a natural Diels–Alderase revealed in molecular detail *J. Am. Chem. Soc.* **2016**, *138*, 6095–6098.

54. Zhu, Y.; Zhang, W.; Chen, Y.; Yuan, C.; Zhang, H.; Zhang, G.; Ma, L.; Zhang, Q.; Tian, X.; Zhang, S.; Zhang, C. *ChemBioChem* **2015**, *16*, 2086–2093.

55. Oikawa, H.; Tokiwano, T. Characterization of heronamide biosynthesis reveals a tailoring hydroxylase and indicates migrated double bonds *Nat. Prod. Rep.* **2004**, *21*, 321–352.

56. Oh, D.-C.; Poulsen, M.; Currie, C. R.; Clardy, J. Sceliphrolactam, a Polyene Macrocyclic Lactam from a Wasp-Associated *Streptomyces* sp. *Org. Lett.* **2011**, *13*, 752–755.

57. Moss, S. J.; Martin, C. J.; Wilkinson, B. Loss of co-linearity by modular polyketide synthases: a mechanism for the evolution of chemical diversity *Nat. Prod. Rep.* **2004**, *21*, 575–593.

58. Olano, C.; Wilkinson, B.; Sánchez, C.; Moss, S. J.; Sheridan, R.; Math, V.; Weston, A. J.; Braña, A. F.; Martin, C. J.; Oliynyk, M.; Méndez, C.; Leadlay, P. F.; Salas, J. A. Biosynthesis of the Angiogenesis Inhibitor Borrelidin by *Streptomyces parvulus* Tü4055 *Chem. Biol.* **2004**, *11*, 87–97.

59. Tatsuno, S.; Arakawa, K.; Kinashi, H. Analysis of modular-iterative mixed biosynthesis of lankacidin by heterologous expression and gene fusion *J. Antibiot.* **2007**, *60*, 700–708.

60. Busch, B.; Ueberschaar, N.; Behnken, S.; Sugimoto, Y.; Werneburg, M.; Traitcheva, N.; He, J.; Hertweck, C. Multifactorial control of iteration events in a modular polyketide assembly line *Angew. Chem., Int. Ed.* **2013**, *52*, 5285–5289.

61. Xu, W.; Zhai, G.; Liu, Y.; Li, Y.; Shi, Y.; Hong, K.; Hong, H.; Leadlay, P. F.; Deng, Z.; Sun, Y. An iterative module in the azalomycin F polyketide synthase contains a switchable enoylreductase domain *Angew. Chem., Int. Ed.* **2017**, *56*, 5503–5506.

62. Ng, B. G.; Han, J. W.; Lee, D. W.; Choi, G. J.; Kim, B. S. The chejuenolide biosynthetic gene cluster harboring an iterative trans-AT PKS system in Hahella chejuensis strain MB-1084 *J. Antibiot.* **2018**, *71*, 495–505.

63. Bierman, M.; Logan, R.; O'Brien, K.; Seno, E. T.; Rao, R. N.; Schoner, B. E. Plasmid cloning vectors for the conjugal transfer of DNA from *Escherichia coli* to *Streptomyces* spp. *Gene* **1992**, *116*, 43–49.

64. Kieser, T.; Bibb, M. J.; Buttner, M. J.; Chater, K. F.; Hoopwood, D. A. Practical streptomyces genetics *Practical Streptomyces Genetics*; The John Innes Foundation: Norwich, UK, 2000.

65. Oh, D.-C.; Poulsen, M.; Currie, C. R.; Clardy, J. Dentigerumycin: a bacterial mediator of an ant-fungus symbiosis *Nat. Chem. Biol.* **2009**, *5*, 391−393.

66. Nam, S.-J.; Kauffman, C. A.; Jensen, P. R.; Fenical, W. Isolation and characterization of actinoramides A–C, highly modified peptides from a marine *Streptomyces* sp. *Tetrahedron* **2011**, *67*, 6707−6712.

67. Raju, R.; Khalil, Z. G.; Piggott, A. M.; Blumenthal, A.; Gardiner, D. L.; Skinner-Adams, T. S.; Capon, R. J. Mollemycin A: An Antimalarial and Antibacterial Glyco-hexadepsipeptide-polyketide from an Australian Marine-Derived *Streptomyces* sp. (CMB-M0244) *Org. lett.* **2014**, *16*, 1716−1719.

68. Shin, D.; Byun, W. S.; Moon, K.; Kwon, Y.; Bae, M.; Um, S.; Lee, S. K.; Oh, D.-C. Coculture of marine *Streptomyces* sp. with *Bacillus* sp. produces a new piperazic acid-bearing cyclic peptide *Front. Chem.* **2018**, *6*, 498.

69. Menegatti, C.; Lourenzon, V. B.; Rodríguez-Hernández, D.; da Paixão Melo, W. G.; Ferreira, L. L.; Andricopulo, A. D.; do Nascimento, F. S.; Pupo, M. T. Meliponamycins: Antimicrobials from

Stingless Bee-Associated *Streptomyces* sp. *J. Nat. Prod.* **2020**, *83(3)*, 610−616.

70. Lemay, M.; Ogilvie, W. W. Aqueous enantioselective organocatalytic Diels− Alder reactions employing hydrazide catalysts. A new scaffold for organic acceleration *Org. Lett.* **2005**, *7*, 4141−4144.

71. Yabuuchi, T.; Kushumi, T. Phenylglycine methyl ester, a useful tool for absolute configuration determination of various chiral carboxylic acids *J. Org. Chem.* **2000**, *65*, 397−404.

72. Smith, S. G.; Goodman, J. M. Assigning stereochemistry to single diastereoisomers by GIAO NMR calculation: The DP4 probability *J. Am. Chem. Soc.* **2010**, *132*, 12946−12959.

73. Bagno, A.; Rastrelli, F.; Saielli, G. Toward the Complete Prediction of the ^{1}H and ^{13}C NMR Spectra of Complex Organic Molecules by DFT Methods: Application to Natural Substances *Chem.-Eur. J.* **2006**, *12*, 5514−5525.

74. Kim, E.; Shin, Y.-H.; Kim, T. H.; Byun, W. S.; Cui, J.; Du, Y. E.; Lim, H.-J.; Song, M. C.; Kwon, A. S.; Kang, S. H.; Shin, J.; Lee, S. K.; Jang, J.; Oh, D.-C.; Yoon, Y. J. Characterization of the ohmyungsamycin biosynthetic pathway and generation of derivatives with improved antituberculosis activity *Biomolecules* **2019**, *9*, 672.

Appendix: NMR Spectroscopic Data

Figure S1. ^{1}H NMR spectrum (600 MHz) and ^{13}C NMR spectrum (150 MHz) of acidiphilamide A (**1**) in DMSO-d_6.

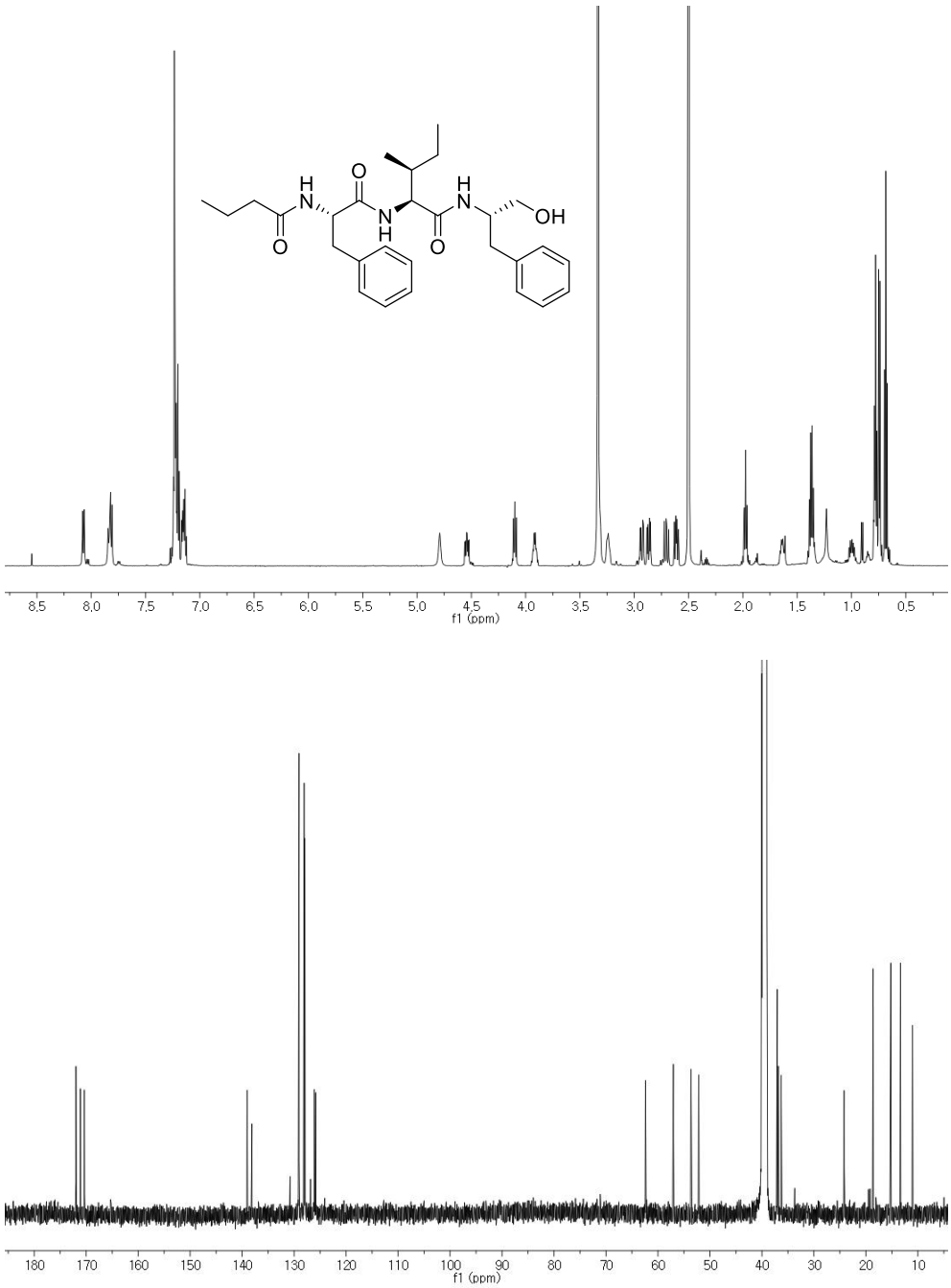

Figure S2. ^{1}H NMR spectrum (600 MHz) and ^{13}C NMR spectrum (150 MHz) of acidiphilamide B (**2**) in DMSO-d_6.

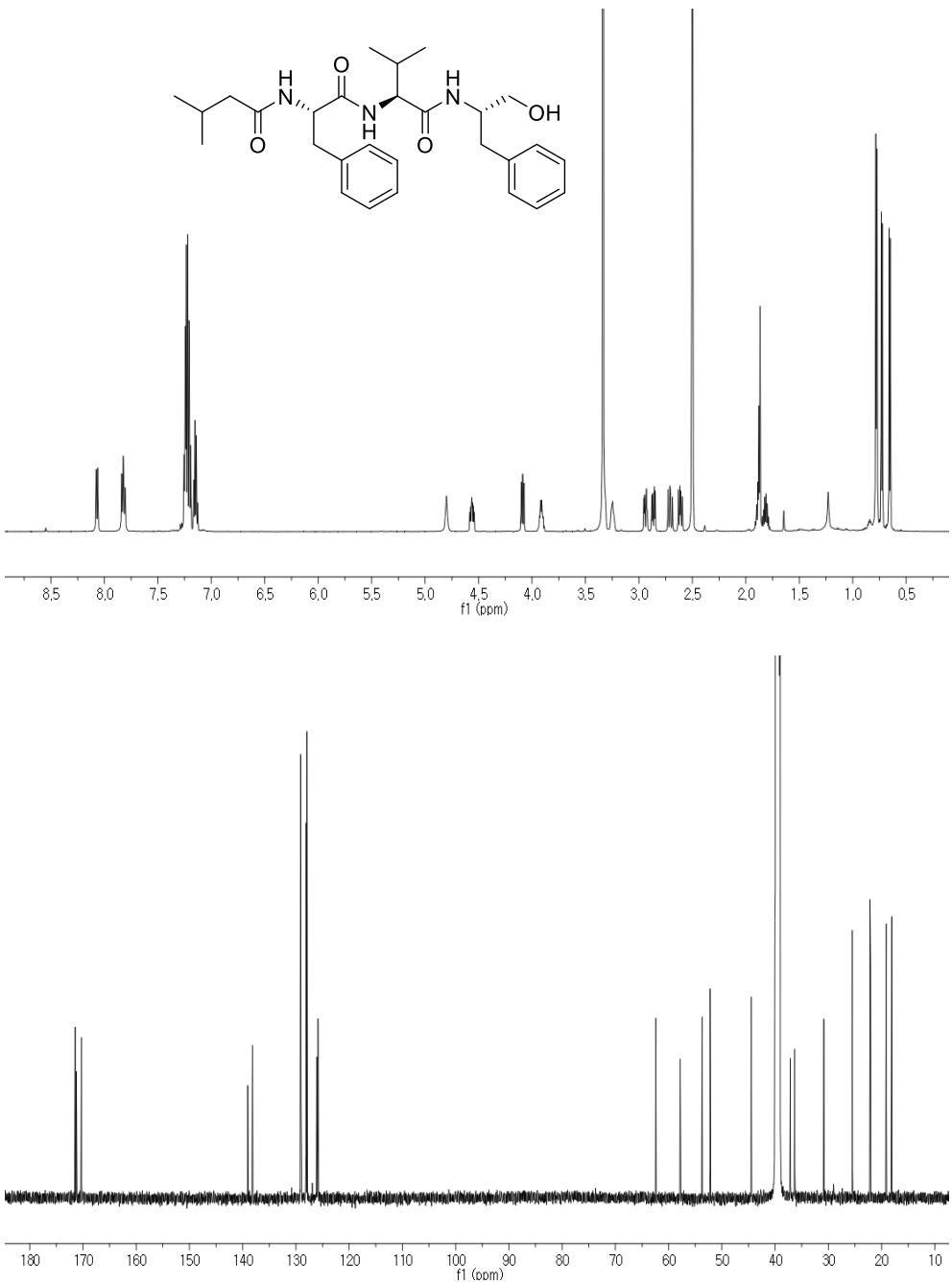

Figure S3. ^{1}H NMR spectrum (600 MHz) and ^{13}C NMR spectrum (150 MHz) of acidiphilamide C (**3**) in DMSO-d_6.

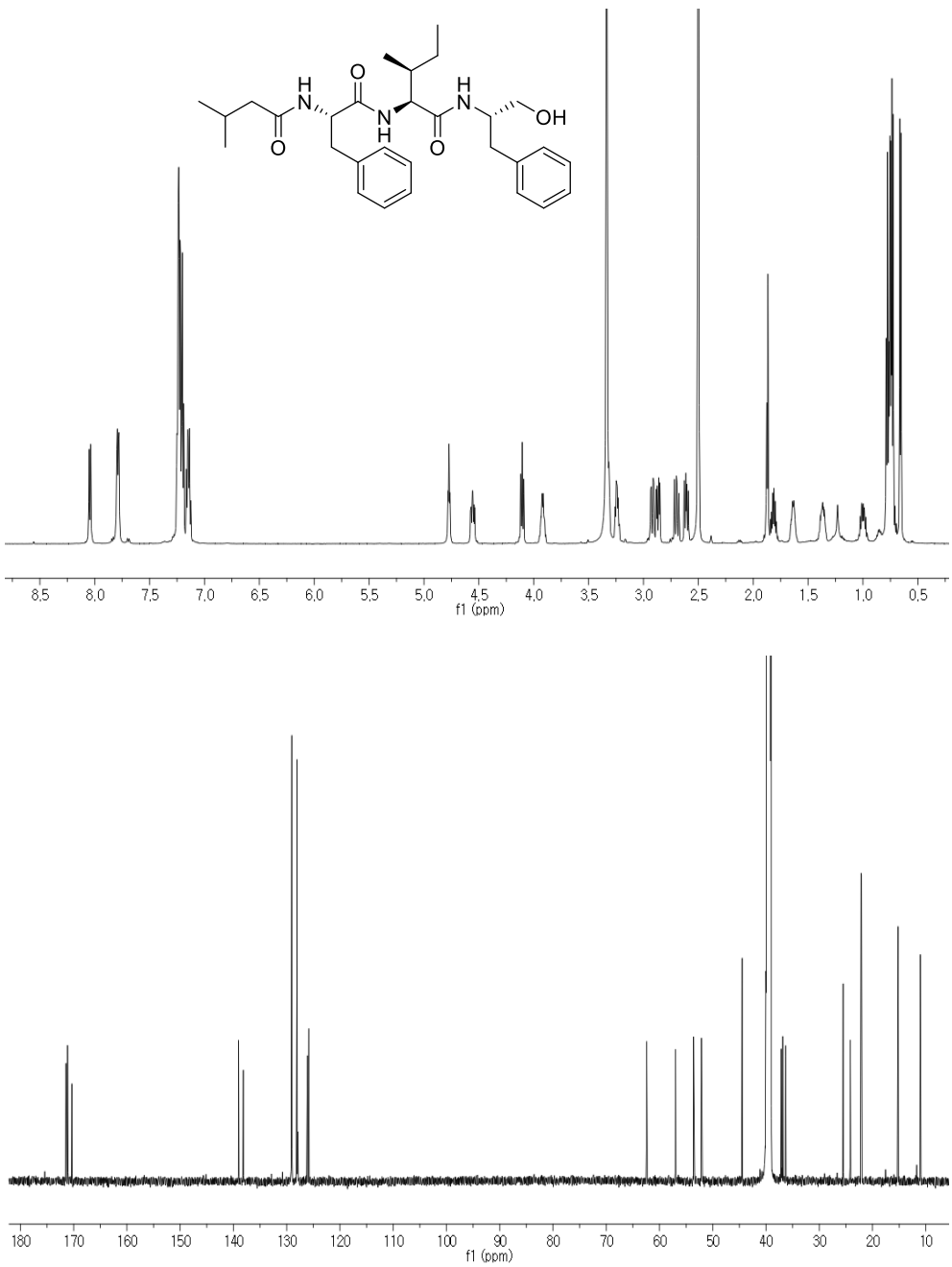

Figure S4. ^{1}H NMR spectrum (600 MHz) and ^{13}C NMR spectrum (150 MHz) of acidiphilamide D (**4**) in DMSO-d_6.

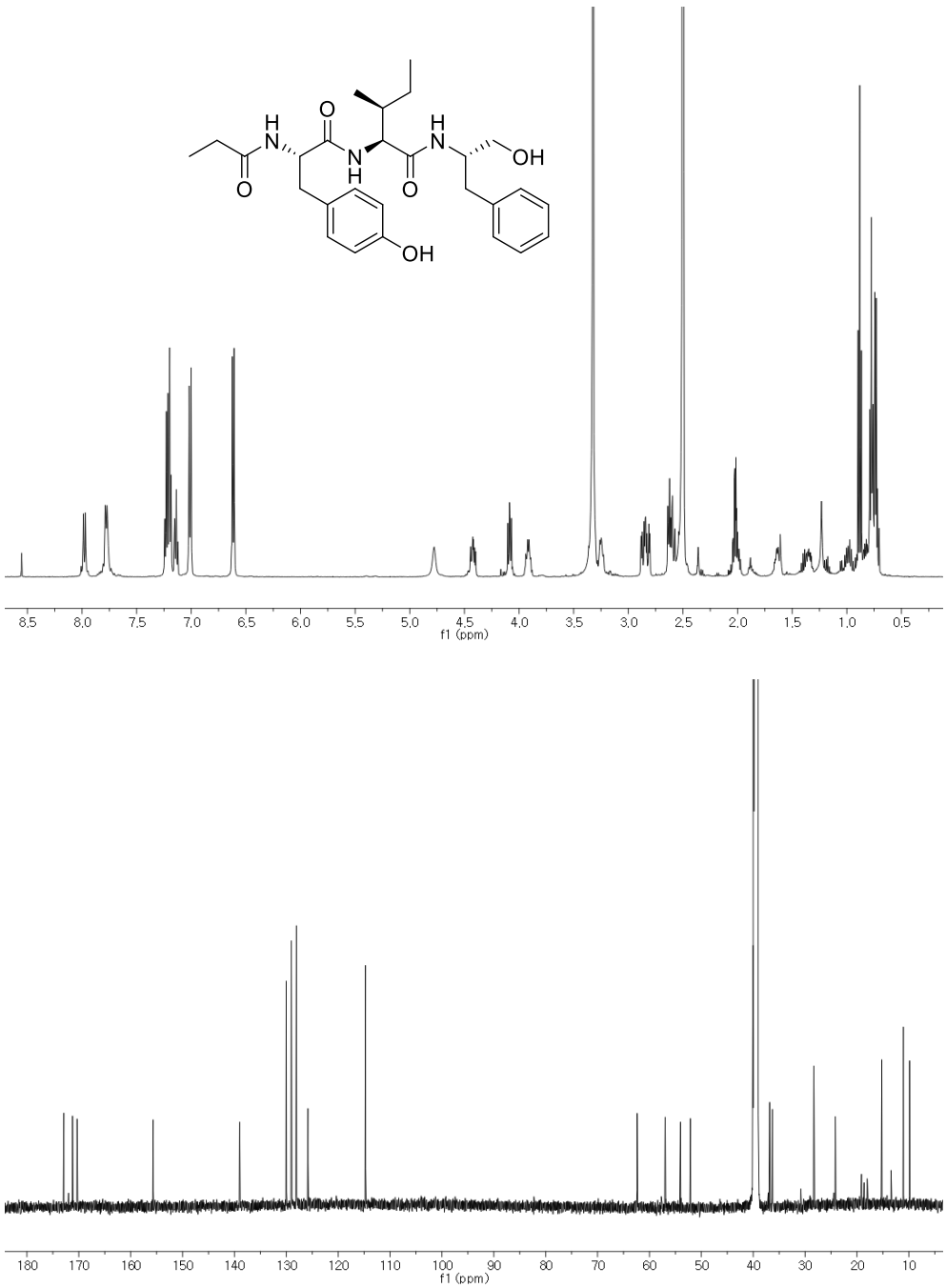

1 2 3

Figure S5. ^{1}H NMR spectrum (600 MHz) and ^{13}C NMR spectrum (150 MHz) of acidiphilamide E (**5**) in DMSO-d_6.

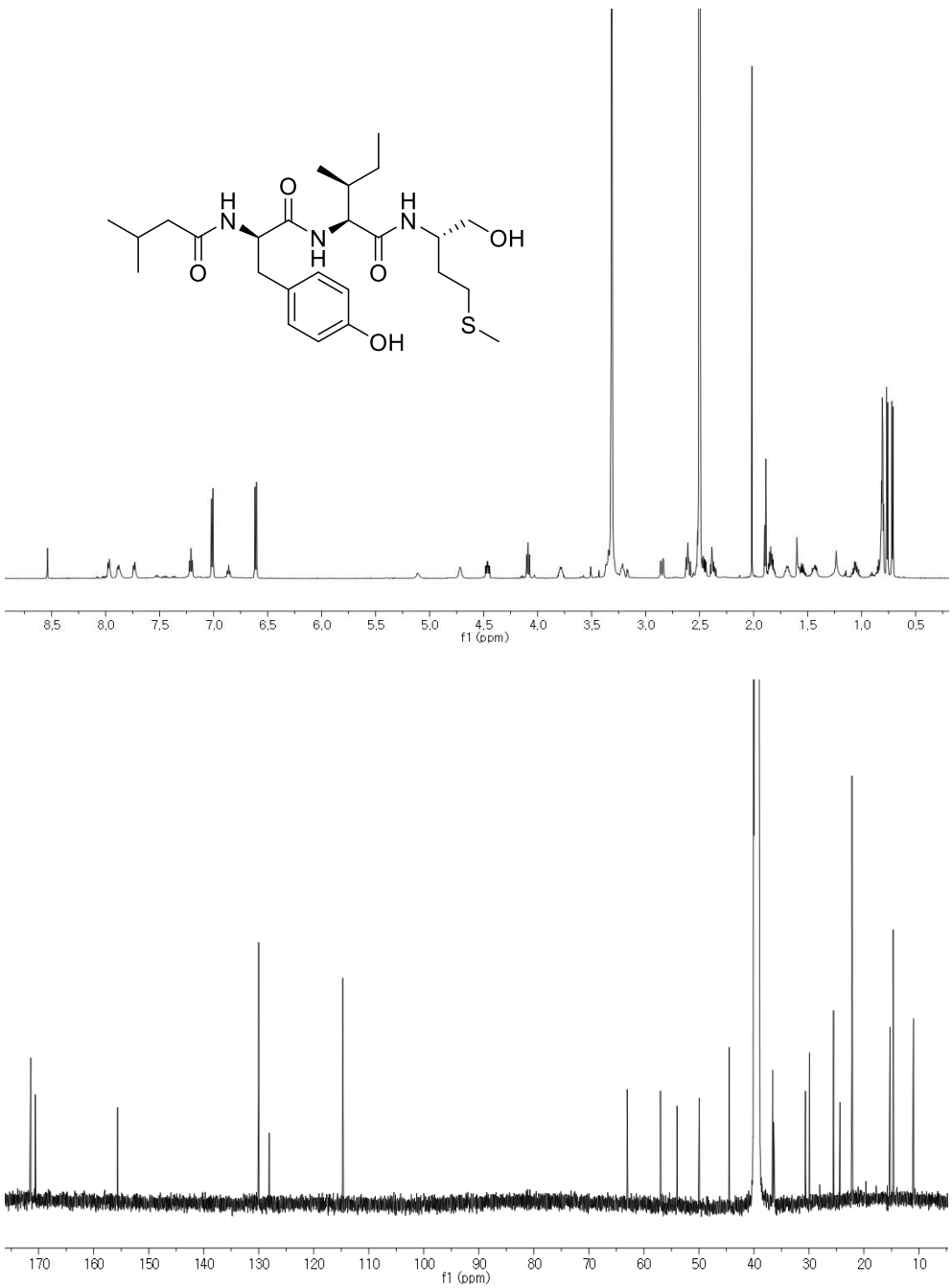

Figure S6. ^{1}H NMR spectrum (800 MHz) and ^{13}C NMR spectrum (200 MHz) of pentaminomycin C (**6**) in DMSO-d_6.

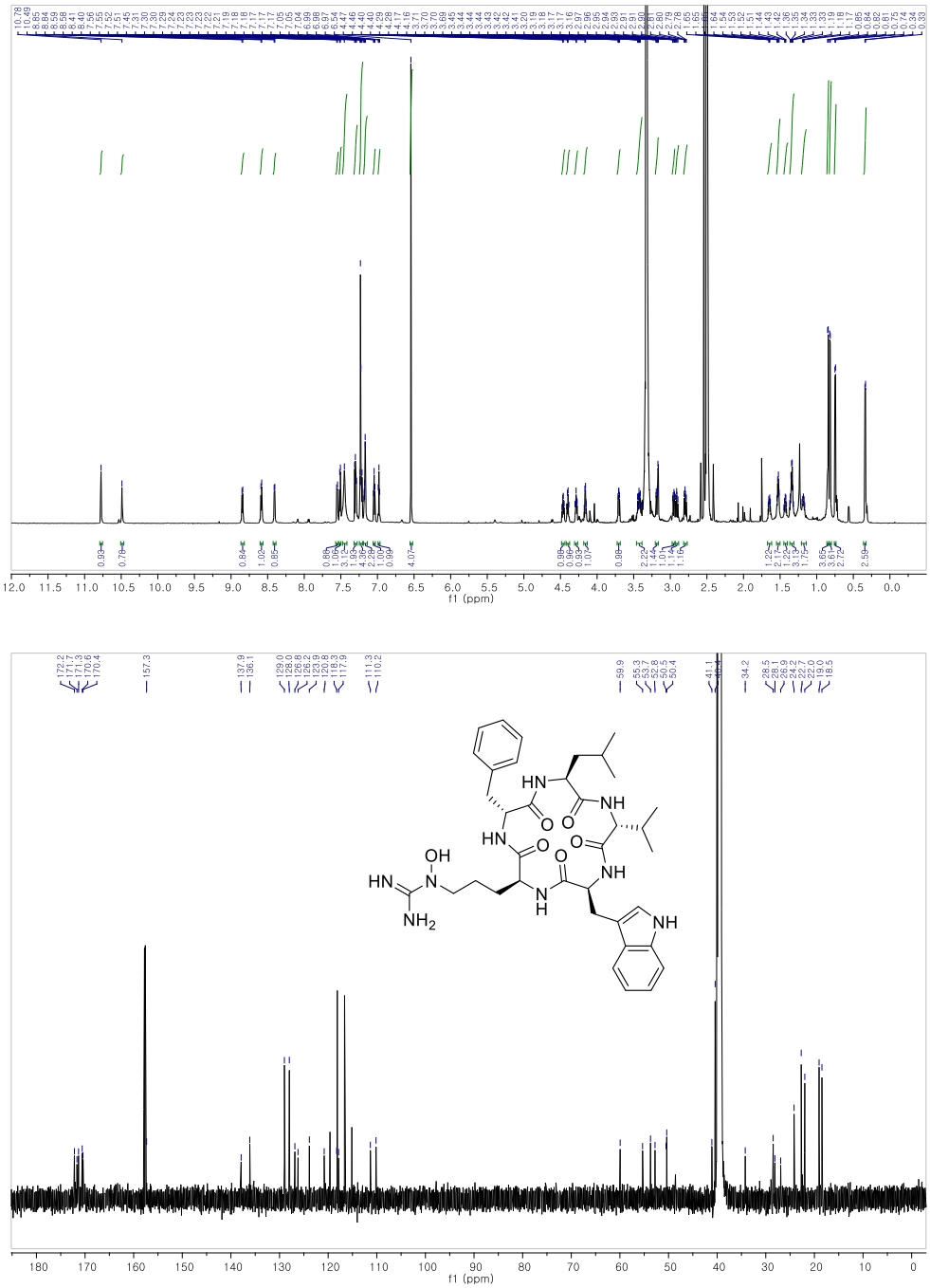

Figure S7. ^{1}H NMR spectrum (800 MHz) and ^{13}C NMR spectrum (200 MHz) of pentaminomycin D (**7**) in DMSO-d_6.

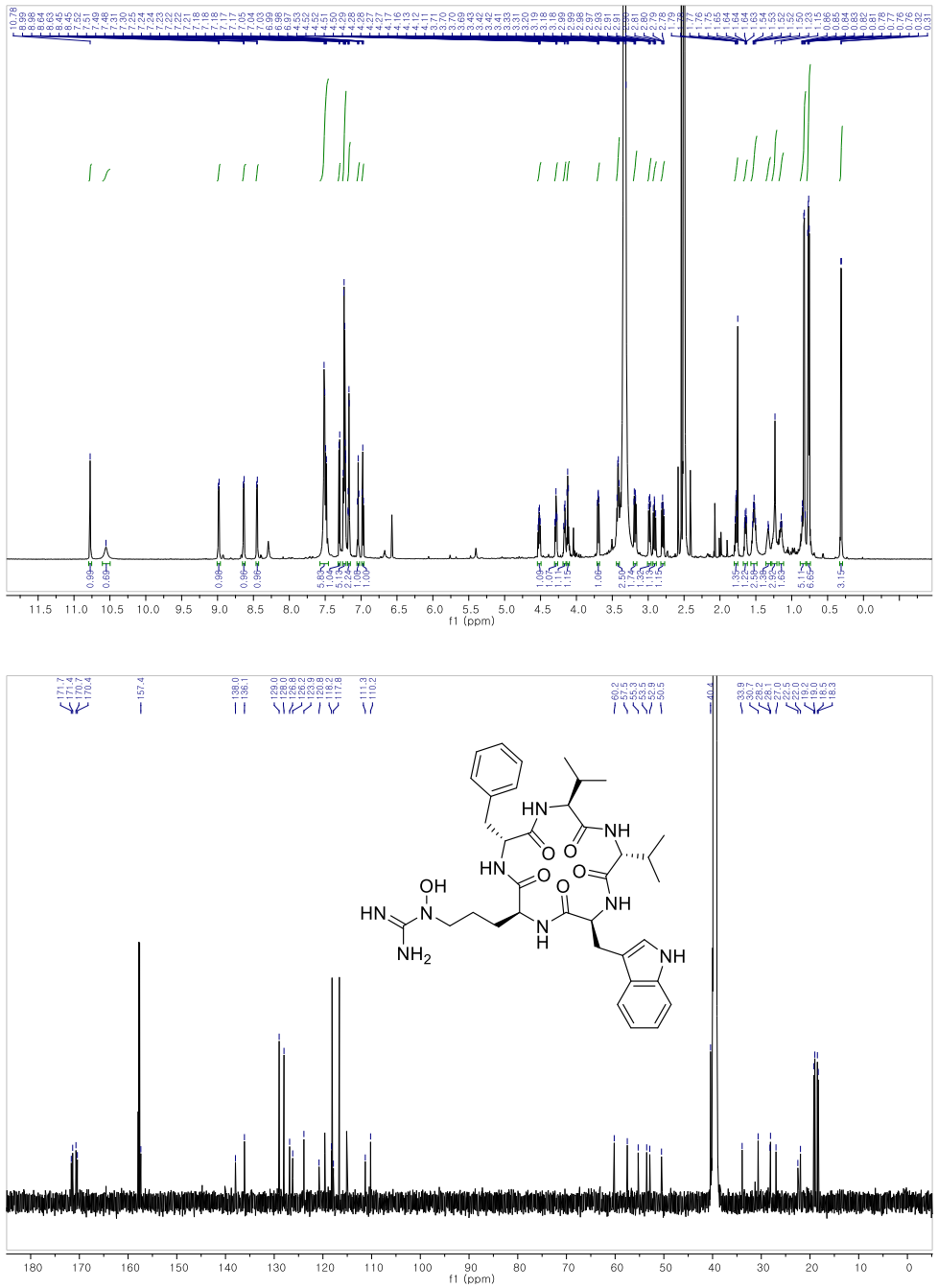

Figure S8. ^{1}H NMR spectrum (800 MHz) and ^{13}C NMR spectrum (200 MHz) of pentaminomycin E (**8**) in DMSO-d_6.

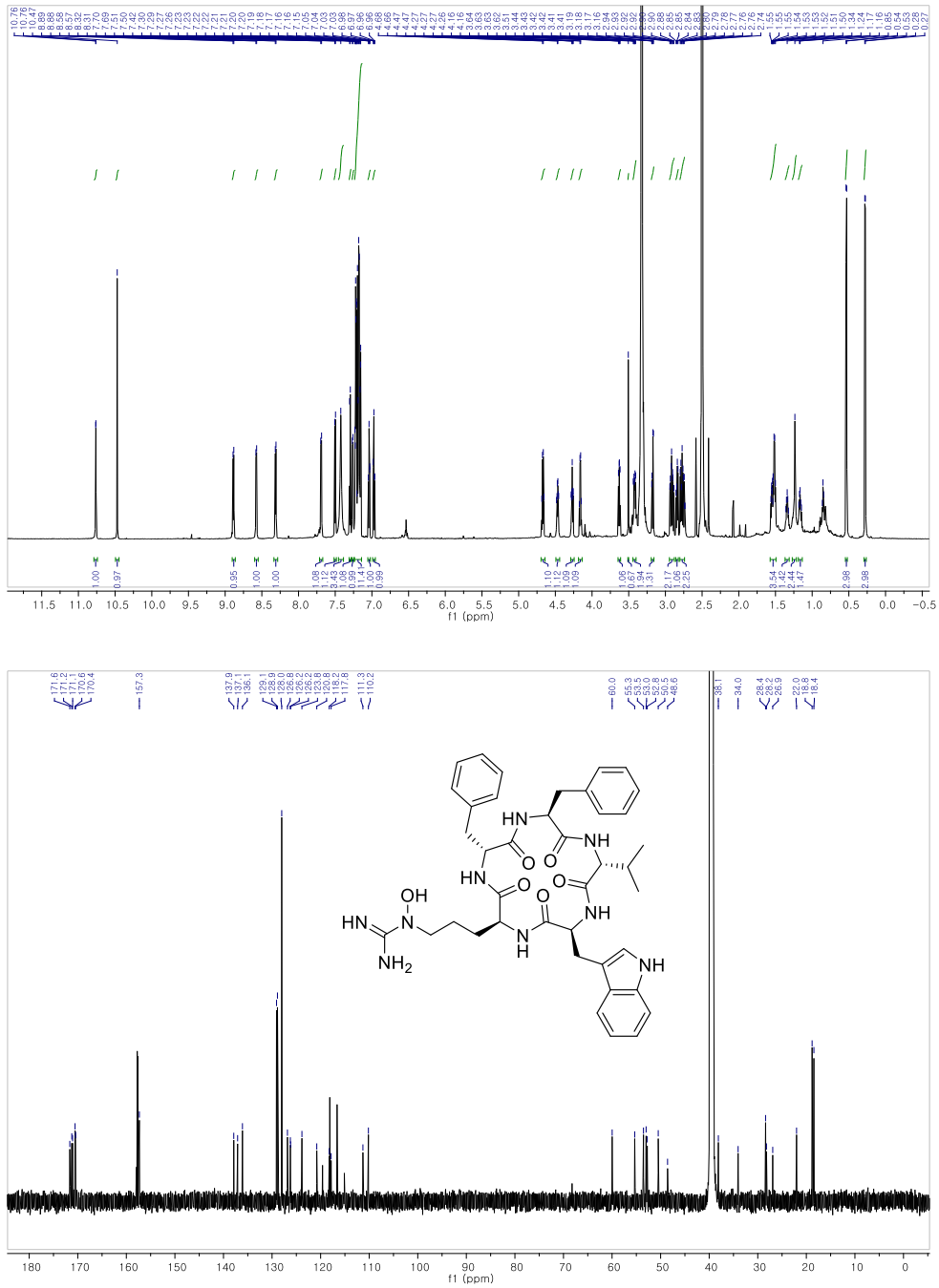

Figure S8. ^{1}H NMR spectrum (850 MHz) and ^{13}C NMR spectrum (212.5 MHz) of tripartilactam (**10**) in DMSO-d_6.

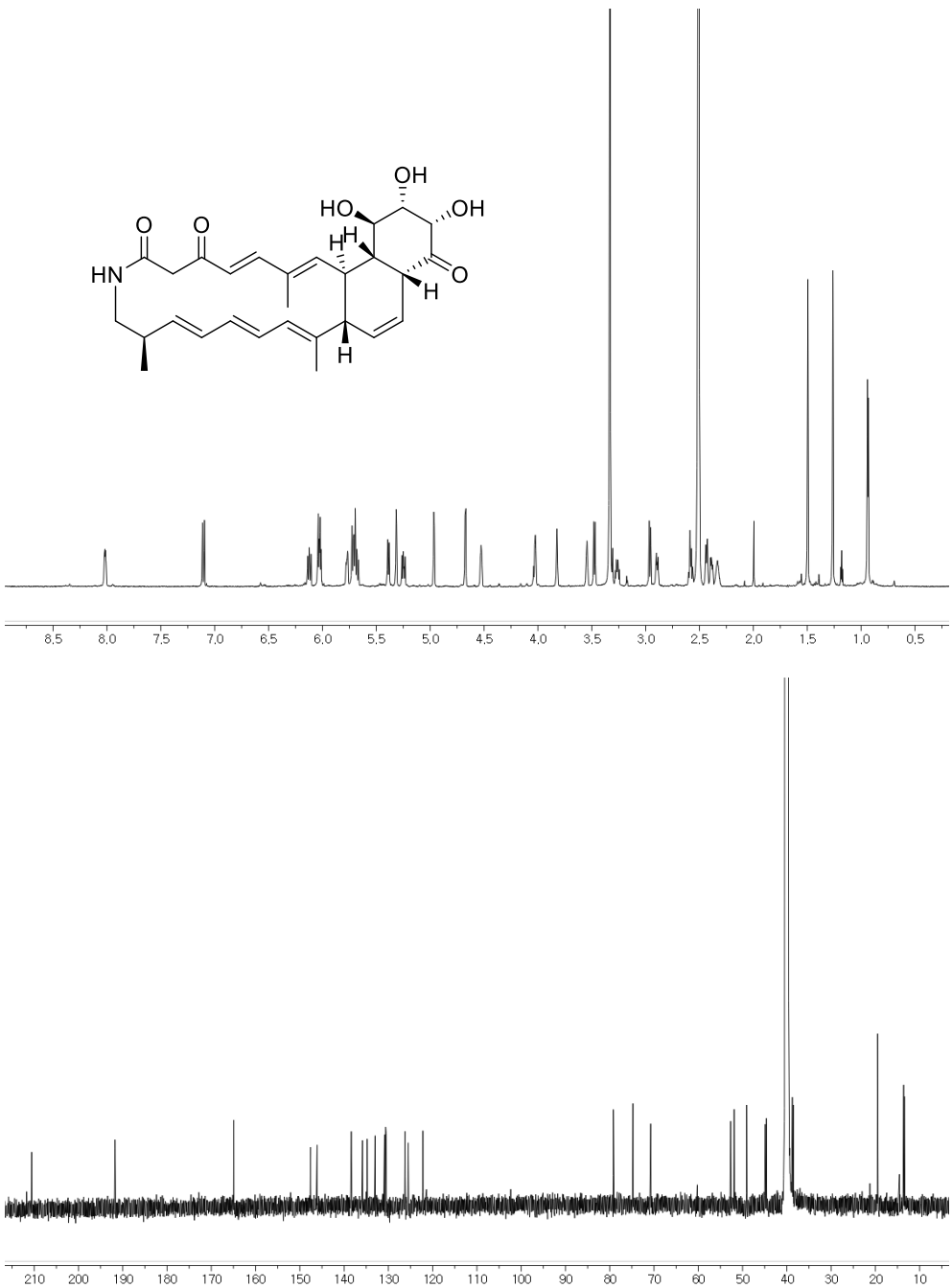

Figure S9. ^{13}C-^{13}C COSY NMR spectrum (200 MHz) of tripartilactam (**10**) in DMSO-d_6.

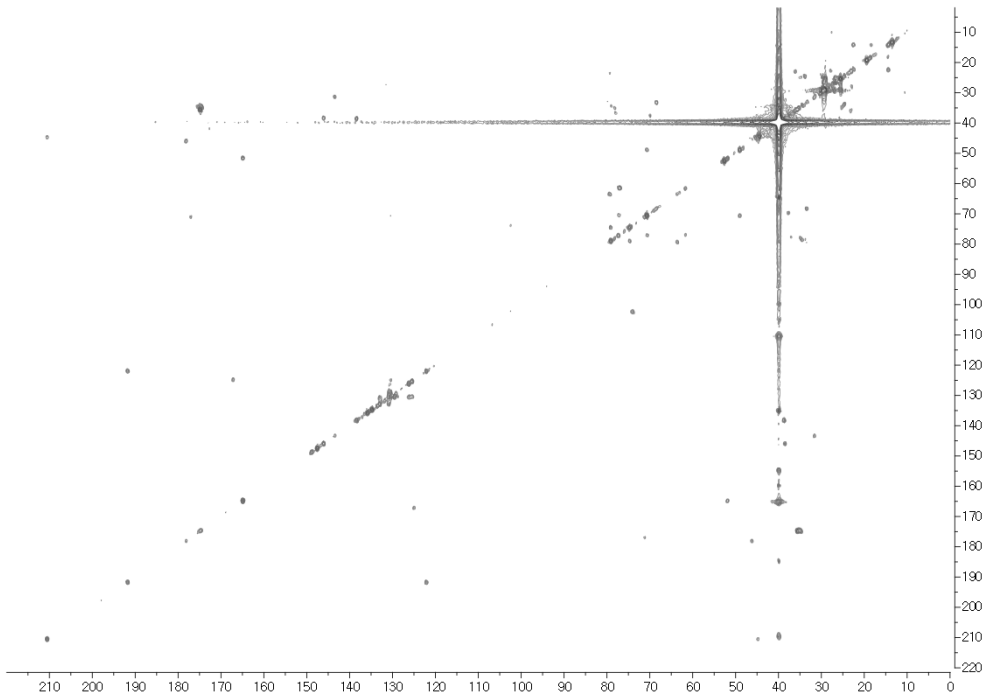

Figure S10. ^{1}H NMR spectrum (800 MHz) and ^{13}C NMR spectrum (200 MHz) of lydiamycin A (**11**) in DMSO-d_6.

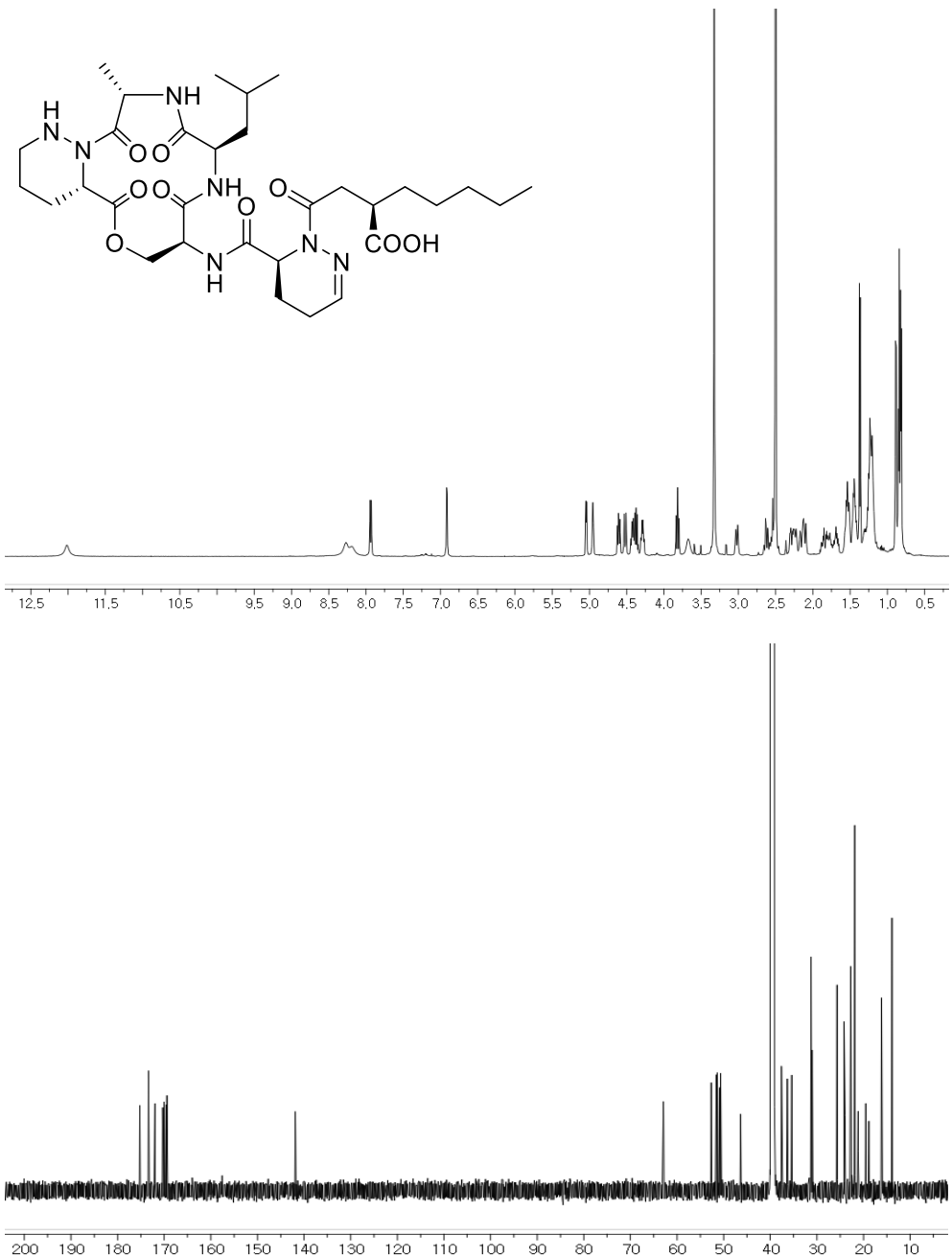

Figure S11. ^{1}H NMR spectrum (800 MHz) and ^{13}C NMR spectrum (200 MHz) of lydiamycin A (**11**) in $CDCl_3$.

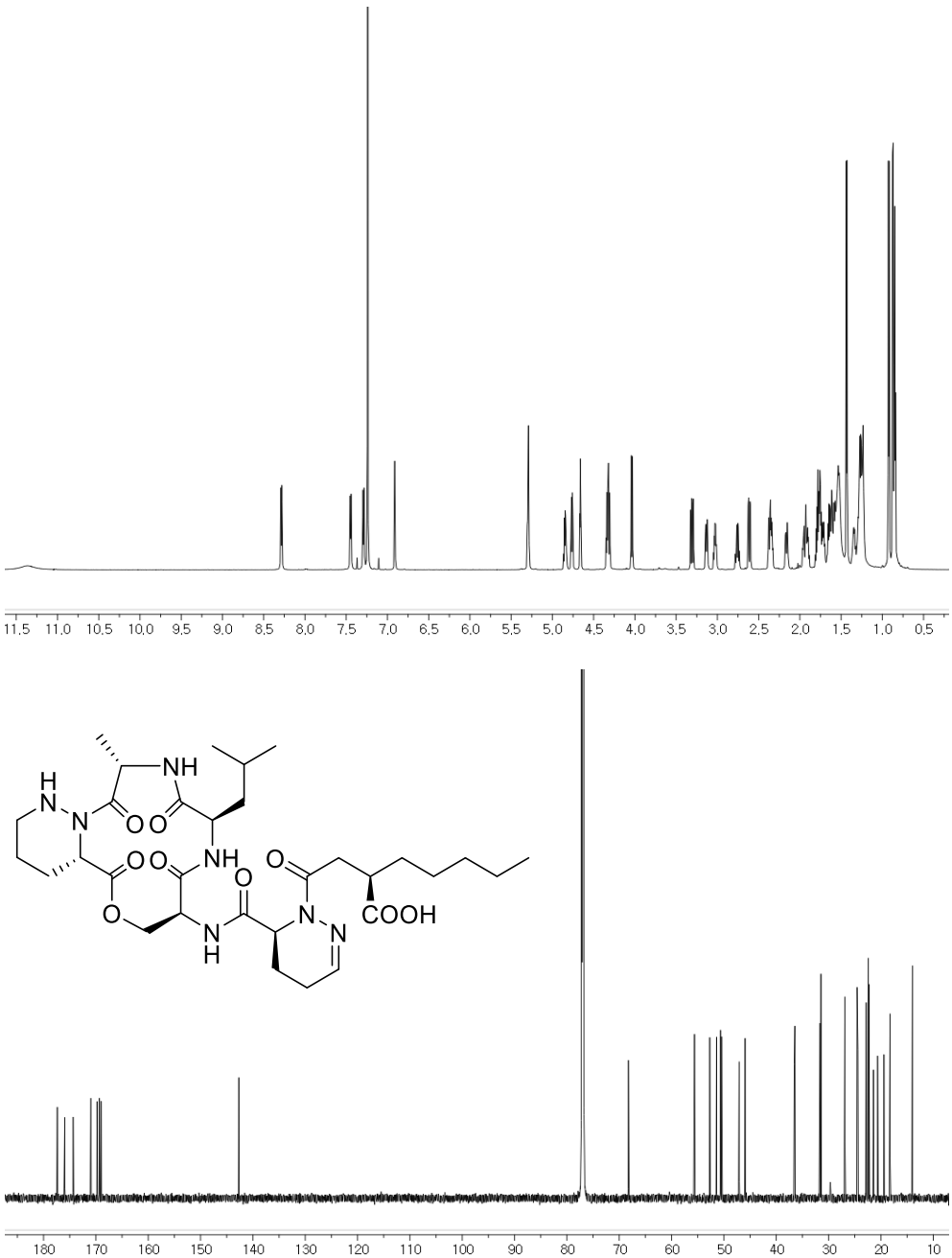

Figure S12. ^{1}H NMR spectrum of reaction product of *S*-piperazic acid with L-FDAA in DMSO-d_6.

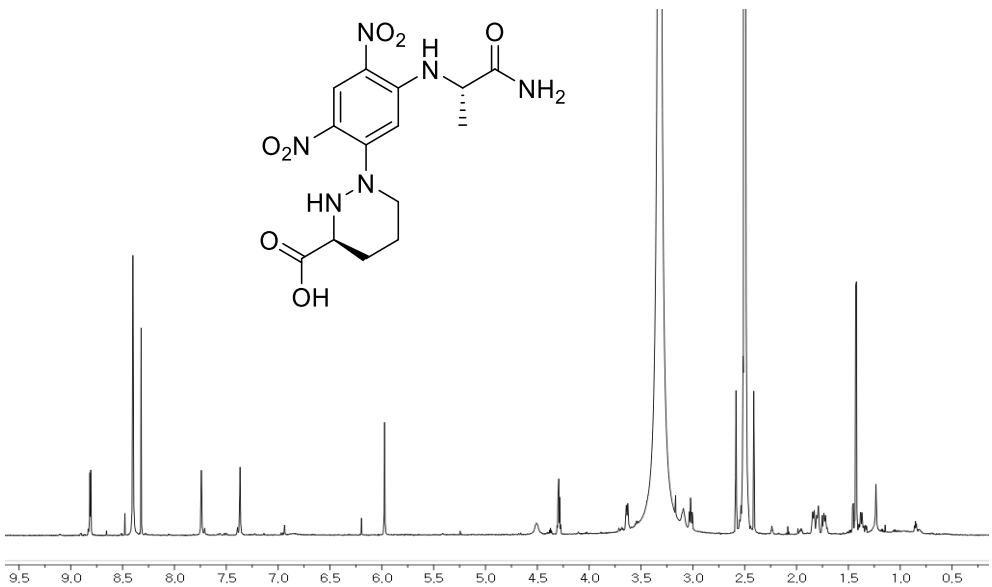

Figure S13. ^{1}H NMR spectrum of reaction product of *S*-piperazic acid with D-FDAA in DMSO-d_6.

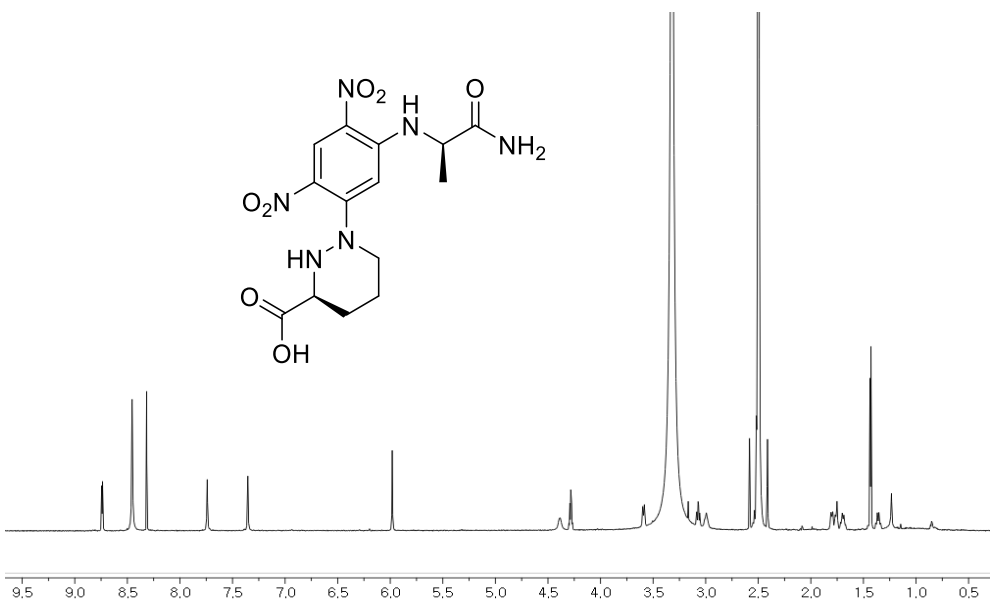

Figure S14. ^{1}H NMR spectrum of *S*-PGME derivatized lydiamycin A (**11a**) in DMSO-d_6.

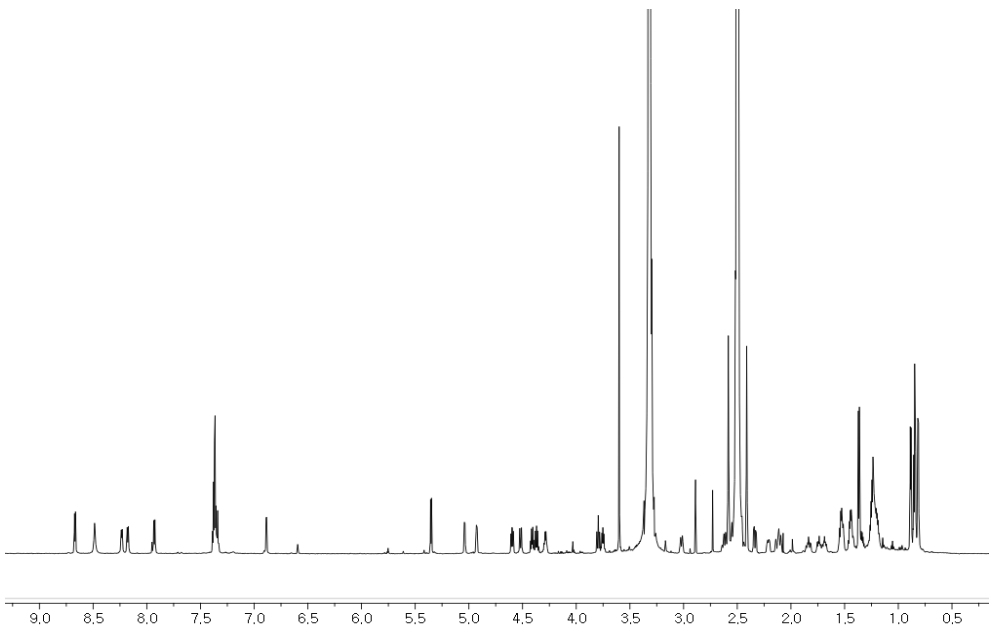

Figure S15. ^{1}H NMR spectrum of *R*-PGME derivatized lydiamycin A (**11b**) in DMSO-d_6.

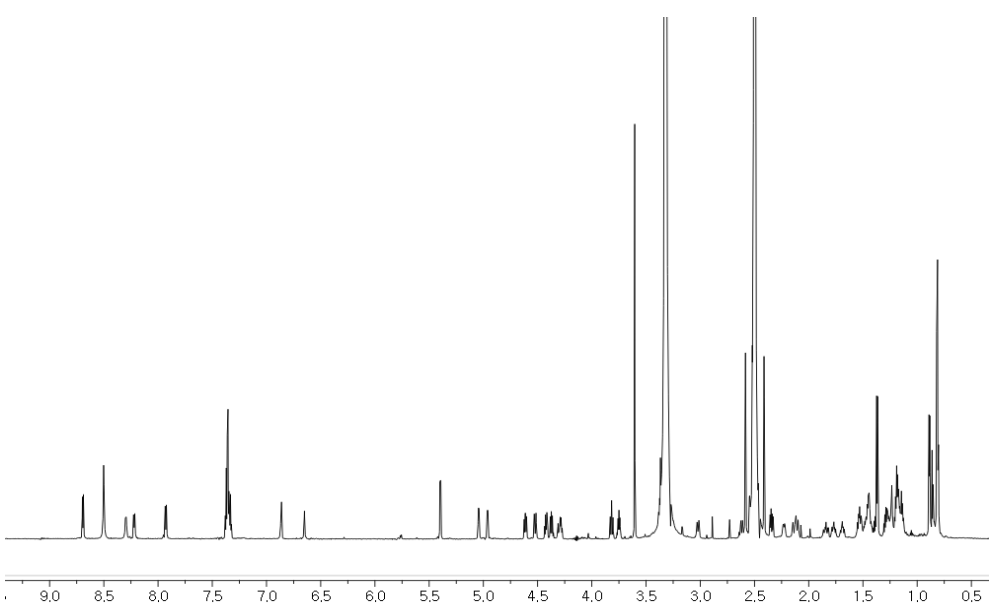

Abstract in Korean

국문논문요지

방선균 유래 신규 천연 펩타이드의 발견과 기지물질에 대한 구조적 오류 수정

황성훈

서울대학교 약학대학 대학원

천연물과학전공

천연물 신약 개발 연구의 기반이 되는 선두 물질의 발견을 위하여 곤충 유래 방선균이 생산하는 이차대사물질의 발견 및 구조 결정 연구를 진행하였다. 특히 방선균이 생산하는 새로운 펩타이드 물질에 대한 연구 (파트 A)와 이미 보고된 기지물질의 구조적 오류를 찾고 이를 수정하는 연구 (파트 B)를 수행하였다.

파트 A. 방선균이 생산하는 새로운 펩타이드 타입의 물질.

5가지 새로운 펩타이드 물질인 acidiphilamides A-E (**1**-**5**) 는 이미 보고된 L-isoleucinamide와 L-valinamide와 함께 산성 토양 유래 호산성 방선균 *Streptacidiphilus rugosus* AM-16으로부터 발견되었다. **1**-**5** 물질의 구조는 phenylalaninol 혹은 methioninol을 포함하며 C_3~C_5 acyl chain을 가지는 변형된 세 아미노산으로 구성된 펩타이드 물질들이며 이는 핵자기공명을 통한 분광분석 (NMR) 및 분광학적 질량분석을 통해 밝혀졌다. 아미노산들의 절대입체구조는 advanced Marfey's method 와 GITC (2,3,4,6-tetra-O-acetyl-β-D-glucopyranosyl isothiocyanate) 유도체화 반응과 LC/MS 분석을 통해 밝혀냈다. Acidiphilamide A와 B는 희귀 방선균인 *Streptacidiphilus* 속에 속하는 균주에 의해 만들어지는 최초로 밝혀진 이차대사물질이며 이 물질들이 HeLa 세포에서 autophagy flux를 효과적으로 억제하는 동시에 proteasome activity를 억제하지 않는 것으로 밝혀졌다. 이 물질들은 주로 세포의 autophagy 마지막 과정의 autophagosome-lysosome의 융합과정을 억제하는 역할을 하는 것으로 보인다.

Pentaminomycins C-E (**6**-**8**)는 갈색거저리 (*Tenebrio molitor*) 샘플의 내장에서 분리된 *Streptomyces* 종의 GG23 균주 배양액으로부터 분리되었다. Pentaminomycin 물질들은 분광학적 1D와 2D NMR 분석 및 질량분석을 통하여 N^{δ}-hydroxyarginine을 포함하는 고리형 펩타이드 물질이라는 것을 규명하였다. 각 아미노산들의 절대입체구조는 Marfey's method와 비리보솜 펩타이드 (NRP) 의 생합성 유전자 (BGC) 정보분석을 통하여 결정하였다. 생합성 유전자에 대한 자세한 분석을 통해 모듈 1의 NRPS adenylation domain 이 낮은 특이성을 가지고 있기 때문에 물질 **6**-**8**의 구조적 다양성이 발생하는 것으로 확인하였고 또한 거대 고리화 과정을 진행하는 효소가 일반적인 효소가 아니고 특이한 페니실린 결합 단백질 타입의 thioesterase (TE) 라는 것을 알게 되었다. 뿐만 아니라 pentaminomycin C 와 D (**6** 과 **7**) 는 autophagy를 유도하는 활성을 가지고 있으며 산화적 스트레스에 대한 보호작용 활성이 있음이 세포 수준에서 확인되었다.

파트 B. 이미 보고된 기지물질의 구조적 오류 및 수정.

Tripartilactam (**9**) 은 거대고리 구조를 가진 락탐계열 천연물로 원래 희귀한 골격인 [18,8,4]-삼고리 구조로 보고되었던 물질이다. 그러나 [18,6,6]-삼고리 구조 골격을 가진 niizalactam C (**10**)가 tripartilactam의 대체 구조로 보고된 2015년 이래로 해당 구조의 타당성에 대한 논의가 있었다. 따라서 이에 대한 확실한 규명이 필요하다고 생각되었고 NMR 분광분석 결과에 대한 종합적인 재조사와 ^{13}C-^{13}C COSY NMR 실험을 통한 ^{13}C-^{13}C 직접 커플링을 확인하여 tripartilactam 의 구조가 niizalactam C 와 동일하다는 것을 명백하게 했다. 이에 덧붙여서 tripartilactam 을 생산하는 생합성 균주에 대한 전장유전체 분석 및 유전자 정보 분석과 돌연변이화 분석을 통해 물질의 생합성 경로를 확인할 수 있었다. 이를 통해 확인된 생합성 경로의 특징은 type I polyketide synthase 모듈들 중에서 하나가 반복적으로 사용되며 PKS 후과정으로 자발적인 [4+2] 고리첨가 반응을 통하여 전구물질인 sceliphrolactam에서 tripartilactam으로 생합성 된다는 것이다.

Lydiamycin A (**11**) 는 이미 보고되었던 *Streptomyces* 로부

터 생산된 piperazic acid 모핵을 가지고 있는 고리형 펩타이드 물질이다. Lydiamycin A의 절대입체구조는 여러 차례 유기합성을 통해 규명하려는 시도들이 있었지만 완전히 규명되지 않았다. 이에 따라 lydiamycin A (**11**) 의 입체구조를 확실히 규명하기 위하여 advanced Marfey's method, 화학적 유도체화 반응 및 양자역학 기반의 컴퓨터 분석 등의 방법을 진행했고 결국 구조의 수정과 절대입체구조의 결정을 완료할 수 있었다. 또한 Lydiamycin A (**11**) 는 세포수준에서 약한 항결핵활성을 가지고 있음도 확인되었다.

주요어: 방선균, 미생물의 이차대사물질, 생합성 경로, 구조적 오류 수정

학번: 2015-21908

Permission for Republication of the Published Paper in Thesis

*Reproduced from [**Hwang, S.**; Yun, Y.; Choi, W. H.; Kim, S. B.; Shin, J.; Lee, M. J.; Oh, D.-C. Acidiphilamides A–E, Modified Peptides as Autophagy Inhibitors from an Acidophilic Actinobacterium, *Streptacidiphilus rugosus*. *Journal of Natural Products*, **2019**, *82(2)*, 341–348.]

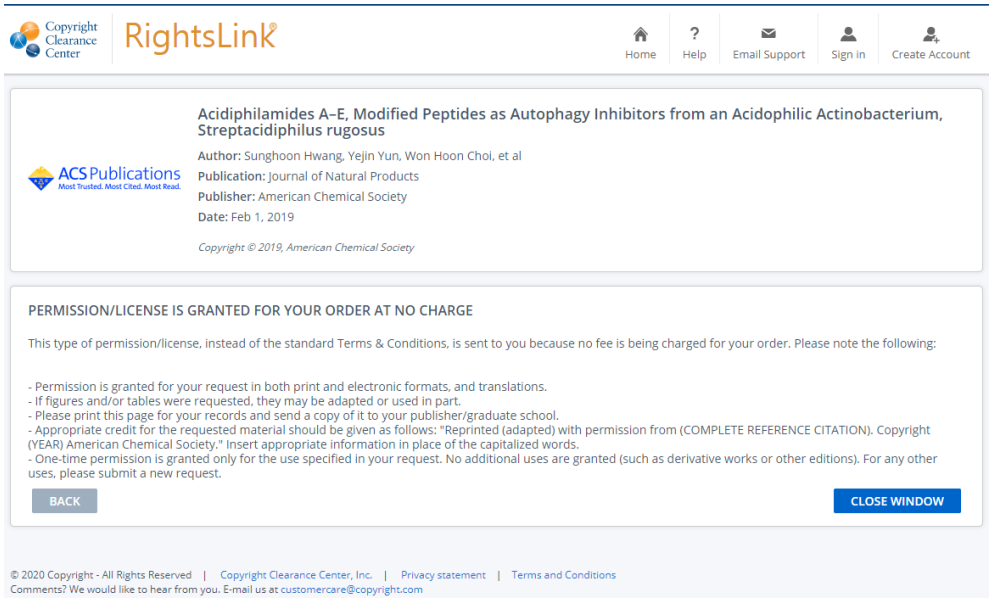

*Reproduced from [**Hwang, S.**; Kim, E.; Lee, J.; Shin, J.; Yeo, Y. J.; Oh, D.-C. Structure Revision and the Biosynthetic Pathway of Tripartilactam. *Journal of Natural Products*, **2020**, *83(3)*, 578–583.]

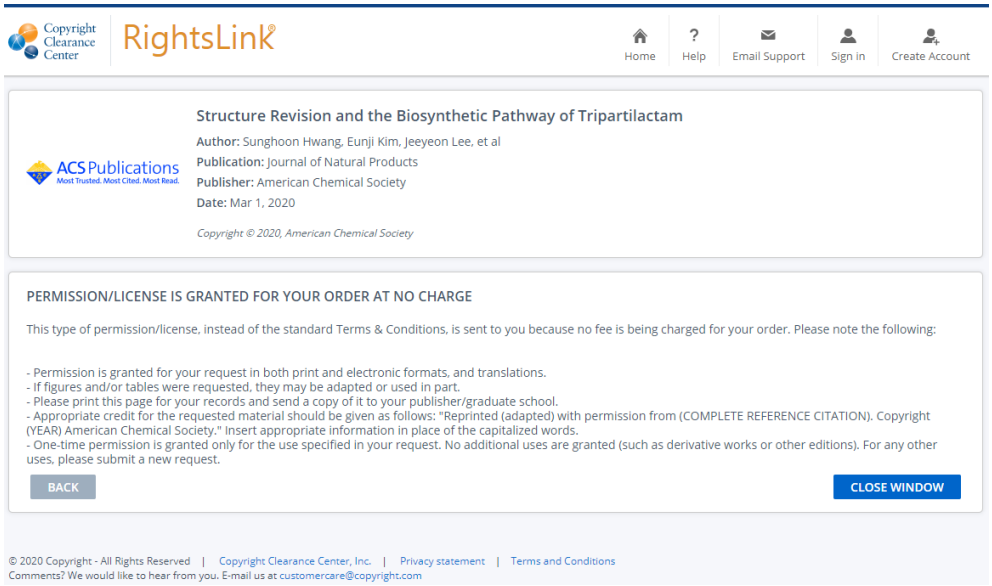

*Reproduced from [**Hwang, S.**; Shin, D.; Kim, T. H.; An, J. S.; Jo, S.-I.; Jang, J.; Hong, S.; Shin, J.; Oh, D.-C. Structural Revision of Lydiamycin A by Reinvestigation of the Stereochemistry. *Organic Letters*, **2020**, *22(10)*, 3855–3859.]

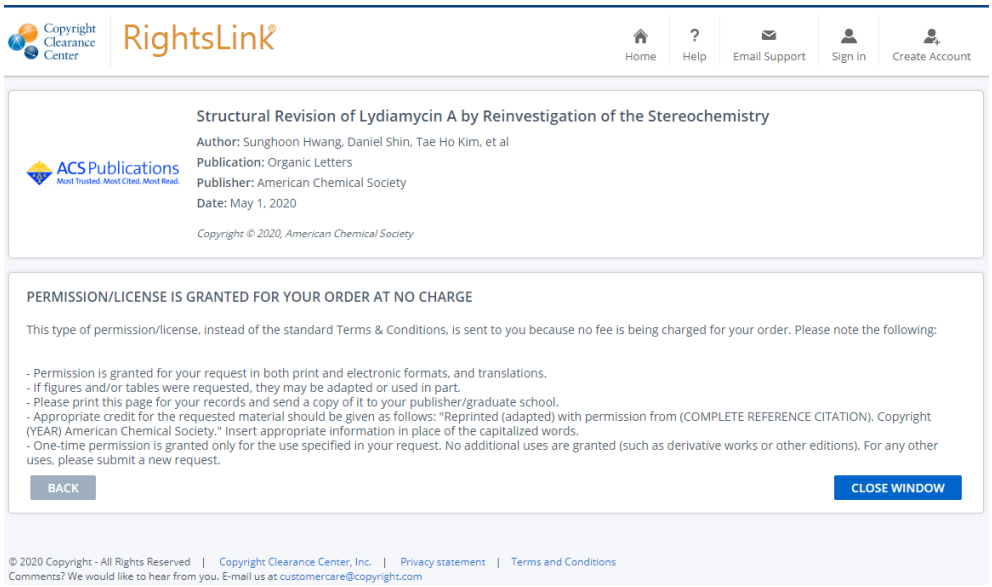

Acknowledgement

감사의 글

6 년의 대학원 학위과정동안 여러 선후배들께서 논문을 쓰고 졸업을 하여 새로운 곳으로 떠나는 것을 보며 저도 언젠가 졸업을 하겠지 막연하게 생각해왔는데 어느새 제 차례가 다가왔습니다. 학위과정 중에는 그리도 시간이 느리게 가는 것 같고 끝이 보이지 않는 길고 긴 터널을 터벅터벅 걸어가는 느낌이었는데 막상 끝에 다다르니 어느새 이렇게 시간이 빠르게 지나갔나 하는 생각이 드는 것이 참 감회가 새롭습니다. 학위과정동안 학문적인 것은 물론이고 그 외에도 많은 것을 배웠고 얻었습니다. 그 덕분에 제 자신도 이전보다 많이 성장했다는 생각이 듭니다. 물론 아직도 너무나 부족하고 더 배우고 경험해야할 것들이 넘치도록 많다고 생각하지만 학위과정 기간은 저에게 박사학위 말고도 여러가지 의미있는 것들을 알려준 소중한 시간이었습니다. 특히 삶에서 참고 인내하고 노력하는 법을 알게 되었고 세상은 내 기대와 예상대로 흘러가지 않는다는 것도 깨닫게 되었습니다. 수없이 많은 실패의 경험들이 저를 겸손할 수 있게 해주었고 그 속에서 이뤄낸 작은 성취에도 기뻐하는 법을 알려주었습니다. 그 노력의 순간들이 모여 얻을 수 있었던 학위라 생각하니 더욱 감사하고 뜻깊습니다.

학위과정동안 많은 지원과 훌륭한 가르침을 주셨던 지도교수님이신 오동찬 교수님께 진심으로 감사의 말씀을 드립니다. 교수님께 학문적인 지식뿐만 아니라 진정 학자로서 학문을 탐구하는 자세를 배웠고 스승으로서 제자들을 보살피고 이끌어주시는 모습을 존경하게 되었습니다. 저도 후에

누군가를 가르칠 위치에 오르게 되는 날이 온다면 아마도 오동찬 교수님을 떠올리며 교수님께 배웠던 것을 그들에게 가르쳐주고자 노력할 것입니다.

항상 저를 걱정해주시고 그럼에도 믿고 응원해주시는 부모님께도 감사드립니다. 가족들의 응원과 사랑이 없었다면 지금의 저는 없었을 것입니다. 표현을 잘 못하는 아들이지만 항상 감사하고 사랑합니다.

함께 동고동락했던 실험실 구성원들께도 감사의 말씀을 전하고 싶습니다. 저보다 앞서 졸업한 선후배 분들과 지금도 옆에서 실험하고 있는 친구들 모두에게 많은 것들을 배웠고 덕분에 길고도 고단했을 학위과정 기간이 오히려 즐거웠고 또 보람찼습니다. 여기서 만났던 소중한 사람들 모두 나중에 시간이 지나서 다시 만나면 함께했던 시간을 추억하며 웃고 떠드는 날이 오겠지요. 벌써 그 날이 기다려집니다.

서울대학교에서의 10 년은 제 인생에서 너무나도 큰 의미가 있었던 시간이었습니다. 학교 곳곳에 지난 10 년간의 추억이 서려있는 이 곳을 떠난다는게 조금은 아쉽고 두렵기도 하지만 익숙했던 곳을 벗어나 한 발 더 나아가야 할 때가 된 것 같습니다. 지금의 저를 있게 해준 저의 모교에 감사드리고 함께 했던 모든 이들에게 감사합니다. 그리고 마지막으로 제 박사학위과정의 대부분의 시간 동안을 힘들 땐 격려해주고, 기쁠 땐 함께 기뻐해주며 곁을 지켜줬던 고마운 친구, 故신준호 형에게 진심으로 감사하다는 말을 전하고 싶습니다. 고마워 형.